Artifact Noise Removal Techniques and Automatic Annotation on Seismocardiogram Using Two Tri-axial Accelerometers

A Thesis Submitted
to the College of Graduate and Postdoctoral Studies
in Partial Fulfillment of the Requirements
for the Degree of Master of Science
in the Department of Electrical and Computer Engineering
University of Saskatchewan
Saskatoon, Saskatchewan, Canada

by

Loc Gia Luu

PERMISSION TO USE

In presenting this thesis in partial fulfillment of the requirements for a Postgraduate degree from the University of Saskatchewan, I agree that the Libraries of this University may make it freely available for inspection. I further agree that permission for copying of this thesis in any manner, in whole or in part, for scholarly purposes may be granted by the professor who supervised this thesis work or, in their absence, by the Head of the Department of Electrical and Computer Engineering or the Dean of the College of Graduate and Postdoctoral Studies at the University of Saskatchewan. It is understood that any copying, or publication, or use of this thesis, or parts thereof for financial gain shall not be allowed without my written permission. It is also understood that due recognition shall be given to me and to the University of Saskatchewan in any scholarly use which may be made of any material in this thesis.

Request for permission to copy or to make any other use of material in this thesis in whole or in part should be addressed to:

Head of the Department of Electrical and Computer Engineering
57 Campus Drive
University of Saskatchewan
Saskatoon, Saskatchewan, Canada
S7N 5A9

ABSTRACT

Heart disease are ones of the most death causes in the world. Many studies investigated in evaluating the heart performance in order to detect cardiac diseases in the early stage. The aim of this study is to monitor the heart activities in long-term on active people to reduce the risk of heart disease. Specifically, this study investigates the motion noise removal techniques using two-accelerometer sensor system and various positions of the sensors on gentle movement and walking of subjects. The study also ends up with algorithms to detect cardiac phases and events on Seismocardiogram (SCG) based on acceleration sensors.

A Wi-Fi based data acquisition system and a framework on Matlab are developed to collect and process data while the subjects are in motion. The tests include eight volunteers who have no record of heart disease. The walking and running data on the subjects are analyzed to find the minimal-noise bandwidth of the SCG signal. This bandwidth is used to design bandpass filters in the motion noise removal techniques and peak signal detection. There are three main techniques of combining data of the two sensors to mitigate the motion artifact: analog processing, digital processing and fusion processing. The analog processing comprises analog ADDER/SUBTRACTOR and bandpass filter to remove the motion before entering the data acquisition system. The digital processing processes all the data using combinations of total acceleration and z-axis only acceleration. The fusion processing automatically controls the amplification gain of the SUBTRACTOR to improve signal quality as long as a signal saturation is detected. The three techniques are tested on three placements of sensors including *horizontal*, *vertical*, and *diagonal* on gentle motion and walking. In general, the *total acceleration* and *z-axis acceleration* are best techniques to deal with gentle motion on all placements which improve average systolic signal-noise-ratio (SNR) around 2 times and average diastolic SNR around 3 times comparing to only one accelerometer. With walking motion, overall the ADDER and *z-axis acceleration* are best techniques on all placements of the sensors on the body which enhance about 7 times of average systolic SNR and about 11 times of average diastolic SNR comparing to only one accelerometer. The combination of two sensors also increases the average number of recognizable systole and diastole on walking corresponding to 71.3 % and 43.8 % comparing to

only one sensor. Among the sensor placements, the performance of horizontal placement of the sensors is outstanding comparing with other positions on all motions.

There are two detection stages to detect events in the SCG for automatic annotation. First, two algorithms including moving average threshold and interpolation are applied to locate the systolic and diastolic phases. Then, based on those identified phases, cardiac events are found in the searched intervals using two outstanding characteristics of the SCG. The two algorithms of phase detection are examined on the stationary data sets of *digital processing* and *horizontal* placement. The *total acceleration* of only one sensor is also calculated for comparison. With moving average threshold algorithm, the average error and missing rates of *total acceleration* and *z-axis acceleration* are 1.8 % and 2.1 % respectively which are lower than using one accelerometer (3.6 %). With interpolation algorithm, the average error and missing rates of *total acceleration* and *z-axis acceleration* are in the order of 2.3 % and 2.4 % which are still lower than one accelerometer. The average calculation time of the moving average algorithm is lower than the interpolation counterpart. The real-time mode of detection algorithms is also demonstrated on Matlab framework to prove the possibility of practical applications.

ACKNOWLEDGEMENTS

I would like to send my hearty gratefulness to my dear supervisor Dr. Anh Van Dinh for his continuous support and encouragement throughout my graduate program at the University of Saskatchewan.

I truly appreciate my parents, my parents-in-law, my wife, my sisters and my sisters-in-law for their endless love, backing and sharing during my life.

Lastly, I would like to say thank to everyone involved in this study and to my great friends for their sharing and help.

TABLE OF CONTENTS

LIST OF FIGURES

LIST OF TABLES

LIST OF ABBREVIATIONS

ABS	Absolute
AC	Aortic Valve Closure
ACC_MOV	Accelerometer on the ECG negative (right) electrode
ACC_SCG	Accelerometer on the ECG positive (left) electrode
ADC	Analog-To-Digital Converter
AGC	Auto Gain Control
AO	Aortic Valve Open
AS	Atrial Systole
BCG	Ballistocardiogram
BPM	Beat-Per-Minute
CAD	Coronary Artery Disease
CSCW	Cardiac Sound Characteristic Waveform
CT	Computed Tomography
DAQ	Data Acquisition
DTV	Diastolic Timed Vibrations
ECG	Electrocardiogram
EMD	Empirical Mode Decomposition
FIR	Finite Impulse Response
GUI	Graphic User Interface
IM	Isovolumic Movement
LVET	Left Ventricular Ejection Time
MC	Mitral Valve Closure
MO	Mitral Valve Open
MRI	Magnetic Resonance Imaging
PEP	Pre-Ejection Period
RE	Rapid Ejection

RF	Rapid Diastolic Filling
S:D	Systolic and Diastolic Ratio
SCG	Seismocardiogram
SNR	Signal Noise Ratio
STI	Systolic Time Intervals
TOTAL_ACC	Total Acceleration of three axes of two accelerometers
VPP	Peak-to-Peak voltage
Z_ACC	Combination of z-axis of two accelerometers

CHAPTER 1
INTRODUCTION

As a report of the World Health Organization in January 2017, cardiovascular diseases including ischemic heart disease and stroke were the biggest killers in the top ten causes of death in the world from 2000 to 2015 [1]. Cardiovascular diseases claimed 26.7% of the 56.4 million deaths worldwide in 2015. In Canada, heart disease is also the second leading cause of death. Following the data in 2012 and 2013 from Public Health Agency, around 2.4 million Canadian adults were diagnosed heart disease with the age of twenty up, and every hour, about twelve of those Canadian adults die due to heart disease [2]. Therefore, early diagnosis of cardiovascular diseases is needed before the diseases getting worse. Heart assessment has an important role in that process. Myocardial infarction, angina, arrhythmias and cardiomyopathy, for instances, were identified by analyzing the features of heart signal - electrocardiogram or the segments of heart moving images – echocardiogram [3]. Having the right evaluation and treatment for current heart condition can prevent it from progressing to a serious stage. There are many techniques to observe and evaluate the heart from simple as symptoms and physical signs associated with patients or blood work to complex as X-Ray, computed tomography (CT) or magnetic resonance imaging (MRI). However, symptoms and physical signs cannot identify the heart disease accurately because they might conflict with other diseases. Although X-Ray, CT and MRI can diagnose the cardiac diseases precisely, they are too complicated and expensive techniques which are only required in some special cases. For early diagnosis, the heart should be tracked in long-term by a device to daily monitor important information from heart activities. The device should be light-weight, long-lasting, ease-of-use, and wearable which can be carried comfortably all day and provides information of the heart instantly using simple and reliable techniques. Electrocardiography (ECG) and Seismocardiography (SCG) are simple, non-invasive and inexpensive as well as providing much useful and reliable information about the heart; hence, they are suitable for wearable devices in long-term monitor [4-11].

ECG are electrical signals generated by a combination of depolarization and repolarization processes of the hearts muscle cells when they contract or relax. Depolarization is the loss of the cell external positive charges that are substituted by the negative ones; repolarization represents the recovery of the cell external positive charges [12]. These signals are captured through the

electrodes placed in different positions on a human body. The electrodes can be the wet ones which require conductive gel between the electrodes and the skin. They also can be the dry ones which use capacitance technique to measure and require no gel between. There are total twelve standard ECG signals corresponding to various places of ten electrodes on the chest and limbs. The components of a typical ECG signal consist of P wave, QRS complex and T wave representing repolarization and depolarization processes [12]. The abnormalities of ECG features and the change of the inter-component intervals helped doctors to evaluate and monitor some types of heart disease on patients [13,14].

Differ from ECG, SCG are mechanical signals generated by the force of heart activities pushing on the chest wall. SCG signals are measured using an accelerometer placed on the chest. The SCG signals provide the timing of closing and opening of the heart valves corresponding to the signal peaks. These events are divided into two groups. The group of systolic events includes mitral valve closure (MC), aortic valve open (AO), isovolumic movement (IM) and peak of rapid ejection (RE). The group of diastolic events contains aortic valve closure (AC), mitral valve open (MO), peak of rapid diastolic filling (RF) and peak of atrial systole (AS) [15]. These events of SCG signals also have correlation with ECG signal. With corrected timing, the MC should be in the end of ECG QRS complex, and the AC should be near to the end of ECG T wave. Figure 1.1 is extracted from [16] to illustrate the timing relationship between the ECG components and the SCG events.

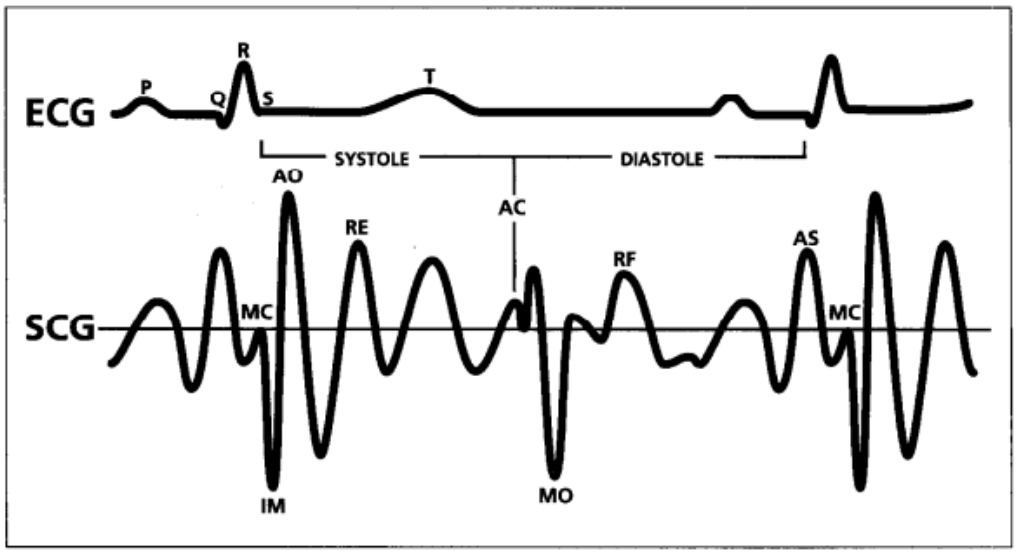

Figure 1.1 The relation between SCG events and ECG components [16].

1.1 Applications of Seismocardiography

The ECG signal has been already investigated by many research and was also applied in clinical applications while the SCG signal still needs more studies to make it more reliable before utilizing in clinical trials. Before the millennium, many studies showed the high potential of SCG in diagnosis of heart disease. Compared to ECG, SCG was proven to have a better sensitivity than ECG for identifying anatomic and physiologic ischemic coronary artery disease during exercise stress testing on women and on patients who did not reach the maximum heart beat in the test. Moreover, the technique also gave more information for diagnosis than exercise ECG [16]. The authors in [17] proposed the benefit of SCG when observing the left ventricular function during myocardial ischemia. It showed the significant differences on SCG of a patient during ischemia from SCG of other five normal volunteers [17]. In a research of medicine doctors, the change of SCG before and after balloon angioplasty was also analyzed to prove that SCG varied due to ischemia changes caused by decreased coronary blood flow [18]. Another study examined on 58 subjects with SCG at rest and limited exercise after within 2 minutes. The authors measured the left ventricular functions and compared with literature; the SCG provided good data for all functions even with exercise while literature did not [19]. The cardiac time intervals measured by SCG and ECG were studied on two groups of 12 women running on treadmill to find out how difference between trained and untrained women [20]. Medicine doctors in [21] investigated the systolic time intervals (STIs) with left ventricular ejection time (LVET) and pre-ejection period (PEP) extracted form an accelerometer on the chest of young patients in head upright and tilt testing. They concluded that the fast response of STIs changes could be helpful in pacemakers with adaptive rate to the posture [21]. In some special cases, the patients were required to monitor cardiac function under stress test with MRI. However, the ECG was not compatible for cardiac function with MRI due to the distortion of high electrical voltages caused by MRI. In contrast, SCG was experimented on animal in the same configuration to prove SCG as a solution to detect myocardial ischemia during MRI [22].

After the millennium, the potential of SCG in diagnosis of cardiac diseases was still investigated by many researchers. One study re-estimated left ventricular functions on two groups of 50 patients associated with coronary heart disease using exercise stress test and SCG. The study again showed the benefit of SCG in tracking left ventricular function in patients with

heart disease [23]. One study on 77 patients with coronary artery disease (CAD) confirmed that SCG was low cost, simplicity, more accurate and sensitive than ECG stress test in the detection of ischemia resulted by coronary stenosis [24]. Other investigation also proved the usefulness of SCG to assess patients with exercise-caused ischemia by observing the changes of the left ventricular function on exercise tolerance test [25]. The SCG was also used to estimate the diastolic onset and ending for improving performance in application of diastolic timed vibrations (DTV). The DTV device delivers direct mechanical vibrations during diastolic phase on the chest of patients associated with acute coronary thrombosis [26-28]. In another research, the intervals of PEP and LVET which reflect the cardiac contractility were extracted and validated with previous studies to prove SCG as a possible method for the assessment of cardiac mechanics [29]. Due to the limitation of clinical integration on human, one study investigated with more clinical integration on 9 pigs to confirm the alterations of myocardial function correlated with the changes on SCG [30].

1.2 Current Research of Cardiac Events on Seismocardiogram

Due to the huge potential applications in clinical environment as well as in daily life, SCG signal was studied by many researchers to accurately detect its events. In two studies, two points AO and AC were automatically detected based on sliding the templates, which were formulated from the ensemble average of few SCG beat cycles. Then, the algorithms searched in narrow-down window based on the location of peaks obtaining from sliding process [31,32]. In another research, IM and AC, which are most extrema points, were identified automatically using four different envelopes including cardiac sound characteristic waveform (CSCW), absolute (ABS), Shannon and Hilbert on high frequency acceleration signal [33]. However, the works of [31-33] still used ECG signal as a timing reference. A study to detect IM, AO and AC events automatically without the need of ECG uses multiple envelopes derived from high-pass filtering with different cut-off frequencies and triple integration. The envelopes included heart rate envelope used to replace the ECG R wave, diastolic and systolic envelopes were used to detect SCG points [34]. Other research also annotated automatically SCG events including AO and IM points without the need of ECG signal using Morlet wavelet transform and continuous wavelet transform [35,36].

1.3 Motivation

A patient feeling unusual about the heart would arrange to visit a doctor for checkup. All vital signs of the patient relating to the disease including heartbeat, ECG, blood pressure or even blood work are measured and sent to a specialist for further diagnosis. In some cases, after receiving the test results, additional specialized tests may be required such as CT and MRI which are very costly. In addition, when the patient clearly experiences the heart abnormalities, the disease might be near to the worst stage. Depending on the condition of the disease, the diagnostic may affect the effectiveness of treatment process and patients' mental health. From all the above situations, if the early stage of the heart disease can be detected, the cost of treatment will be tremendously reduced and the process of treatment may be simpler and more effective.

With the rapid development of new technologies, the sensors are more sensitive, much smaller, light-weight and consume less power than in the past. That leads to a tendency of wearable devices for personal health care in long-term monitoring and real-time interpretation of the recorded signals. Although there are many gadgets such as watch, bracelet which can monitor in real-time some health information from body activities, they do not provide any further than step counting, body temperature and maybe heartbeat. Having a wearable device which can interpret some important signs of your heart condition and detect the early phase of heart disease would be very helpful for elderly people, patients with cardiovascular diseases or even for healthy people who want to track their heart. As mentioned before, some simple, non-invasive, inexpensive and reliable techniques which can help to monitor the heart activities include Electrocardiogram and Seismocardiogram.

1.4 Problem Statement

Although many works were conducted to detect SCG's events, there are still some limitations which have not yet or less been investigated. Firstly, most of studies acquired data using wire connection which restricted subject to movement which causes motion noise. Such setup cannot be used to monitor SCG signal in daily activities [31-36].

Secondly, the motion artifact removal of SCG signals has not been studied thoroughly. A study analyzed, identified and eliminated the segments of SCG signal containing some kinds of noise which was created at a specific time during recoding [15]. The authors in [15] did not

describe the method to eliminate the noise beyond an analog band-pass filter before going to analog-to-digital converter. In another work, various types of noise affecting to SCG signal in different situations were only analyzed without the methods to remove those noises [37]. The authors also did not have any method to reduce the noise rather than a digital band-pass filter in the preprocessing stage. Although some techniques were applied to remove the motion artifact of SCG signals, they were still complicated and not fully conducted in different types of motion noise [38,39]. The authors in [38] used the normalized least mean square (NLMS) adaptive filter to reduce the motion artifact caused by walking around 1.3 m/s. In [39], empirical mode decomposition (EMD) was used to denoise walking motion on SCG. All the above studies used only one accelerometer placing on the sternum, and multi-accelerometer concept has not been yet investigated.

Thirdly, most algorithms to process the SCG signal only applied to z-axis of one accelerometer [31-36] while the accelerometer has three axes, and each axis provides acceleration of the heart activations in a different plane. The combination of all three axes can improve the quality of SCG signal leading to better accuracy for event detection. Lastly, many algorithms were developed to detect cardiac points, but they almost required ECG as timing reference [31-33]. In addition, some detection algorithms are complicated to implement in real-time fashion [34-36]. Therefore, removing the need of ECG while having the detection of cardiac events relying only on SCG signal with simplicity and acceptable accuracy can make the concept of using SCG to monitor long-term heart wellness feasible in everyday life.

1.5 Objectives of the Thesis

This study proposes solutions to the missing gaps and bring to the final aim which is detecting all cardiac events on SCG signal measuring on people with daily activities. In the following, the objectives of this thesis are described and briefly discussed:

1. Design a wearable data acquisition device which can collect biomedical signals including ECG and six axes of two accelerometers simultaneously with high resolution of timing (1000 sample-per-second). This setting can help to erase the restriction of wire connection in settings and easily conduct different types of motion artifact. This device combining with Matlab framework is also designed to test algorithms in real-time mode.

In addition, it is low-cost and the hardware and firmware can be maximally customized to fit the requirements of this thesis work. This system is not to be compared to other commercially available devices due to its unique design. The system can also work as a standalone device with embedded detection algorithms in future applications.

2. Investigate into motion noise removal methods using a system of two accelerometers placed in various positions on the chest to find out which positions can achieve the high quality SCG signal while the subjects are moving in different scenarios including moving gently and walking. In addition, the combination of all three axes of the accelerometer is also to be examined to see if a better detection can be obtained rather than using only z-axis as in many previous studies.

3. Develop two algorithms to firstly locate zones comprising systolic and diastolic events without using ECG as timing maker. Then, a less-complex method detects automatically all SCG cardiac points by focusing on the located zones. This process can reduce the calculation time and increase the accuracy of detection by narrowing down the regions to detect cardiac events. Hence, that makes the process possible in real-time fashion.

1.6 Thesis Organization

The remaining part of this thesis is divided into four chapters. Chapter 2 provides more background details of seismocardiography to obtain a better understanding. The history and methods people used to discover cardiac events on SCG will be described. The relations of SCG with other signals such as Electrocardiogram and Ballistocardiogram will also be discussed in this chapter.

Chapter 3 describes all the methods applied on SCG signal. Firstly, the design of data acquisition system to acquire ECG and six-axis of two accelerometers will be detailed. Next, the pair accelerometers with one captures combination of vibrations and motion, and one is referred as motion reference will be placed in different positions to investigate the effects of motion while subjects sitting/moving gently and walking. Various motion removal techniques using two accelerometers with analog ADDER/SUBTRACTOR, digital signal processing and automatic gain control are also explained then. After dealing with motion artifacts, two algorithms will be introduced to locate the regions containing systolic and diastolic events. One uses the slope, a

moving average threshold and systolic interval constraint whereas another takes the advantage of the slope and interpolation technique to locate systole and diastole. The purpose of this step is to narrow down the searching window of cardiac events, increase the accuracy of detection in next step and eliminate the need of ECG as timing reference. Finally, based on the located regions, all cardiac points of SCG will be identified based on the special characteristics of seismocardiogram.

Chapter 4 presents all visual and statistical results which show the advantages and disadvantages of the sensors placements, motion artifact removal techniques as well as the accuracy of the methods detecting the systolic and diastolic phases on SCG signal based on eight volunteer subjects who have no record relating to heart disease.

Chapter 5 emphasizes specific contributions of the thesis. All the thesis works will also be summarized. There still have some limitations of this study which are needed to be investigated to bring SCG closer to actual clinical use. Lastly, some suggestions are also presented to provide some ideas for further research.

CHAPTER 2
SEISMOCARDIOGRAPHY

In this chapter, the development of seismocardiography is discussed in details. Then, the waveform and characteristics of SCG are explained in following section.

2.1 History of Seismocardiography

Seismocardiography is a non-invasive technique measuring the cardiac vibrations on the chest wall caused by heart operation using an accelerometer. The first idea of measuring cardiac vibration was documented by Gordon in 1877. The author recorded the movement on a person standing upright on a special bed. The bed was described as a weighing machine with normal spring. When the person stood perfectly still on the bed, a rhythmic movement synchronizing with heart pulse was observed; however, only systoles were captured by this setting [40]. Later, in 1905, Henderson re-measured the body vibration using an improved bed which was limited the swing and used a magnifying mechanism to write result on a smoked drum. The author did that to secure the recording in horizontal movements with accuracy [41]. Thirty years later, Doctor Starr, who firstly named the measuring technique as Ballistocardiography (BCG), struggled to reproduce Henderson's method because of the large effect of respiration to the results. Then, Starr made another bed working on higher frequency than Henderson's bed which require no breath holding on patients when measuring, and Starr's table has been used to monitor patients for long period [42,43].

A new measuring technique of BCG was introduced in 1949 by Dock. The author captured the velocity of vibrations on the shin of subject, and many studies were drawn by the new technique because of simple setup. However, the method still had a drawback which was very sensitive to coupling between subject and measuring device [44]. In 1954, another new instrument using electrical charges at the surface effect was designed by Elliott. The device was also attached on patients' leg to measure BCG, and the author noticed some new waves when recording on normal subjects [45]. In 1956, the instrument of Elliott was reused in a clinic trial on twelve healthy subjects. However, the device was mounted on the subjects' chest specifically on apex beat or apical area [46]. In the same year, Scarborough proposed the names for peaks of BCG waveform. The systolic waves include H wave is upward and near to R peak of ECG, I

wave is downward and following H wave, J is largest upward peak following H wave and K is downward peak staying near to the systolic end. The diastole includes small amplitude L, M and N waves in sequence [47].

Recently, some new methods of measuring BCG were investigated using chairs [48,49], beds [50,51] and scales [52]. Figure 2.1 illustrates the different records of BCG and their name convention.

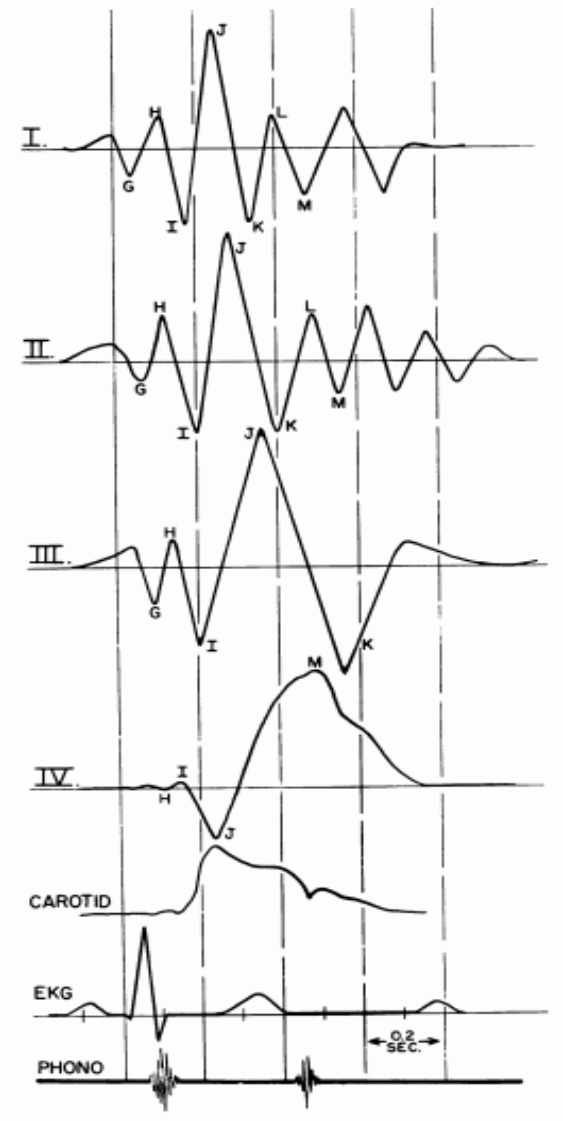

Figure 2.1 Different waveforms of BCG with ECG. (I) High frequency BCG. (II) Direct-body BCG. (III) Low frequency BCG. (IV) Ultra-low frequency BCG [47].

The precordial vibration was studied firstly by Bozhenko in 1961. Bozhenko placed an accelerometer on the chest of people with abnormal hearts to acquire precordial vibration

waveforms from 4 to 40 Hz then compared with the waveforms of normal people to observe the difference [53]. In 1964, Baevskii also measured precordial vibrations using an electromechanical accelerometer placed various positions on the torso along with ECG signal. The author calculated the average time intervals between the Q wave of ECG signal and systoles and diastoles of SCG signal [54]. Later, Zanetti and Salerno revived the precordial measuring technique in 1990 and called it as Seismocardiography (SCG). They captured the acceleration from an accelerometer on the sternum in supine position with dorsal-ventral direction [55]. They also proposed a technique to determine cardiac mechanics on SCG by measuring ECG, SCG at the same time with M-mode echocardiograph image. They found that the closing and opening times of echocardiogram correlating with upward and downward peaks of SCG with ECG as timing maker [56]. With the development of electronic devices, the accelerometers became steadily smaller size, higher sensitive, better accuracy and lower power consumption. Lately, new accelerometers designed based on microelectromechanical systems (MEMS) technology with very tiny size and high sensitive were implemented in some studies to recording SCG on the chest [57,58].

2.2 SCG Waveform

Comparing to other cardiac vibration signals, a typical SCG waveform have distinguishing systolic and diastolic complexes [59]. According to a review, there are to groups of opinion about SCG frequency range. The first group believed the SCG frequency range stays mostly smaller than 25 Hz while the second group thought the range is above 25 Hz [60]. Although the SCG frequency was investigated in many research, but the signal amplitudes were not usually mentioned. In this study, the average amplitudes of raw SCG signal captured on the chest have been noted around 20 mV with the sensor sensitivity of 660 mV/g equivalent to 0.03 g.

The peaks of SCG waveform was proposed to occur at the same time with cardiac events of the heart, and these events were identified and published in the past. They are the peak of the atrial systole (AS), mitral valve closure (MC), isotonic contraction (IC), isovolumic movement (IM), isovolumic contraction (IVC), aortic valve opening (AO), the peak of rapid systolic ejection (RE), mitral valve opening (MO), aortic valve closure (AC) and rapid filling (RF) [56,61,62]. Figure 2.2 is shown again to depict the components of ECG and SCG and their correlation.

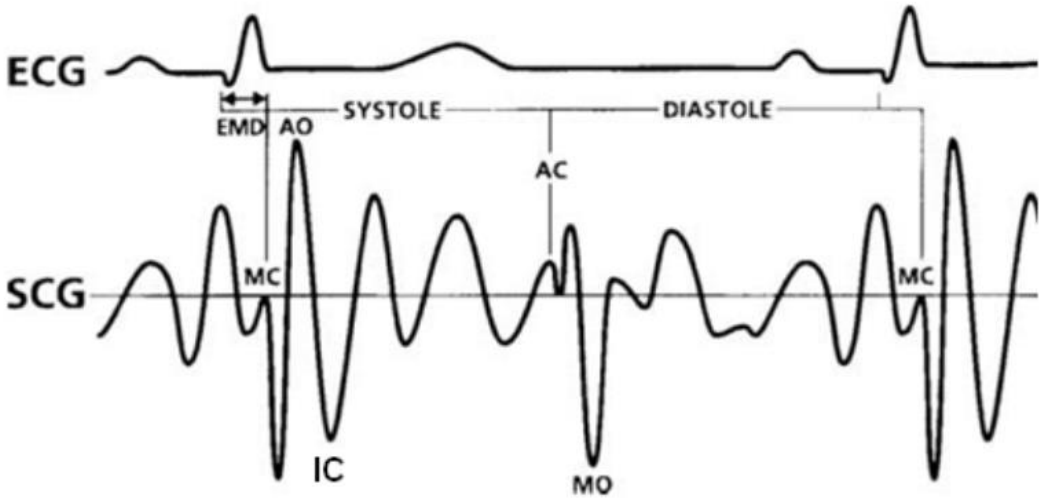

Figure 2.2 SCG signal annotated based on the collation of echocardiogram cardiac events and SCG peaks [56]

The conventional measuring technique using one accelerometer on the sternum can only observe the cardiac events of atrial valve and mitral valve on the SCG signal. A new study was proposed to use four accelerometers placing on the clinically four-valve auscultation areas of 25 subject to capture waveforms corresponding to each heart valves, then comparing with simultaneous echocardiogram with ECG as timing reference. As the result, six new cardiac events were identified in this study [63]. Figure 2.3 displays the six new feature points on SCG signals.

In conclusion, both BCG and SCG measure the vibrations caused by cardiac activities, but the BCG captures the vibrations of the whole body caused by circulation of blood in the main arteries while SCG records the vibrations caused by the heart operation. Both BCG and SCG are influenced easily by body movement. However, SCG promises the applications not only in clinic but also in daily tracking due to simple configuration and more information about cardiac mechanics comparing with BCG.

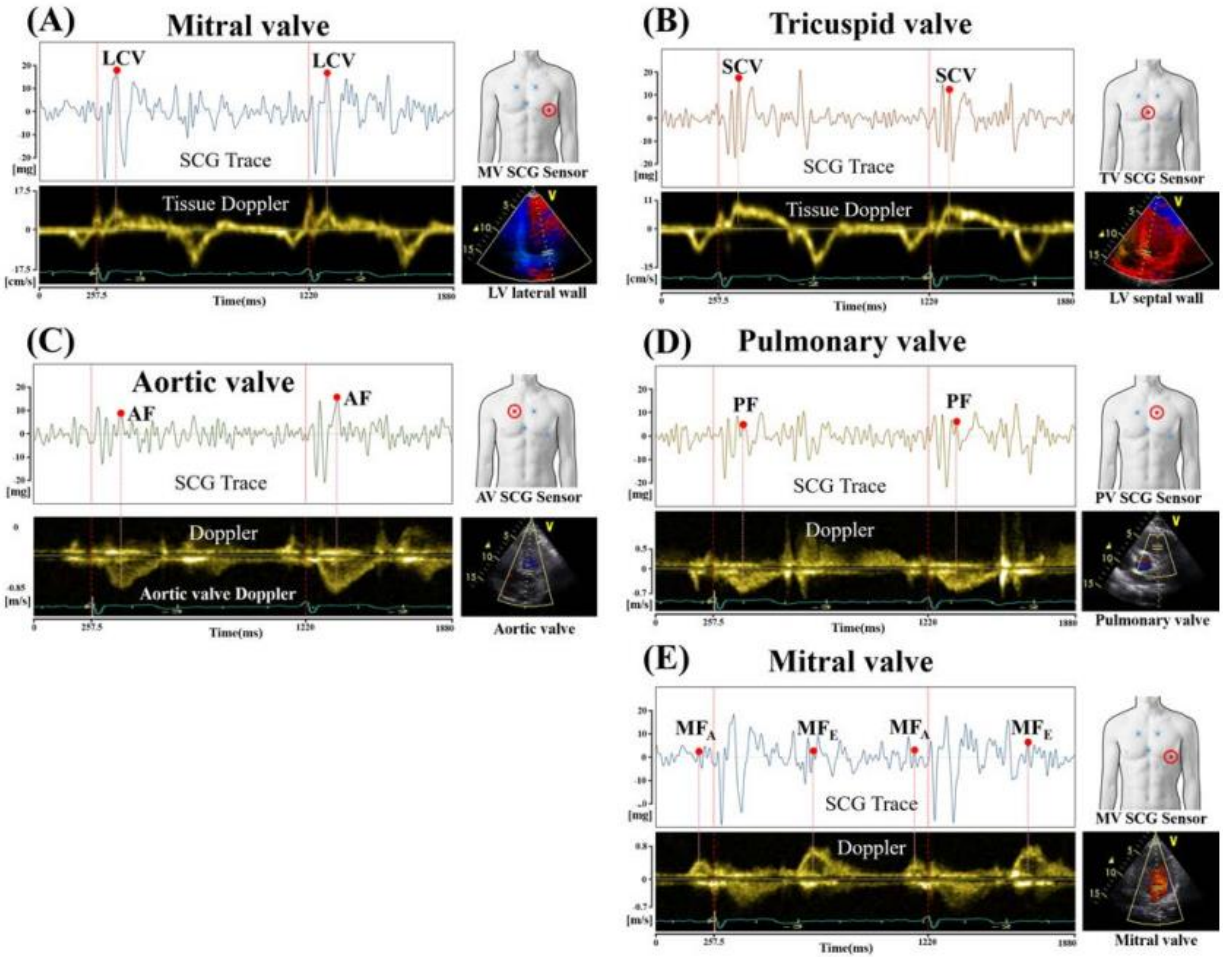

Figure 2.3 Six new identified events [63]

2.3 Noises in SCG

Accelerometer is a device measuring acceleration of a motion. When using as a sensor to measure the heart vibration on a subject (i.e., SCG), it also picks up other movements related to the subject such as respiratory, voice, and body movement (gentle motion, walking, running, etc.). Figure 2.4, 2.5, 2.6 and 2.7 show different SCG waveforms with various types of motion noise. The extracted respirations in Figure 2.4 are low-pass filtered signals with a cut-off frequency of 0.7 Hz. The extracted voices in Figure 2.5 are band-pass filtered signals with cut-off frequencies of 80-500 Hz. The extracted motions in Figure 2.6 and 2.7 are low-pass filtered signals with a cut-off frequency of 20 Hz. The above cut-off frequencies will be discussed in details in Section 3.4.1, SCG bandwidth analysis.

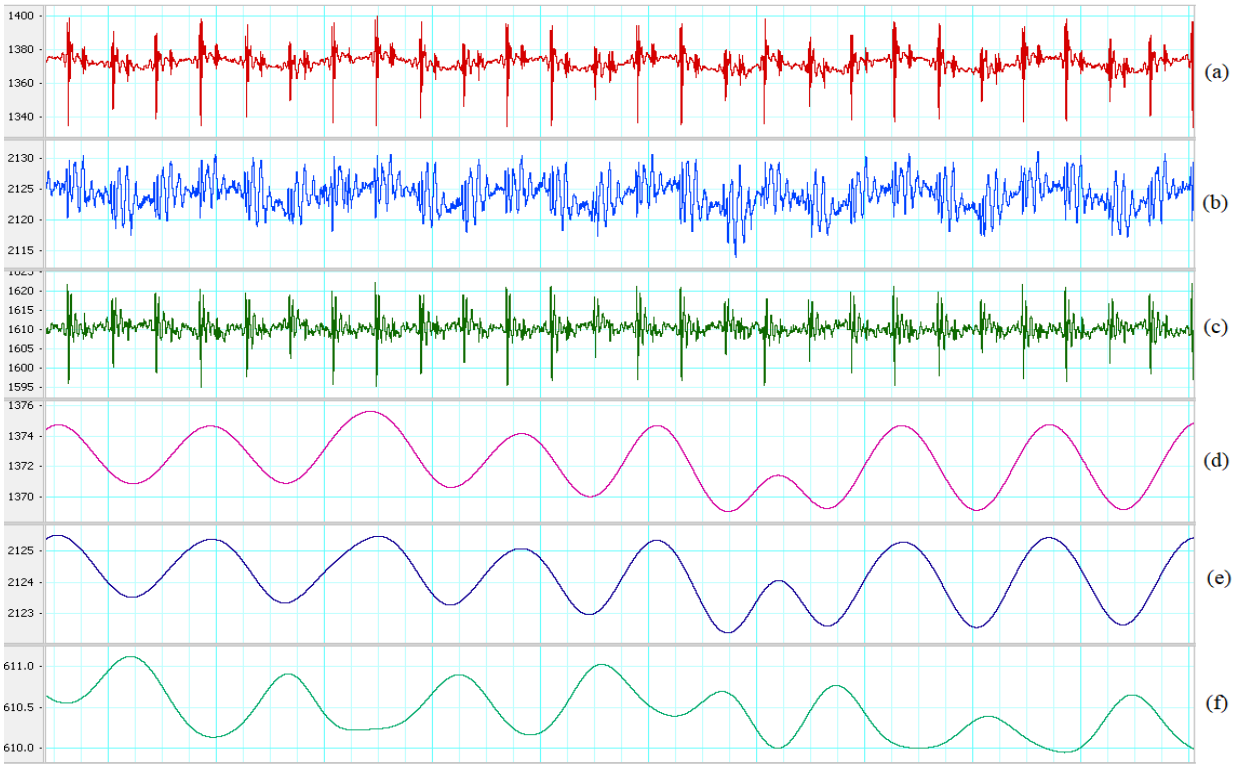

Figure 2.4 Respiration with SCG on all three axes of an accelerometer. (a) z-axis. (b) y-axis. (c) x-axis. (d) Extracted respiration on z-axis. (e) Extracted respiration on y-axis. (f) Extracted respiration on x-axis.

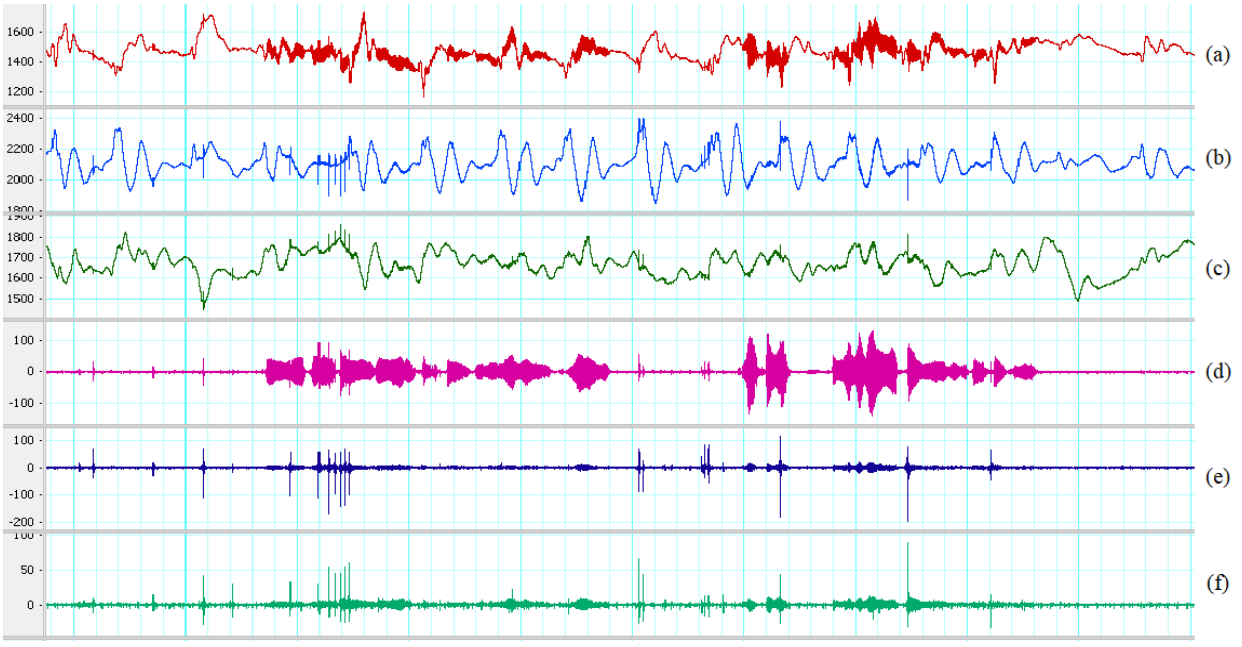

Figure 2.5 Subject's voice with SCG on all three axes of an accelerometer. (a) z-axis. (b) y-axis. (c) x-axis. (d) Extracted voice on z-axis. (e) Extracted voice on y-axis. (f) Extracted voice on x-axis.

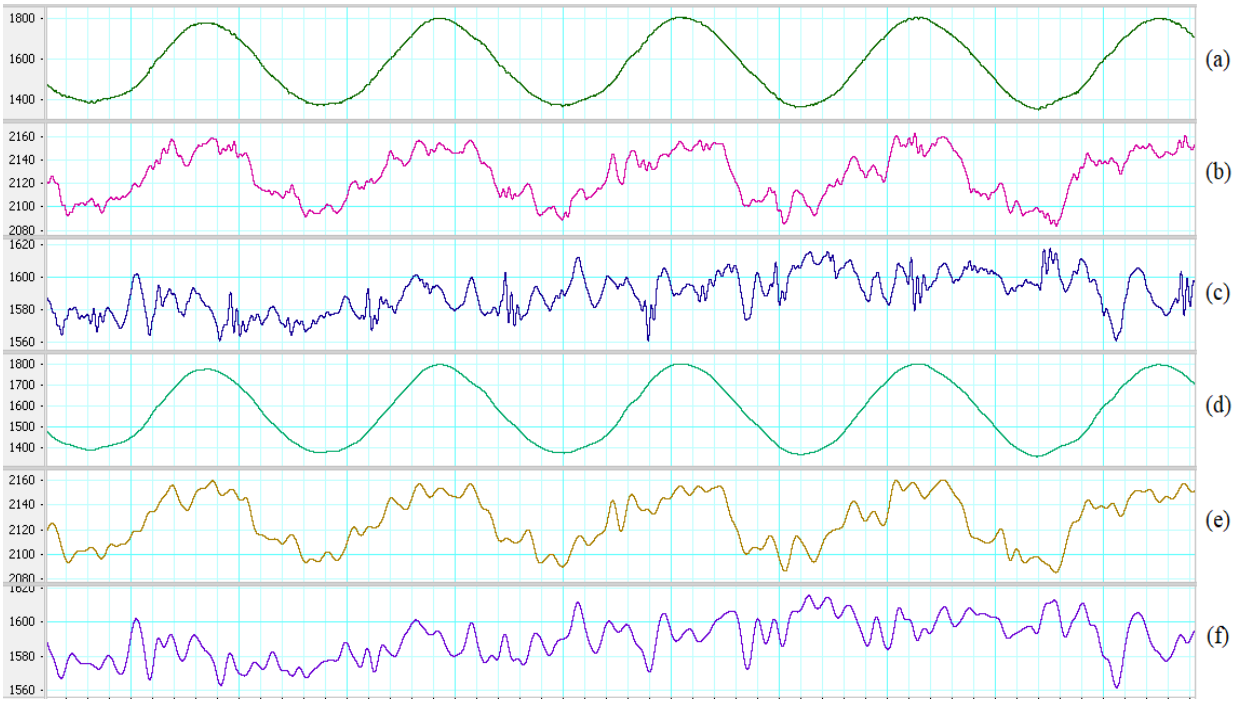

Figure 2.6 Gentle motion with SCG on all three axes of an accelerometer. (a) z-axis. (b) y-axis. (c) x-axis. (d) Extracted motion on z-axis. (e) Extracted motion on y-axis. (f) Extracted motion on x-axis.

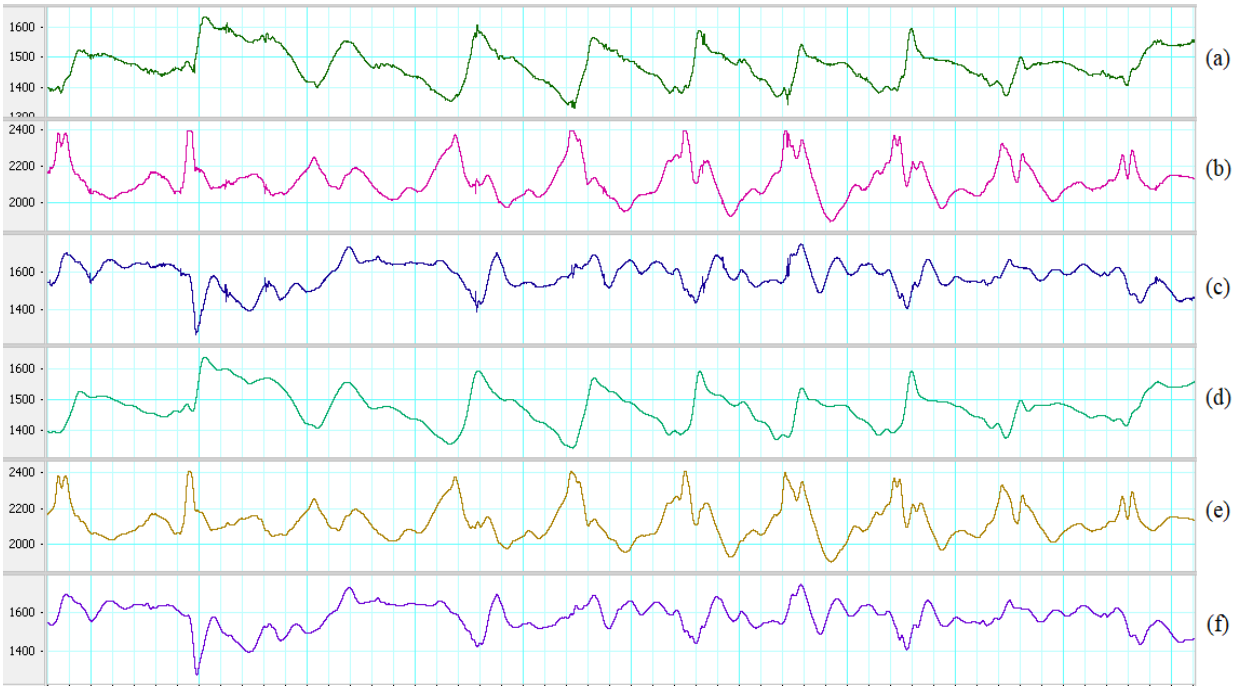

Figure 2.7 Walking motion with SCG on all three axes of an accelerometer. (a) z-axis. (b) y-axis. (c) x-axis. (d) Extracted motion on z-axis. (e) Extracted motion on y-axis. (f) Extracted motion on x-axis.

To acquire quality SCG signals, the measurement procedure should minimize the other motion sources. For example, the subject should lay down and stay still during acquisition time. However, doing that is only suitable for clinic and laboratory and is not practical in measuring SCG on active people. Therefore, it is needed to develop methods which can minimize the effect of body motions on the SCG while the person is in action. To do so, two accelerometers will be used instead of only one accelerometer to reduce the body motion noises in the SCG signals.

CHAPTER 3
METHODOLOGY

In this chapter, all techniques were used to conduct the research are reported in details. The chapter is divided into seven parts. First part presents all hardware and software designs of the wireless data acquisition system. The following part provides specifications of the sensors and the reasons to choose them for the sensing system. The third part describes the placement in various positions of a pair sensors on the chest to exam the effect of motion noise on the SCG signal. Then, all methods were used to remove the motion artifact on the SCG signal are explained in the fourth part. In the fifth part, to improve the accuracy and performance of cardiac event detection methods, two algorithms are to be applied to firstly locate the systolic and diastolic zones on denoised SCG signal. Then, in the sixth part, systolic and diastolic points will be identified insides the searching intervals around detected systolic and diastolic zones. The real-time mode of event detection is also exposed in the last part.

3.1 Wireless Data Acquisition System

This wireless DAQ was designed with two main purposes. One is erasing the wire connection between the subject and the computer to allow easily investigate on motion artifact in different scenarios. Another intent is saving all data in a user-defined format and testing the algorithms of noise removal and event detection of the collected data in real-time mode using Matlab software. This section consists of three subsections which are overviewed about the system design, the hardware, and the software.

3.1.1 System design

The DAQ system consists of a rechargeable power supply, an 8-channel analog to digital converter, an ARM microcontroller, and a Wi-Fi module packed in a single PCB. All components are commercially available. Figure 3.1 shows the block diagram of the designed system including sensing front-ends, wireless DAQ and the receiving devices.

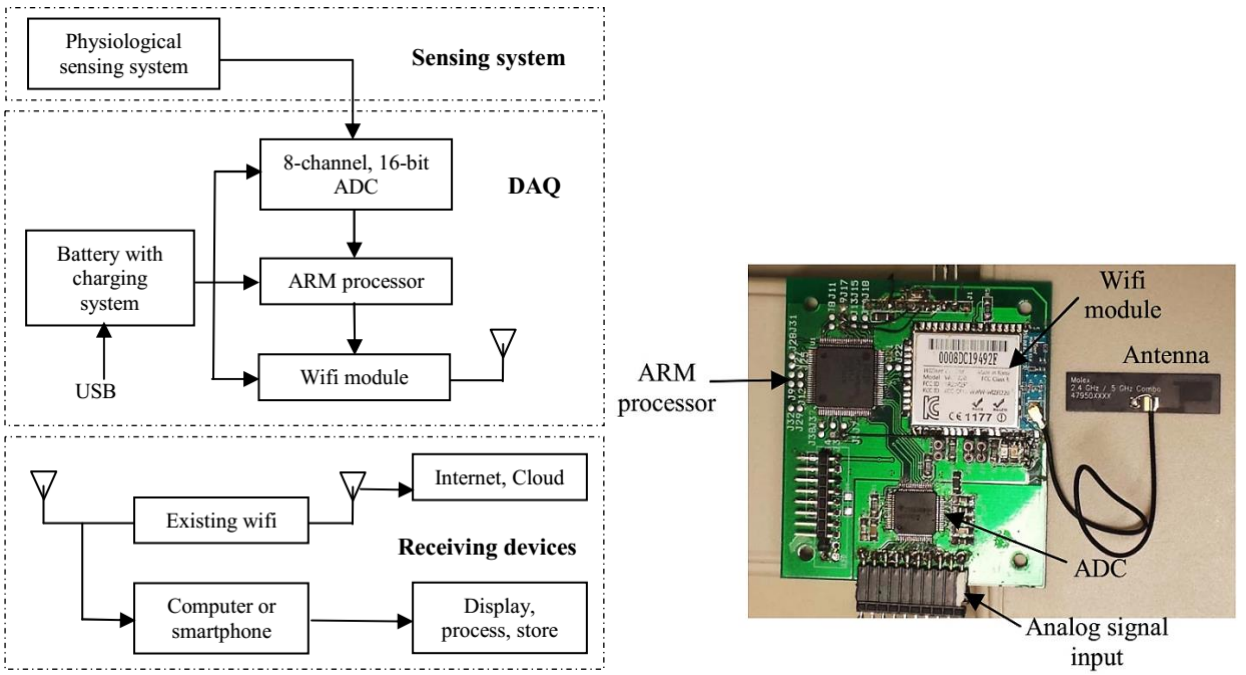

(a) (b)

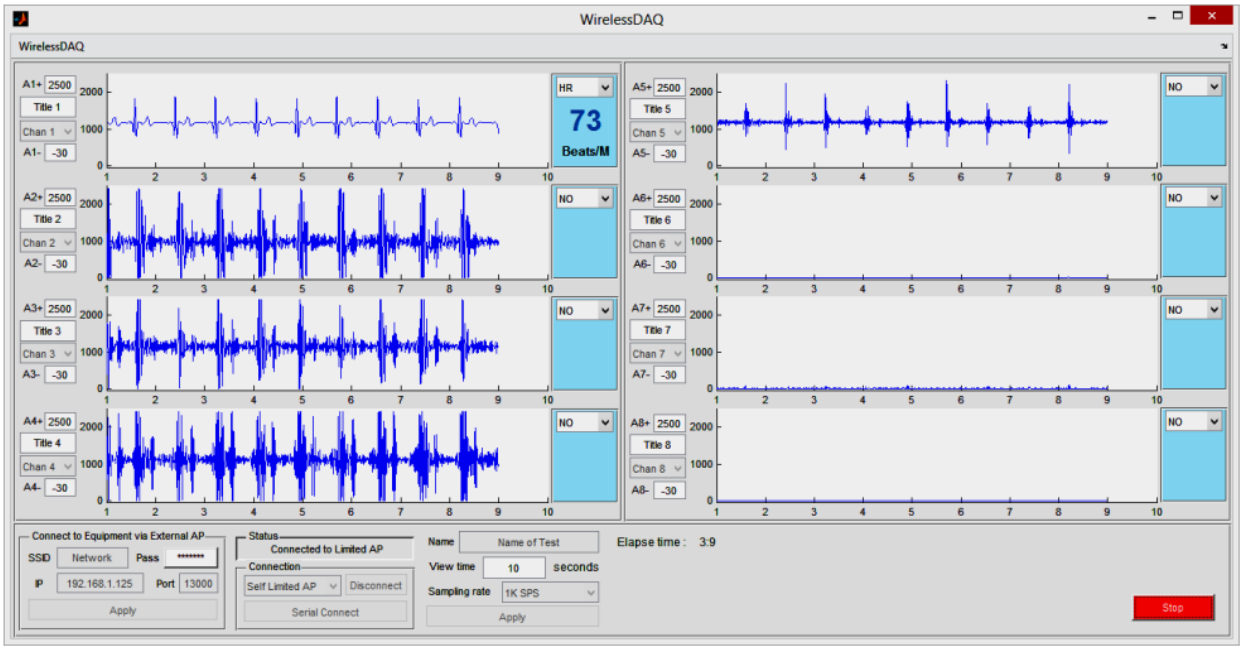

(c)

Figure 3.1 (a) System block diagram, (b) Photograph of the wireless DAQ (power supply and rechargeable battery are not shown) and (c) Screen capture of the DAQ user interface on the computer.

The microcontroller is the LPC1768FBD100 ARM processor made by NXP Semiconductors [64]. This is a Cortex-M3 based microcontroller featuring a high level of integration and low power consumption. The microcontroller contains 512 Kilo-Byte (KB) flash, 64 KB data memory, runs with a maximum speed of 100 MHz and packed in a 100-pin Plastic-Quad-Flat-Pack (LQFP) package. Although the microcontroller has internal analog-to-digital converter (ADC), an external ADC - ADS131E08 made by Texas Instrument (TI) was used instead [65]. The reason is that the internal ADC has low resolution with 12-bit (1.5 bytes per sample) which has less efficient in real-time data communication comparing with higher resolution 16/24-bit (2 or 3 bytes per sample) [66]. In addition, this study requires a precise correlative timing among channels, and the cycle sampling of the internal ADC can cause timing delay among channels while the TI ADC converts signals simultaneously for eight channels. This ADC is a 16/24-bit with a maximum sampling rate of 64 Kilo-Sample-Per-Second (KSPS) and packaged in the 64-pin Thin-Quad-Flat-Package (TQFP) package. However, due to the real throughput of Wi-Fi module which is around 40 Kilo-Byte-Per-Second (KB/s), the external ADC - ADS131E08 was set to sample data at a resolution of 16-bit and at a rate of 1 KHz only. It connected to LPC1768 via SPI peripheral and ran at a speed of 12 MHz to minimize the latency. The eight inputs were configured in the single-ended mode and had a dynamic range 0-2.5 V.

The wireless communication is an 802.11B Wi-Fi module with power amplifier, the WizFi220 made by Wiznet [67]. This module is the Wi-Fi 802.11b/g/n using around 130 mA on a 3.3 V supply, running at a maximum speed of 11 Mega-Bit-Per-Second (Mbps) on the 2.4 GHz, and emits a 17 dBm maximum power output. The Wi-Fi module is connected to an external Wi-Fi antenna; this system uses the WUIZ610WI antenna also made by Wiznet. The antenna has a bandwidth of 84 MHz between 2400-2480 MHz of the Wi-Fi spectrum. This is a small size antenna with a gain of 2.5 dBi and an input impedance of 50 Ω. This Wi-Fi module connects to microcontroller LPC1768 via asynchronous UART peripheral with a speed of 1 Mbps to significantly reduce the data transfer time.

As shown in Figure 3.1, the DAQ receives 8 physiological signals from a sensing system, converts the signals and sends the data over the Wi-Fi connection. A computer or a smartphone wirelessly connects to the DAQ. The receiving device with appropriate software processes the data to display, monitor, store, and make decision on physiological information. The device also

can communicate with the DAQ if needed. This Wi-Fi system can also be connected to an existing Wi-Fi in a home or an office setting. This type of connection provides a longer transmission range between the DAQ and the receiving devices. This also opens the way to send the data to the cloud or internet for telehealth applications. Figure 3.1 also shows the photograph of the DAQ board which has a dimension of 7x7 cm and a screen capture of the DAQ software on PC written by Matlab GUI. The DAQ board will fit in an enclosure with the battery and the charging system connected to the 5 V supplied off a USB cable.

3.1.2 ARM microcontroller and Wi-Fi

The DAQ support two types of connections: direct and indirect mode. In direct mode, the DAQ acts as an access point (AP) and a receiving device can connect directly to form a communication link. The direct mode only supports the WEP (Wired Equivalent Privacy) security and up to 6 connected clients due to the limitation of the Wi-Fi module hardware resource. The direct mode creates an AP named WirelessDAQ_XXXX where XXXX is the last four digits of Wi-Fi module MAC. To connect to that self-AP, the users need to enter password **0123456789**. In indirect mode, the receiving device and the DAQ can communicate via another access point. In this mode, the DAQ supports up to the highest standard of security - WPA2 (Wi-Fi Protected Access II). The indirect mode has potential to connect to the internet when the external AP linked to internet.

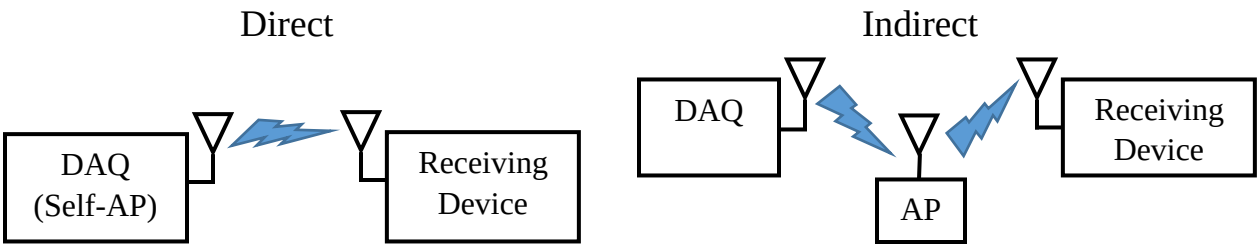

Figure 3.2 Two connection modes with AP is Access Point

As soon as the DAQ supplied with power, it initiates all variables and peripherals including Wi-Fi, serial, SPI and I/O ports. It then checks the Wi-Fi state. If this is a first start (no command is received), the hardware forms the self-AP by default. After the self-AP is created, the DAQ is looking for connection of a receiving device. If a device is connected to the self-AP, the DAQ

waits to accept commands. The *START* command will start the analog to digital process, get data from the ADC, pack them into length-optimized packages and send to the receiving device. The length of data payload of TCP/IP frame was optimized to 1460 bytes to avoid fragment when transferring data. The *HALT* command will disable the ADC and stop sending data. If the first command is the *NETWORK* command, the DAQ will receive a frame data of an external AP's network parameters to stop the self-AP and connect to the external AP with provided information. The flowchart for the microcontroller and the Wi-Fi module is shown in Figure 3.3 below.

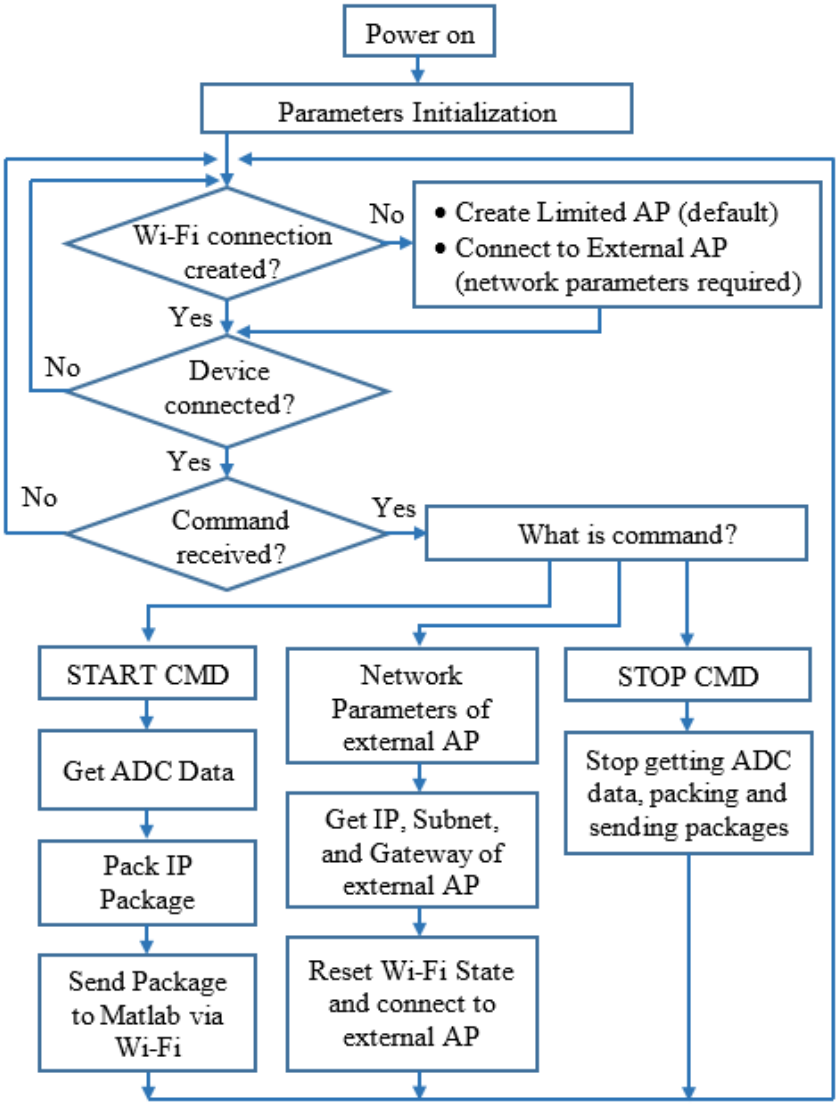

Figure 3.3 Flowchart of the DAQ processor and wireless module.

3.1.3 Computer software

The computer is installed with Matlab, and a framework was written by the MatLab Graphic User Interface (GUI). When the framework receives data from the wireless DAQ, it separates the data for each channel from the received packages. The data of each channel then pass through the corresponding processing streams to be processed by the user-defined algorithms. There are total eight processing streams for each channel, and they can process channel data while receiving packages from the DAQ. The results and processed data are displayed on the user interface. The user can also change the range of the displayed amplitude and the window view during acquisition. For the computers without Matlab installed, a stand-alone version of the code was created for either 32-bit or 62-bit machine. This version is very useful for small computers such as laptops or tablets to be used in the field to collect data. Figure 3.4 describes the internal routine of the framework on a PC.

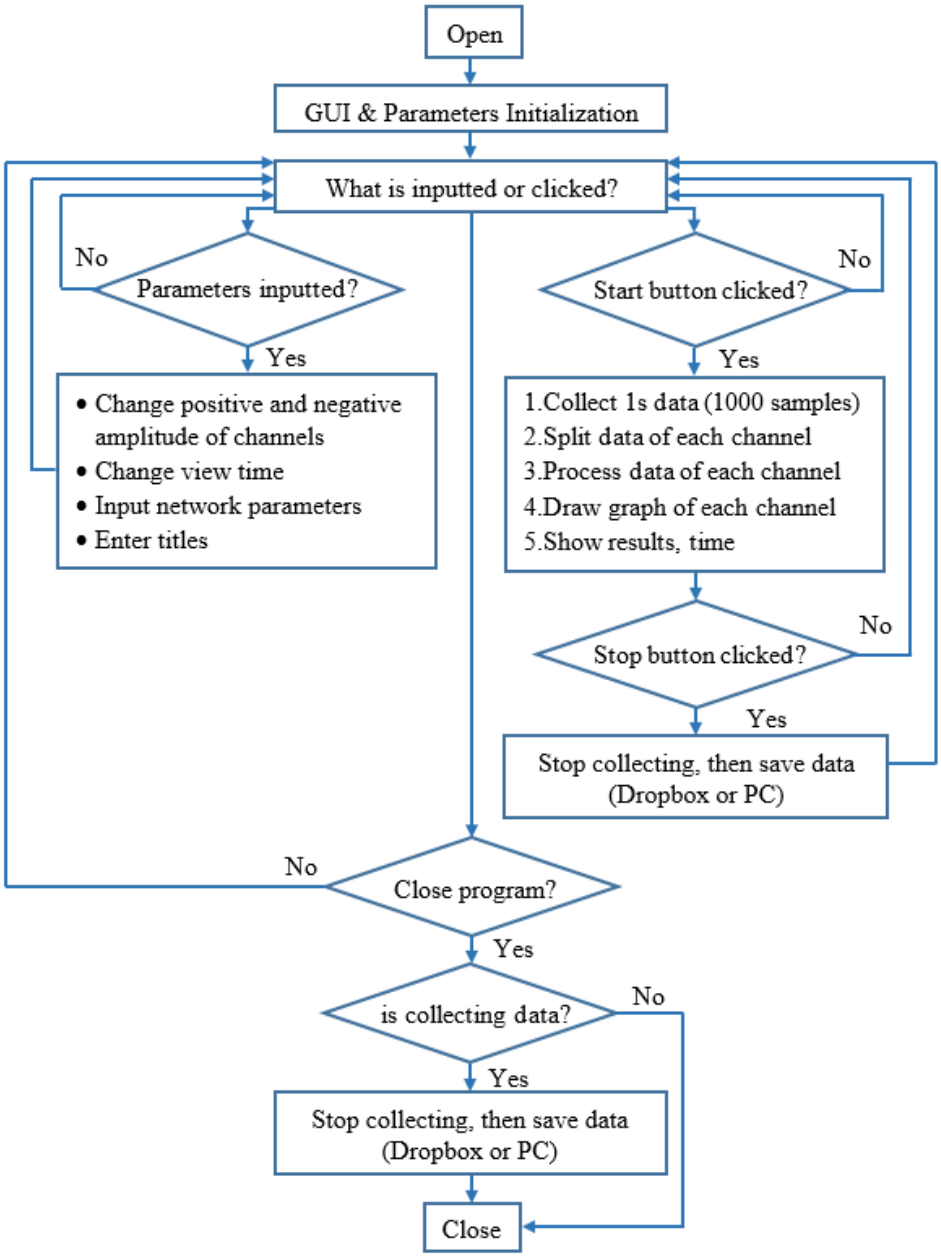

Figure 3.4 Flowchart of the Matlab GUI to receive, display, and store data on a computer.

3.2 Sensing System and Subjects

In the sensing system, different sensors were used to capture the ECG and SCG signals. They are a pair of high sensitive accelerometers and non-contact ECG electrodes. The usage of instrumentation amplifier and op-amp were also for noise removal, amplification and filtration. In addition, a digital potentiometer was utilized in automatic gain control of noise removal

technique. The following sections are brief description and specification of the sensors and components using in this study. The subjects to acquire the data and test the algorithms for this study are also detailed in the last section. Figure 3.5 describes diagram of the sensing system and its picture.

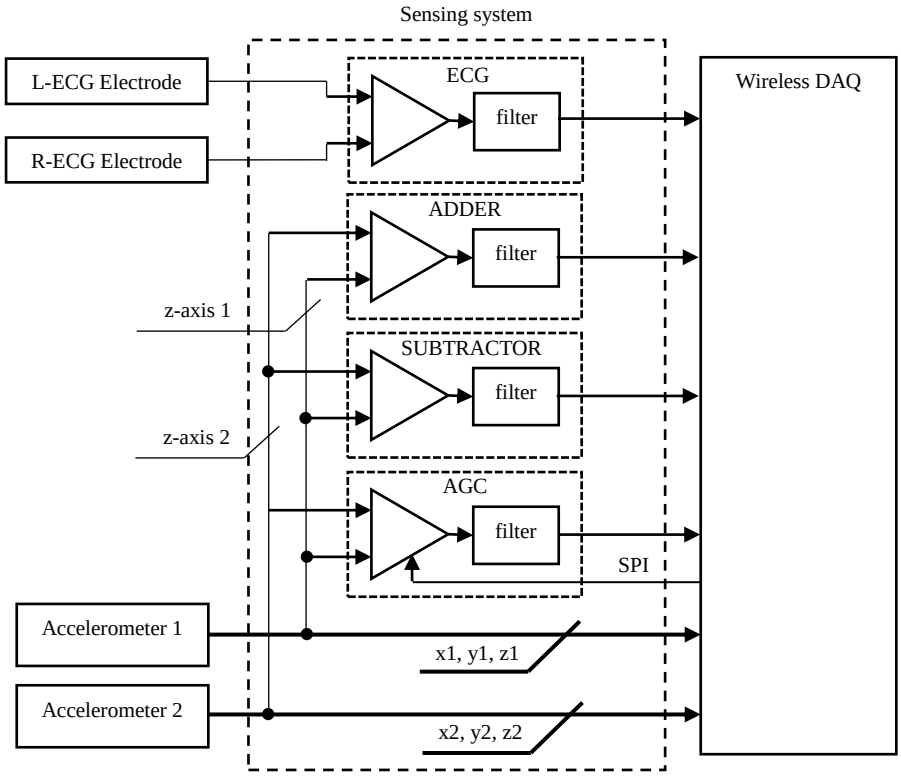

(a)

(b)

Figure 3.5 Diagram (a) and photograph (b) of the sensing system.

3.2.1 Accelerometers

The accelerometers used in this study are KXR94 of Kionix [68]. This accelerometer has a linear response with high SNR. It can operate in a large range of temperature change because of its integrated temperature compensation. The sensitivity and the operative bandwidth are programmable which can be adapted to the need of various applications. In this research, the selected accelerometers have the full-scale output range of ±2 g, the sensitivity 660 mV/g, operative bandwidth 0-50 Hz and the power supply 3.3 V. The reason of limiting the accelerometer bandwidth to 50 Hz is based on the SCG bandwidth is analyzed in Section 3.4.1. Figure 3.6 shows block diagram of the accelerometer.

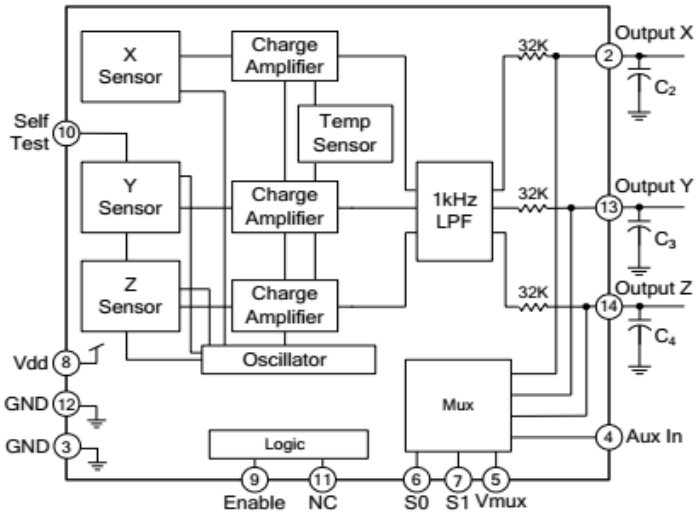

Figure 3.6 The diagram of Kionix KXR94. The capacitors C2, C3 and C4 are selected to limit the analog output bandwidth to 50 Hz [68]

3.2.2 Non-contact ECG sensors

Two non-contact EPIC PS25255 sensors were used to measure ECG in this study [69]. The sensor uses capacitance technology providing ultra-high impedance between the circuit and the patient which are much safer than wet electrode. The sensor also offers a good resolution as wet electrode. The selected sensor has input resistance typically 20 GΩ, input capacitance as low as 15 pF and the effective bandwidth from 200 mHz to 10 KHz. However, the sensors need bipolar power supply from ±2.4 V to ±5.5 V to operate. Figure 3.7 illustrates block diagram of the ECG sensors.

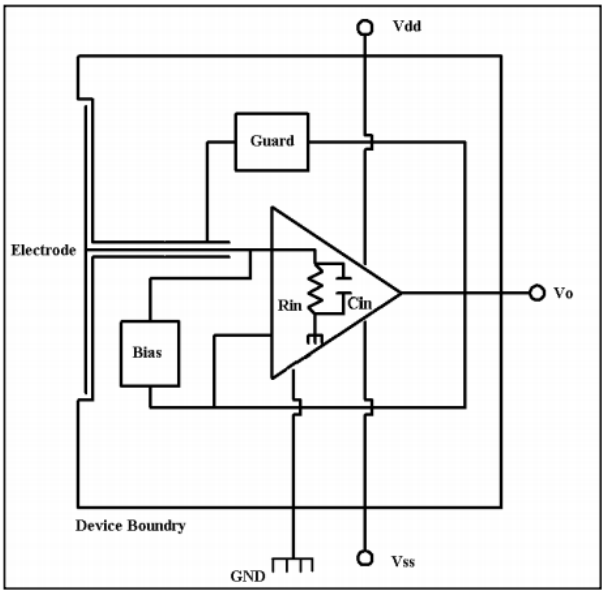

Figure 3.7 Internal circuit of EPIC ECG Sensor [69]

3.2.3 Instrumentation amplifier and op-amp

The instrument amplifier is AD623 made by Analog Device [70]. The AD623 can produce rail-to-rail output swing with possible operation on single-supply from 3 to 12 V. The gain of instrumentation amplifier can be set easily using a resistor. The maximum gain it can be programmed up to 1000. Besides, it offers high common-mode rejection ratio and wide input common-mode range which are considering factors when choosing.

The op-amp is MCP6L02 made by Microchip [71]. This op-amp was chosen due to high performance with the rail-to-rail output, high operative bandwidth 1 MHz, low quiescent power, single supply possibility and very low cost. It offers two op-amps in 8-pin package.

3.2.4 Digital potentiometer

The digital variable resister using in the auto gain control (AGC) method is MCP4351 provided by Microchip [72]. The selected one has 8-bit of control range equivalent to 256 steps of change, and it memory type is RAM for fast response. It value is selected largest 100 KΩ to fit the desire gain required in the AGC method. The potentiometer supports the SPI protocol up to 10 MHz. Figure 3.8 depicts the block diagram of digital potentiometer.

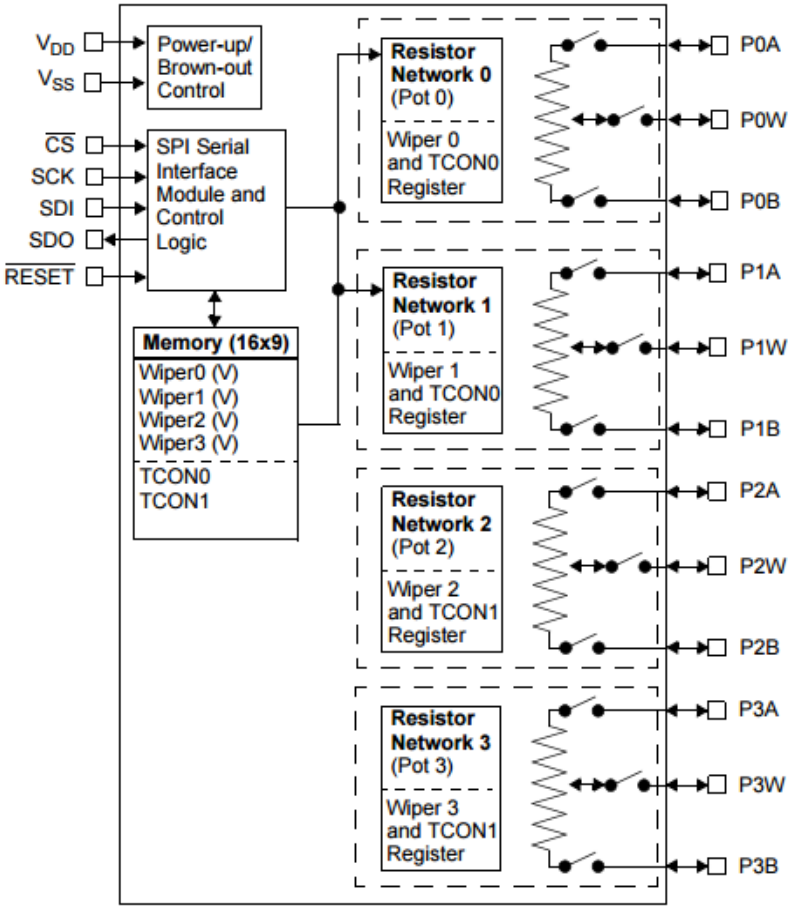

Figure 3.8 Block Diagram of MCP4351 [72]

3.2.5 Subjects in experiments

SCG and ECG were recorded simultaneously on eight volunteers who have no record relating to heart disease with age 32.1 ± 4.5 years, weight 78.2 ± 12.7 kg and height 171.1 ± 7.5 cm. Each subject performed one minute for stationary, one minute for sitting on a chair and moving back and forth gently, one minute for walking on a treadmill with a speed around 5 km/h and one minute for running on treadmill with speed approximately 8 km/h. To collect ECG signal, two non-contact sensors - PS25255 were attached horizontally on the subjects' chest to capture the modified lead-I ECG. The signals from two ECG sensors were then amplified and filtered (5-50 Hz) using instrumentation amplifier and op-amp. Two tri-axial accelerometers were stacked above the two ECG sensors. The accelerometer on the ECG positive electrode

obtained strong SCG signal with motion noise (ACC_SCG) while the accelerometer on the ECG negative electrode collected motion noise and a very weak SCG signal (ACC_MOV).

3.3 Placement of the Two Sensors

The purpose in this study is to measure the SCG signal on active people using accelerometer, so it needs to deal with the body movement noise. Therefore, the idea of using two sensors (accelerometers) placed in different positions on the chest came up. It is supposed that one sensor is placed near to the heart to capture strong SCG signal with body movement, and another one is placed far from the heart to capture body movement with minimized effect of the heart vibration. By observation, the noticed strongest SCG signal was below the chest which is indicated by ✚ in Figure 3.9, but it was decided not to put the sensors there because the signals were highly affected by not only body movement but also respiration. To minimize the effect of respiration, the sensors were placed on the chest bones.

The positions of sensors are 3 types: the same *horizontal* level on chest wall, the same *vertical* line on middle of chest wall and on *diagonal* line goes through the heart on chest wall as depicted in Figure 3.9. The activities will also be divided into two categories: walking and moving body (back and forth) softly while sitting on a rocking chair.

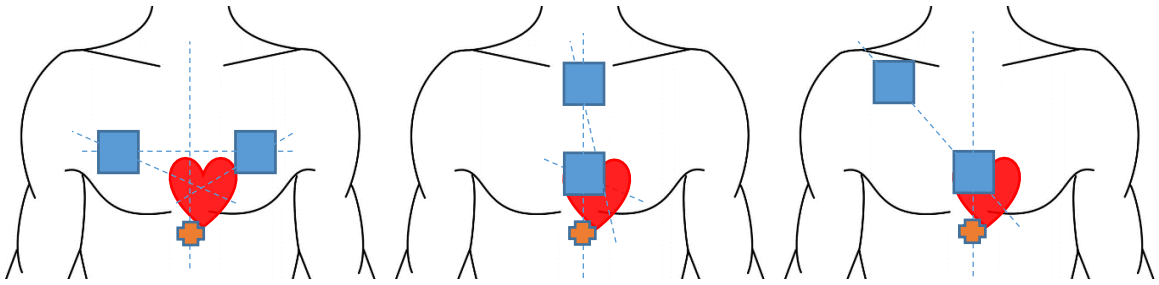

(a) (b) (c)

Figure 3.9 Sensor placement. (a) on the same *horizontal* level. (b) on the same *vertical* line. (c) on the *diagonal* line.

3.4 Motion Noise Removal Techniques

A variety of techniques was applied to eliminate the motion noise on SCG using two accelerometers with different placements. For comparison purpose, the simple motion noise removal technique using only one accelerometer with an analog band-pass filter is also conducted. All techniques using two accelerometers can be classified in three main categories of *only analog processing, only digital processing* and *fusion of both analog and digital processing.* All motion removal methods measured SCG signal along with ECG signal as reference for analysis purpose. However, before discussing the techniques, SCG bandwidth analysis is briefly discussed as frequency of the noise is the main drive in noise reduction methods.

3.4.1 SCG bandwidth analysis

Two sensors were positioned on the chest of the testing subject, one is placed near to the heart to capture SCG signal and motion, and the other one is placed far from the heart to capture motion and a much smaller SCG signal compared to the other sensor. The signal of the sensors placing near to the heart of five subjects were selected and analyzed using Fast Fourier Transform (FFT) to identify the high-energy range of the artificial noise including respiratory, body movement (running and walking) and voice. These noises are picked up by the accelerometers in addition to the clear SCG signal. The respiratory rate is in the range of 8-44 per minute corresponding to 0.13-0.73 Hz [73]. The signal picked up by an accelerometer has a range of 80-500 Hz [74]. Figure 3.10 shows that the motion energy concentrates in the range from 0 to 20 Hz. The frequency of SCG spreads from 0 to 50 Hz [75]; as a result, the effective frequency range was chosen from 20 to 50 Hz.

3.4.2 Motion noise removal using one accelerometer

Many studies used only z-axis of one accelerometer with a filter to measure the SCG signal, in this study, the same configuration on an active person was used to exam the effect of motion noise on the measured SCG signal. The accelerometer was attached on the sternum to obtaining the SCG signal. The results of this configuration were also used to compare the performance with other techniques using two accelerometers. Figure 3.11 depicts the overview of the simple method using one accelerometer and the band-pass filter.

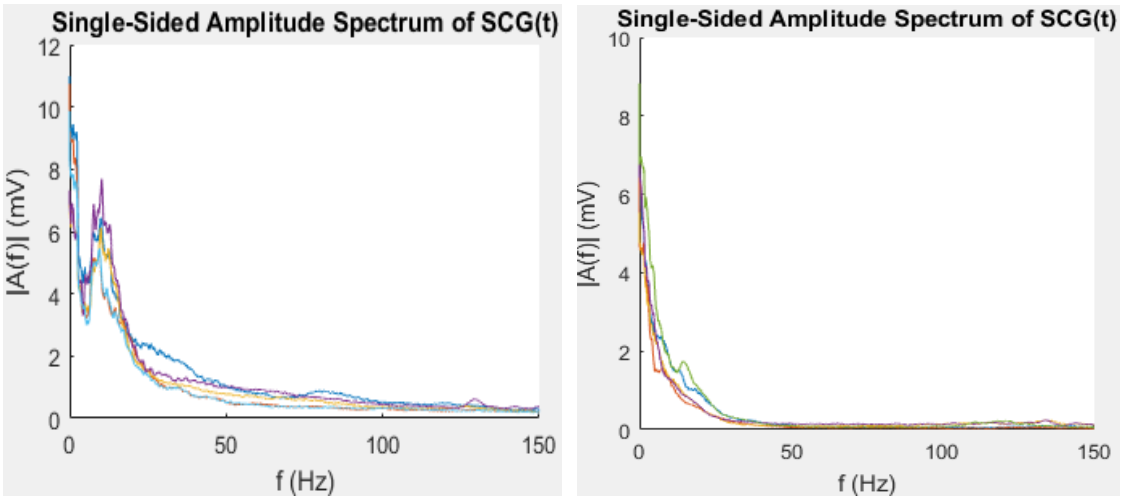

(a) (b)

Figure 3.10 Spectrum of five subjects with (a) running and (b) walking.

In order to achieve good SCG signal, the total amplifier gain of the band-pass filter was set to around 480. The analog band-pass filter was configured as a second-order with a cut-off frequency between 20 Hz and 50 Hz. The output signal has an offset of 1.25 V and in reversed waveform because the amplifier is configured as negative feedback, the signal is to be inverted in Matlab framework. The real schematic of this setting is shown in Figure 3.12.

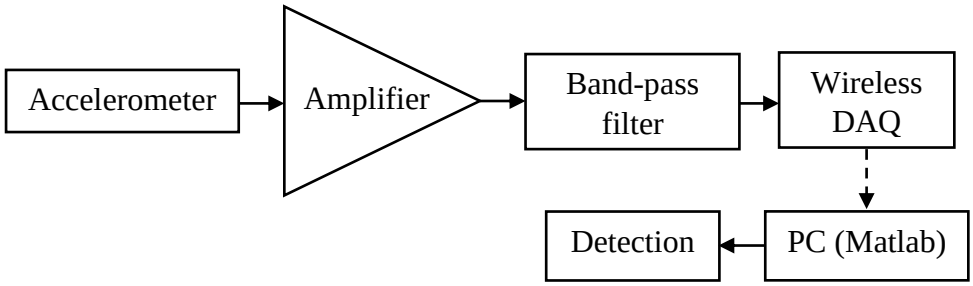

Figure 3.11 Block diagram of noise removal using one accelerometer.

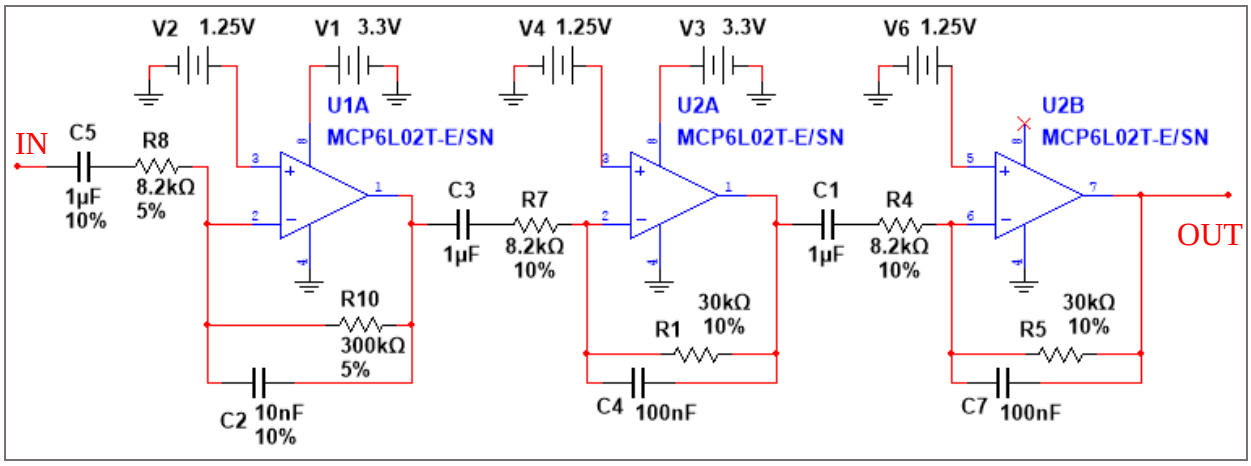

Figure 3.12 Schematic of the amplifier and band-pass filter for using only one accelerometer to reduce artifact noise.

3.4.3 Analog signal processing on two accelerometers

The *analog processing* includes an ADDER and a SUBTRACTOR set-up from an op-amp and an instrumentation amplifier. This configuration removes movement noise by combining two signals from a pair of accelerometers placed at different positions; then, the output signal goes through an analog second-order band-pass filter with a cut-off frequency between 20 Hz and 50 Hz. The filtered signal is then entered the DAQ to go through the detection algorithms. Due to the complexity of hardware configuration, only the z-axis of the two accelerometers are used for ADDER and SUBTRACTOR. The diagram in Figure 3.13 illustrates the *analog processing*.

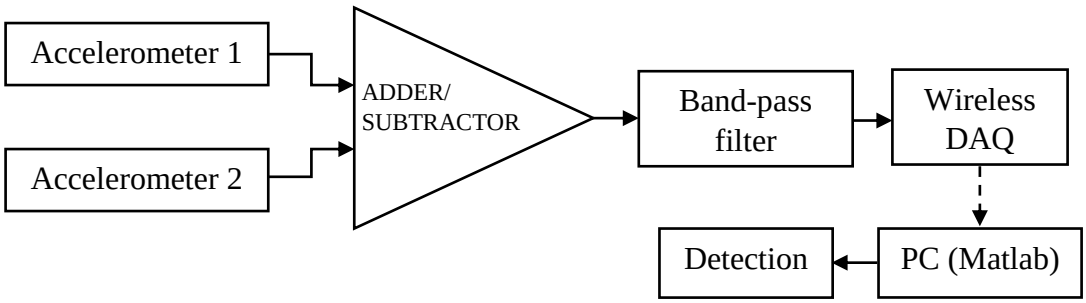

Figure 3.13 Block diagram of the analog processing steps.

To illustrate how two accelerometers can be used to reduce artifact noise, two circuits were simulated using MultiSim (Circuit Design Suite) of National Instruments. Two signal sources, one representing the SCG signal with movement noise and the other one representing only movement noise are added or subtracted to recover the SCG signal. Figure 3.14 and 3.15 are the schematic of the simulated circuits of ADDER and SUBTRACTOR respectively.

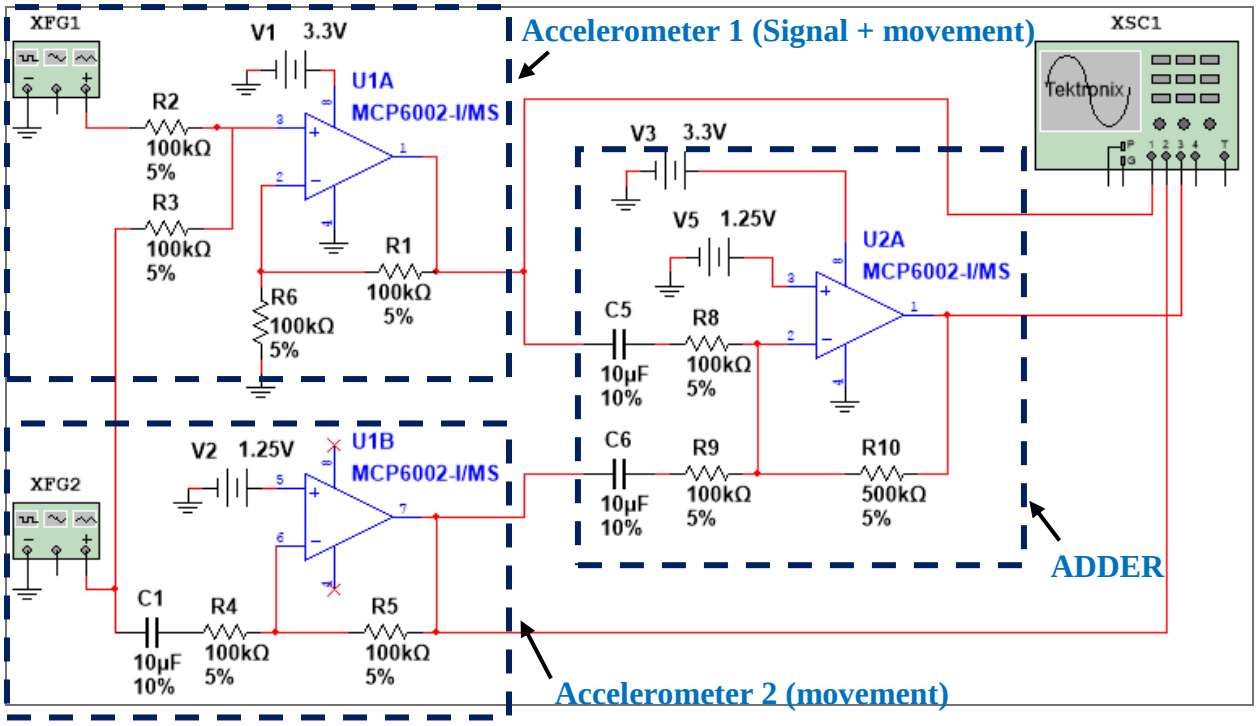

(a)

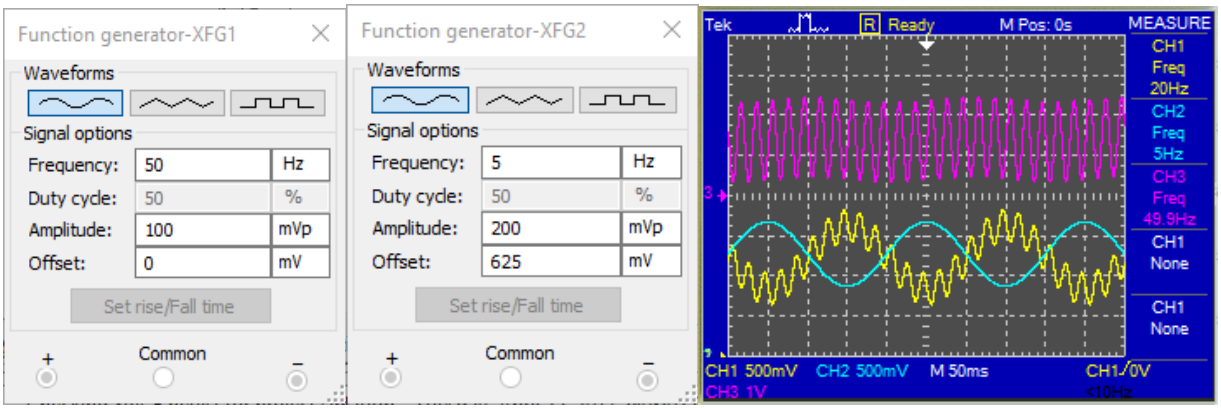

(b) (c) (d)

Figure 3.14 (a) Simulation of the ADDER. (b) Signal generator, (c) Movement generator and (d) Yellow: Signal and movement, Blue: movement, Purple: ADDER output signal.

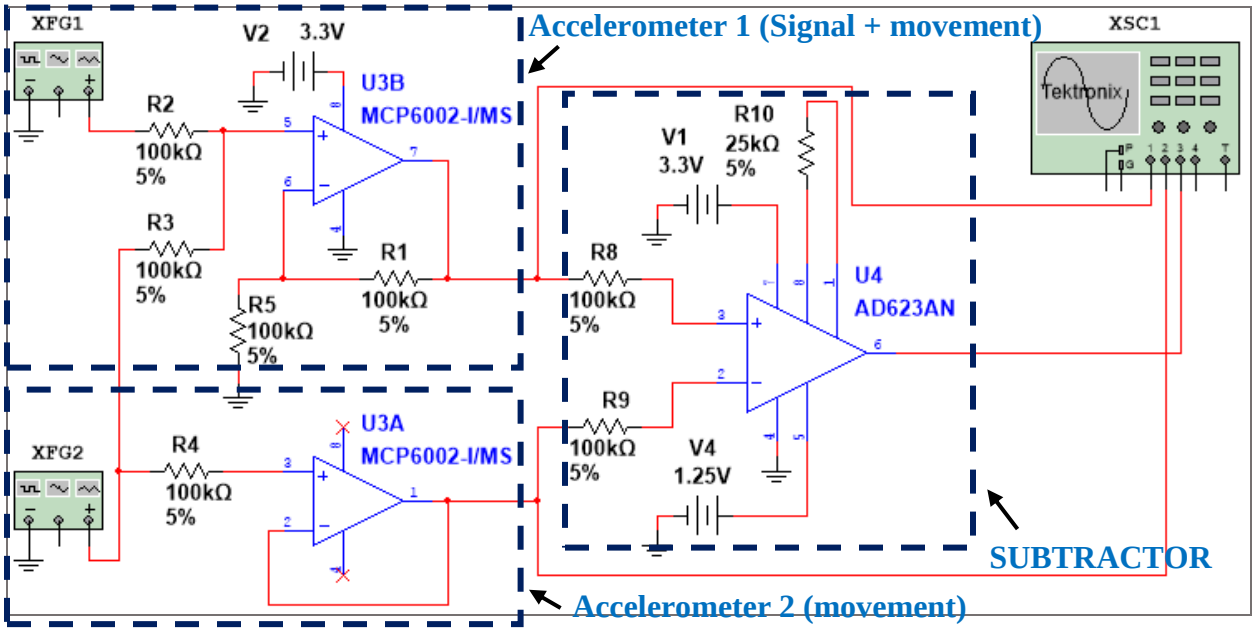

(a)

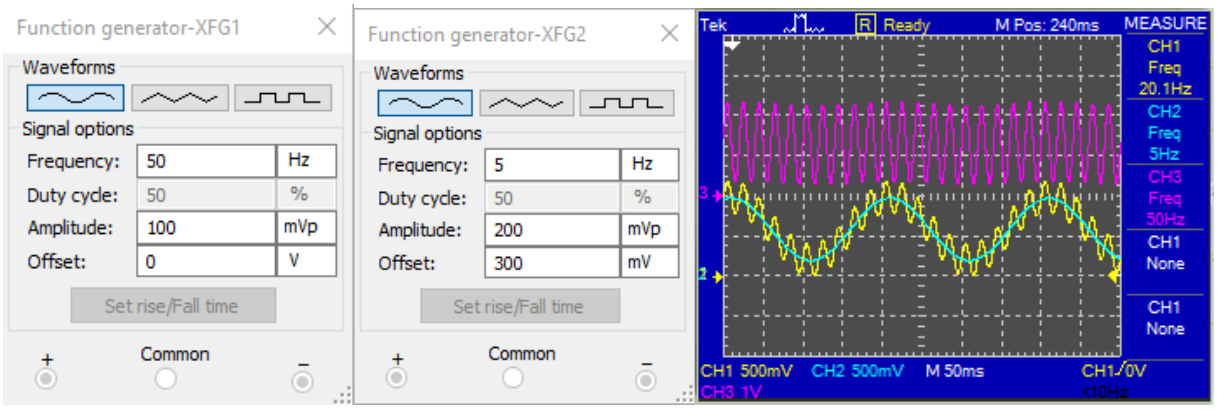

(b) (c) (d)

Figure 3.15 (a) Simulation of the SUBTRACTOR. (b) Signal generator, (c) Movement generator and (d) Yellow: Signal and movement, Blue: movement, Purple: SUBTRACTOR output signal.

A real ADDER and SUBTRACTOR with the same placement of sensors for each type (*horizontal*, *vertical* and *diagonal*) were also tested on a subject made gentle movement and walking. There are two important notices when placing the accelerometers on the chest. To eliminate the motion noise from both accelerometers by summing their z-axes, both sensors z-axis needed to be placed in *opposite directions*. For example, one sensor has z-axis faces outward from the chest, and another must be placed with the z-axis inward to the chest. With the SUBTRACTOR, since the common-mode rejection of the instrumentation amplifier is used to

remove the motion noise, the two z-axes of the accelerometers need to be placed in the *same direction*.

Figure 3.16 shows the schematic of the ADDER along with a band-pass filter. It uses the MCP6L02 op-amps to sum the signals and build the second-order band-pass filter having a cut-off frequency in the range of 20-50 Hz. The total gain from inputs of the ADDER to the output of the band-pass filter is around 480. The output signal has an offset of 1.25V and in reversed form because the ADDER is configured as negative feedback. However, it can be flipped easily in the Matlab framework.

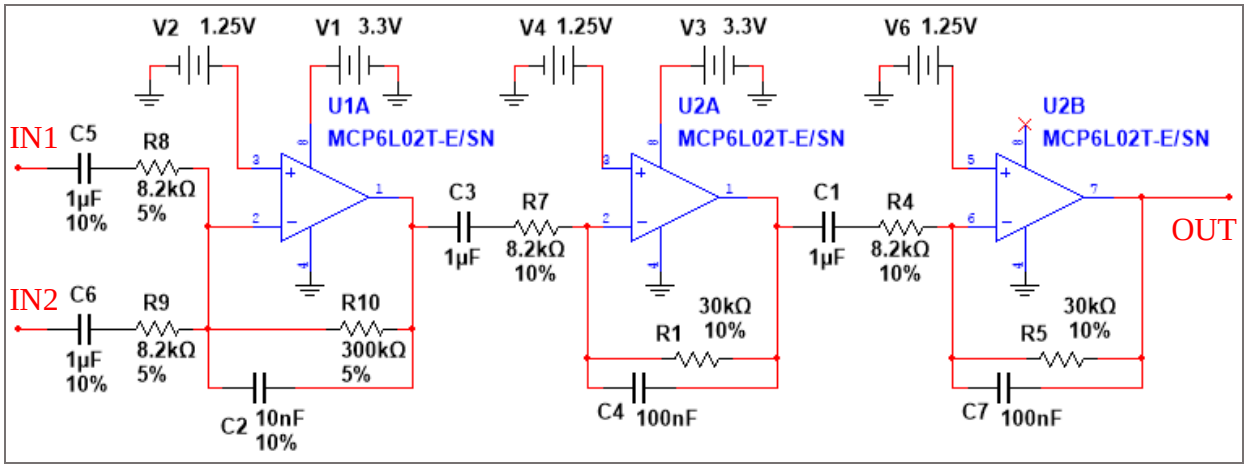

Figure 3.16 Schematic of ADDER and band-pass filter.

The SUBTRACTOR and band-pass schematic is shown in Figure 3.17. It uses the same op-amps for band-pass filter, but an instrumentation amplifier is used to build the SUBTRACTOR. The inputs of the SUBTRACTOR are coupled with a high-pass filter with a cut-off frequency of 20 Hz to bias the inputs and block the DC level from the sensors. The total gain is kept consistently with the ADDER which is around 480 for comparison. It also has the output offset at 1.25 V, but it is not in reversed form as the output of ADDER.

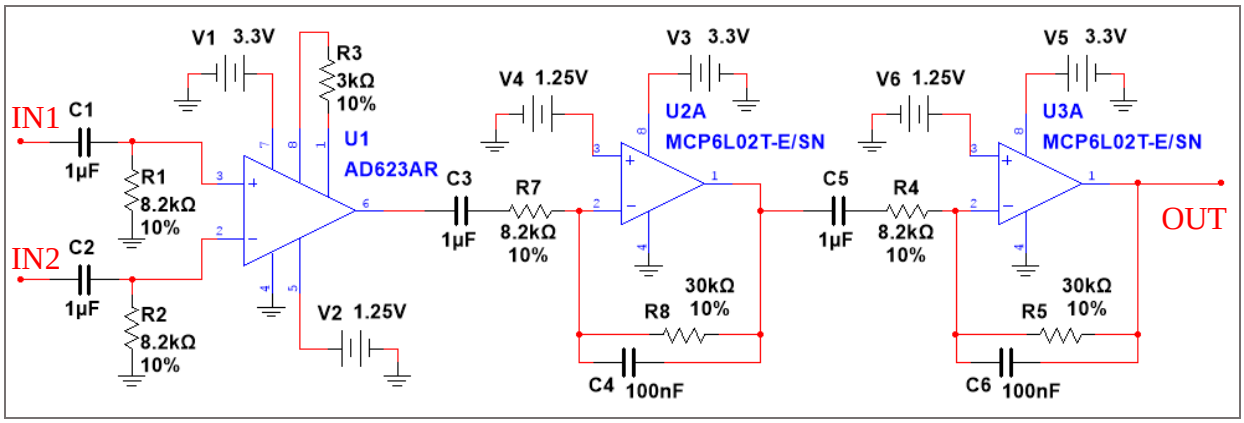

Figure 3.17 Schematic of real SUBTRACTOR and band-pass filter.

3.4.4 Digital signal processing on two accelerometers

The *digital processing* comprises two different combinations of data sets using two accelerometers on the Matlab framework. The signals from the two sensors placed in the same direction of all three axes go directly into the DAQ, and their data are processed in two different strategies. Figure 3.18 shows the diagram of the *digital processing*.

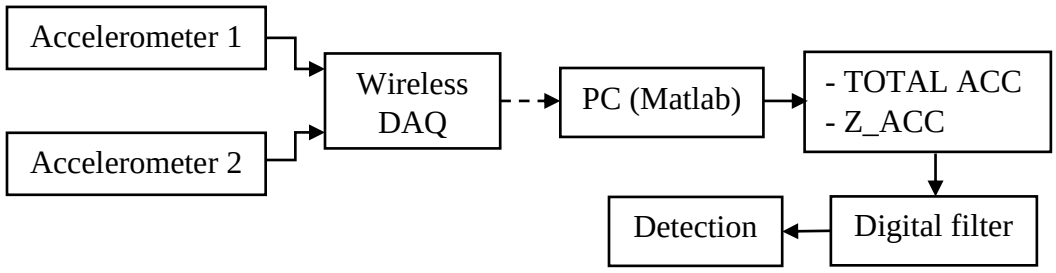

Figure 3.18 Block diagram of the digital processing steps.

The three axes of the tri-axial accelerometer provide acceleration in three different planes. A better SCG signal from the total acceleration (TOTAL_ACC) can be obtained instead of only z-axis as in other previous studies. Therefore, the first strategy removes the motion noise by calculating the TOTAL_ACC of the heart vibration from all data of three-axis of the two accelerometers. Then, the TOTAL_ACC is filtered with a digital zero-phase band-pass filter (20-

50 Hz) for further noise removal. The filtered TOTAL_ACC is used for the detection step. The TOTAL_ACC is calculated using the following equation:

$$\text{TOTAL\_ACC} = \sqrt{(x_1 - x_2)^2 + (y_1 - y_2)^2 + (z_1 - z_2)^2} \quad (3.1)$$

where x_1, y_1, z_1 are the data of three-axis of the first accelerometer and x_2, y_2, z_2 are the data of three-axis of the second accelerometer.

The second strategy uses only the combination of z-axis of both accelerometers; then, the combined data (Z_ACC) is also filtered with a digital zero-phase band-pass filter (20-50 Hz) for further noise removal. The filtered Z_ACC is used for the detection step. The Z_ACC is computed by the equation:

$$\text{Z\_ACC} = \text{abs}\,(z_1 - z_2) \quad (3.2)$$

where abs is the absolute function and z_1, z_2 are the z-axis data of two accelerators. The absolute function is used to ensure the difference of two z-axis data always positive, so that it did not worry about the position interchange of two accelerometers.

The calculated acceleration was then passed through a FIR low-pass filter. The filter is designed by Matlab with the following configurations: 330 orders, 6 dB cut-off frequency at 6.7 Hz, 60 dB of stopband attenuation, and 1 dB of passband ripple. The calculated acceleration is applied zero-phase filtering to maintain timing.

3.4.5 Fusion signal processing on two accelerometers

To achieve high signal-to-noise ratio for the SCG signal using two accelerometers, a fixed and high gain ADDER and SUBTRACTOR are applied. There is no problem with the output SCG signal when the amplitude of motion is not too high such as gentle movement, but when the motion strength increases such as walking, saturation, which causes loss of information for further digital processing, may occur in the output signal. To overcome this drawback, auto gain control (AGC) for ADDER and SUBTRACTOR are used. The AGC combines both analog and digital processing, so it is called fusion processing. Figure 3.19 describes the block diagram of this method.

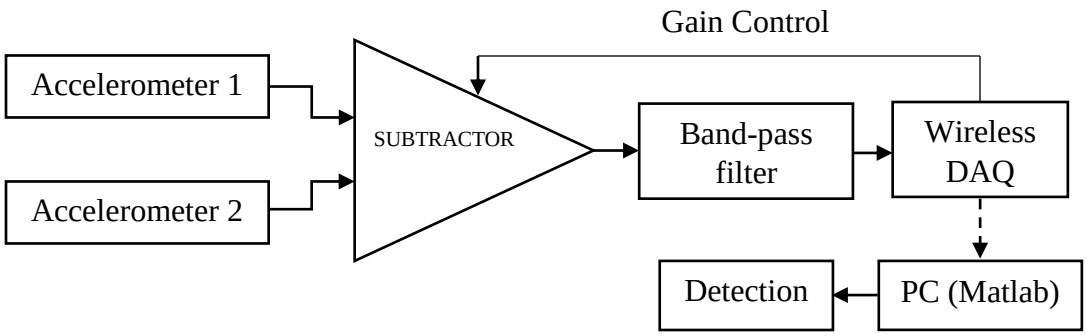

Figure 3.19 Block diagram of the fusion processing steps.

In this setting, the same ADDER and SUBTRACTOR configuration is employed, but the SUBTRACTOR gain-control resistor and the ADDER feedback resistor are replaced by the digital potentiometer – MCP4351 which was controlled by the microcontroller via SPI bus. However, because of the limited resistance of the digital potentiometer which is maximum only 100 KΩ, the ADDER cannot be configured to achieve the maximum desired gain. Hence, only the SUBTRACTOR will be examined in this section.

The wireless DAQ tracks the maximum level of output signal after band-pass filter every second. When any saturation is detected, the DAQ reduces the amplification gain by changing the resistance of the digital potentiometer until the output level stays below the maximum of the dynamic range. When the level of the output signal is lower than a specific threshold, the DAQ increases the gain to bring it above the threshold. There is a reason of tracking output every second. The systolic energy is usually larger than the diastolic energy in one cycle and the heart rate of normal people is typically 60 beat-per-minute (bpm) equivalent to one second per one cycle. Maintaining the tracking every second is to avoid the amplification changing up and down continuously due to the diastolic level is detected lower than the threshold.

The dynamic range of the ADC input is 2.5 V and the output signal swings around the offset level which is 1.25 V; thus, the threshold was set to 0.625 V and 1.825 V which is equivalent to 50 percent of maximum swing. The level of the output signal is kept in a safe range from 0 to 0.625 V and from 1.825 to 2.5 V. Again, due to the complexity of hardware configuration, only the z-axis of the two accelerometers is used for SUBTRACTOR in this

method. The system is then tested on three different positions of the sensors while the subject makes gentle movement and walking.

3.5 Systolic and Diastolic Phase Detection

The procedure of systolic and diastolic phase detection is explained in this section. There are two methods to identify the systoles and diastoles including moving average threshold and interpolation. However, both techniques share some common steps before entering to the detection stage. Those common steps are detailed in pre-processing section, then each detection method will be described. Figure 3.20 shows all the steps of systolic and diastolic phase detection.

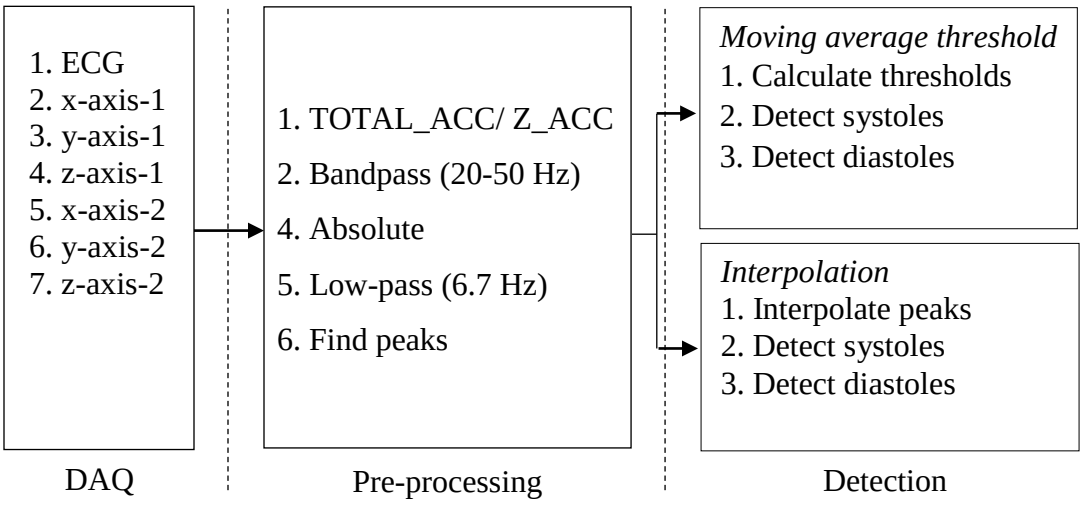

Figure 3.20 Algorithm overview

3.5.1 Pre-processing

There are total of 5 common steps to preprocessing data prior entering to detection in sequential order data combination, band-pass filter, absolute, low-pass filter design and find maxima.

Data combination - Because of the simple configuration and the performance of digital processing of the two accelerometers, only data sets of using two horizontal accelerometers and

digital processing were used for systolic and diastolic phase detection. Those data sets are applied Equation (3.1) and (3.2) to remove the motion noise before going to the next step. However, for comparison purpose, the TOTAL_ACC from data of only one accelerometer in those data sets were also calculated. The reason to do that is to see how different in performance of the detection with different data combinations including using TOTAL_ACC of one accelerometer, using TOTAL_ACC of two accelerometers and using only z-axes of the two accelerometers. All three ways of combining data will be rewritten as following:

1. TOTAL_ACC = $\sqrt{(x_1 - 1650)^2 + (y_1 - 1650)^2 + (z_1 - 1650)^2}$ (3.3)

where x_1, y_1, z_1 are the data of three-axis of one accelerometer which is placed close to the heart and has strong SCG signal with motion. Because the accelerometers are powered at 3.3V, the zero-acceleration point is at the center which is 1.65V for an equivalent of 1650 in ADC data.

2. TOTAL_ACC = $\sqrt{(x_1 - x_2)^2 + (y_1 - y_2)^2 + (z_1 - z_2)^2}$ (3.1)

where x_1, y_1, z_1 are the data of three-axis of the first accelerometer and x_2, y_2, z_2 are the data of three-axis of the second accelerometer.

3. Z_ACC = abs $(z_1 - z_2)$ (3.2)

where abs is the absolute function and z_1, z_2 are the z-axis data of the two accelerators.

Band-pass filter - A FIR bandpass is designed using Matlab with settings: 330 orders, 6 dB cut-off frequency at 20 and 50 Hz, 60 dB of stopband attenuation and 1 dB of passband ripple. The TOTAL_ACC of ACC_SCG is performed the above digital filtering in both forward and reverse directions to remove artificial noise without delaying the signal timing.

Absolute - The filtered TOTAL_ACC contains high frequency components and the spectrum is distributed mostly in the systolic and diastolic areas. To concentrate all energy of those zones in positive domain, the filtered TOTAL_ACC is taken absolute. Squaring function is not applied because it amplifies high frequency with higher gain than low frequency, so it gains up the systolic regions while suppresses the diastolic areas with lower frequency. That causes the reduction of the detection performance and increase the cost of the calculation comparing with the absolute function.

Low-pass filter design - To survive, a person must have systolic and diastolic (S:D) ratio of less than 1.2 or it would increase death or transplant [76]. Maximum heart beat of a human is 220 bpm and a minimum heart rate is 30 bpm. For lowest heart rate, the total of systolic duration and diastolic duration is 2000 ms and the S:D ratio must be maintained below 1.2; therefore, the systolic interval must be below 1091 ms. For highest heart rate, one heart beat cycle takes 273 ms, and the S:D ratio must be no more than 1.2; as a result, the systolic period must be under 149 ms. It means that the constraint of systolic interval increases from 149 ms to 1091 ms respectively from 6.7 to 0.9 Hz when the heart rate decreases from 220 to 30 bpm.

After absolute, the signal has high peaks (high energy) at systole and diastole regions. To locate and distinguish those areas, a low-pass filter with cut-off frequency corresponding to the systolic interval is used and the output signal is called the output SCG energy signal. However, that interval depends on the change of heart rate, the frequency 6.7 Hz is picked for cut-off frequency to cover all heart rate range. The FIR low-pass filter is designed by Matlab with configurations: 330 orders, 6 dB cut-off frequency at 6.7 Hz, 60 dB of stopband attenuation and 1 dB of passband ripple. The signal is also applied zero-phase filtering to maintain the timing.

Find maxima - A custom function is built to find maxima on the low-pass filtered signal by following conditions with T is the sampling period:

$$y(nT - T) < y(nT) > y(nT + T) \text{ for maximum at } y(nT) \tag{3.4}$$

The below figure shows the result waveforms of all the steps in the pre-processing stage.

3.5.2 First detection method - Moving average threshold

Calculate thresholds - A moving average window is used to calculate the average threshold array of the maxima. The average thresholds are then multiplied with a scaler to optimize the accuracy and effectiveness. Because each cycle has at least three maxima, the smallest window length must be three. The window length is also adjusted from 3 to 48 to inspect the detection performance. This will be discussed in the evaluation part.

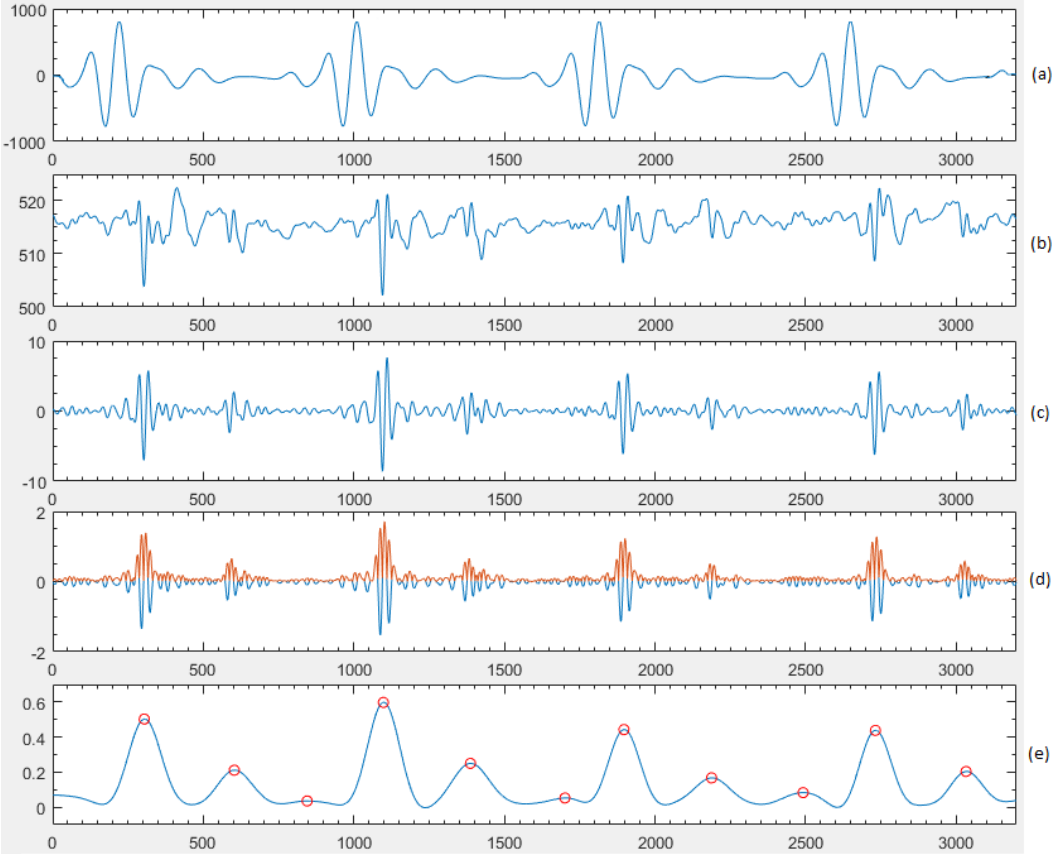

Figure 3.21 Pre-processing steps. (a) 5-15 Hz filtered ECG as reference. (b) Total acceleration of SCG. (c) Bandpass filtered SCG. (d) Absolute indicated as brown signal (e) Low-pass filtered signal (SCG energy signal) with maxima (red circles).

Detect systoles and check constraint - After having thresholds array, each maximum is compared to the threshold corresponding to maximal location. If the amplitude of the peak is higher than the threshold, it will be marked as a systolic candidate. Then, the systolic interval, discussed in subsection 3.5.1, is used to recheck the systolic candidate before marking it as a real systole. The systolic interval expands from 149 ms to 1091 ms when the heart beat drops from 220 to 30 bpm. The average heartbeat of all testing subjects in this study at standing is 75bmp, so an average duration – 436 ms is selected for the restriction of systolic interval on all data set. The time difference between a new systolic candidate and previous detected systole is calculated. If that duration is larger than 436 ms, the systolic candidate will be marked as a correct systole and added to an array contained location and amplitude of all detected systoles for accuracy statistic

at the end. If that duration is smaller than 436 ms, the systolic candidate will be marked as a faulty systole and be removed.

Detect diastoles - Based on the correct detected systoles, all maxima are searched within a forward range which equals to the systolic interval – 436 ms. It may have more than one maximum insides that screening range because some motion noise frequencies still reside in the less-noise bandwidth of the SCG and cannot be removed completely by the first bandpass filter. However, the diastolic regions still have higher energy than the noise peaks in that scope for all stationary data set, the largest peak is selected in the screening range as a diastolic candidate. If the amplitude of the candidate is smaller than the amplitude of the based systolic, it will be marked and stored as a correct diastole. If not, it will be removed and the next large peak in the screening range will be chosen as a new diastolic candidate. The checking process continues until the diastolic candidate qualified both conditions: be in the screening range and has the large amplitude but must be smaller than the based systole. Figure 3.22 illustrates the moving average window method with the length of 3 maxima and scaler of 1.1 which were optimal for both accuracy and performance and will be discussed in section 4.3 of Chapter 4. The purple line is moving average thresholds after scaled.

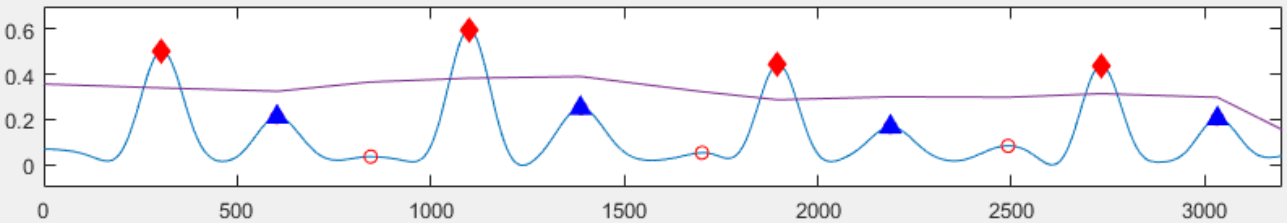

Figure 3.22 Moving average window with a length of 3 maxima and scaler 1.3, detected systoles (red diamonds), detected diastoles (blue triangles).

3.5.3 Second detection method - Interpolation

Interpolation and Find minima - When analyzing the SCG energy signal, a pattern of maxima as a sine wave was realized. Then, interpolation of maxima is taken to gain the sine wave pattern. The sample points of interpolation are the maxima of the SCG energy signal, and the coordinates of the query points are the coordinates of the SCG energy signal. The method to

interpolate is spline. All minimum peaks of interpolation waveform are detected using a custom function with condition:

$$y(nT - T) > y(nT) < y(nT + T) \text{ for minimum at } y(nT) \quad (3.5)$$

Detect systoles and diastoles – It was also found that between two minima of the sine wave pattern contains one systole which has the highest amplitude among maxima of the SCG energy signal. The diastole may lie inside that interval or may pass out of the interval, but it is the one also has high amplitude next to the systole. Therefore, all maxima of the SCG energy signal which reside in the range between two minima of interpolation waveform are searched. The peak has largest amplitude is marked as systole. The next high amplitude one is ticked as diastole. Figure 3.23 demonstrates the interpolation algorithm with the purple line is the interpolation waveform.

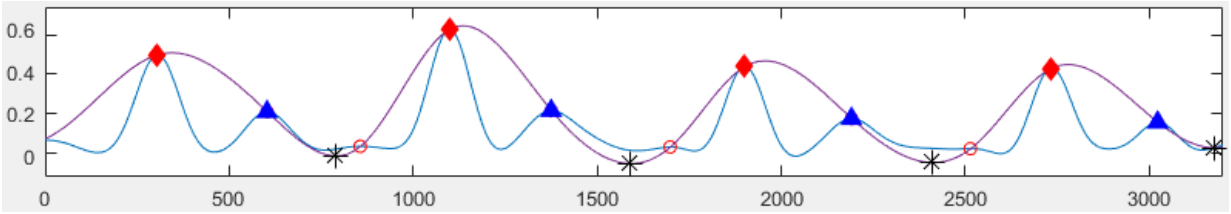

Figure 3.23 Interpolation method with detected systoles (red diamonds), detected diastoles (blue triangles) and minima of interpolation waveform (black stars).

3.6 Systolic and Diastolic Events Detection

There are two outstanding characteristics of SCG signal derived from a descriptive photo in a patent [77]. First, the rate of change of SCG signal from the nadir point IM to the peak AO is highest comparing to the slopes of other systolic points. Second, the steepness between MO and the peak after MO is largest comparing to the slopes between other diastolic points. Figure 3.24 shows the characteristics of SCG signal concurrent to the ECG signal.

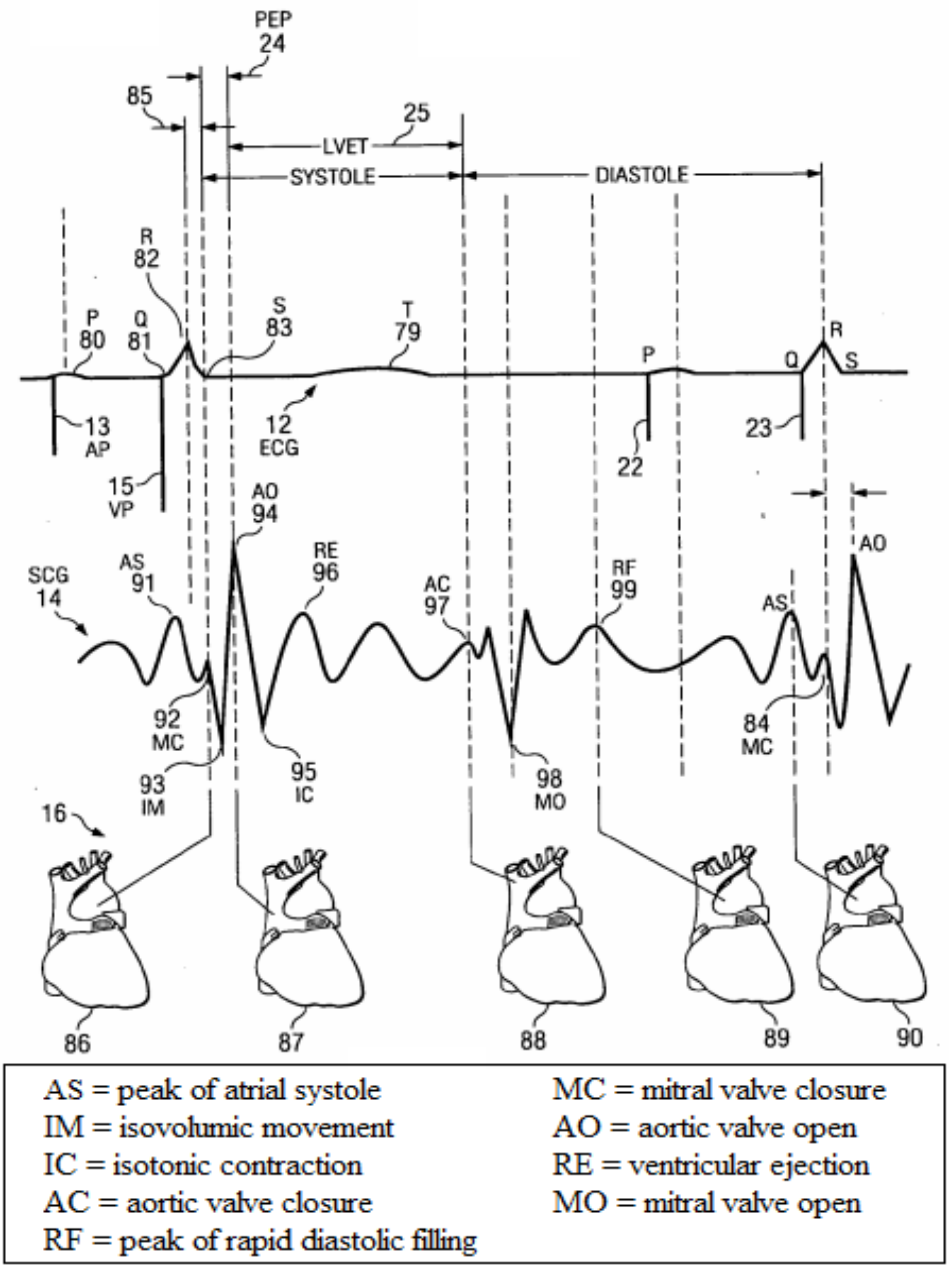

AS = peak of atrial systole	MC = mitral valve closure
IM = isovolumic movement	AO = aortic valve open
IC = isotonic contraction	RE = ventricular ejection
AC = aortic valve closure	MO = mitral valve open
RF = peak of rapid diastolic filling	

Figure 3.24 Characteristics of the SCG signal concurrent to the ECG signal [77].

Using those two characteristics, almost all cardiac events can be located. Figure 3.25 briefly describes the steps to detect cardiac events.

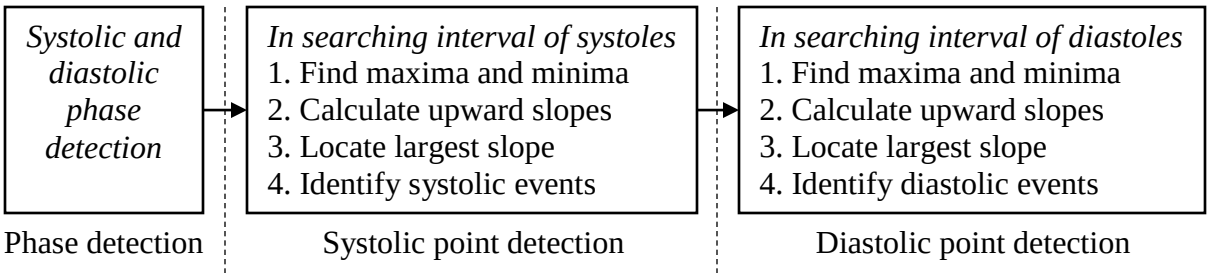

Figure 3.25 Block diagram of the cardiac events detection.

To identify the systolic events, based on the detected systolic phase indicated as red diamond in Figure 3.24(a), all maxima and minima are found inside the systolic searching interval which has value of 260 ms and is shown as light red rectangle. All systolic maxima are illustrated by red circle, and all systolic minima are represented by magenta circle in Figure 3.24(b). Then, all upward slopes between systolic minima and systolic maxima are calculated by following equation:

$$\text{up\_slope} = \frac{\text{max\_amplitude} - \text{min\_amplitude}}{\text{max\_timing} - \text{min\_timing}} \tag{3.6}$$

where up_slope is upward slope between two consecutive systolic minimum and maximum. min_amplitude and min_timing are value and timing index of the systolic minimum, respectively. max_amplitude and max_timing are value and timing index of the continuous systolic maximum, respectively.

Performing such step can reduce the calculation time because only maximum and minimum points are used to compute the slopes rather than doing differential on all in-search-interval data points. Based on the first characteristic, the largest systolic upward slope is picked and is annotated by the red line in Figure 3.26(b). The peak of the largest systolic upward slope is identified as AO, and the nadir of the largest systolic upward slope is marked as IM. The peaks before AO are MC and AS sequentially, and the peak after AO is RE. The nadir right after IM is IC.

To detect diastolic points, also based on the detected diastolic phase indicated as blue triangle in Figure 3.26(a), all maxima and minima are found inside the diastolic searching interval which has value of 220 ms and is shown as light blue rectangle. All diastolic maxima are illustrated by the blue circle, and all diastolic minima are represented by the black circle in

Figure 3.26(b). Then, all upward slopes between diastolic minima and diastolic maxima are also calculated by Equation (3.6). Based on the second characteristic, the largest diastolic upward slope is picked which is annotated by the blue line in Figure 3.26(b). The nadir of the largest diastolic upward slope is marked as MO. The peak right after the maximum point of the largest diastolic upward slope is RF, and the second peak before the maximum point of the largest diastolic upward slope is AC. Figure 3.26 illustrates an example of event detection procedure.

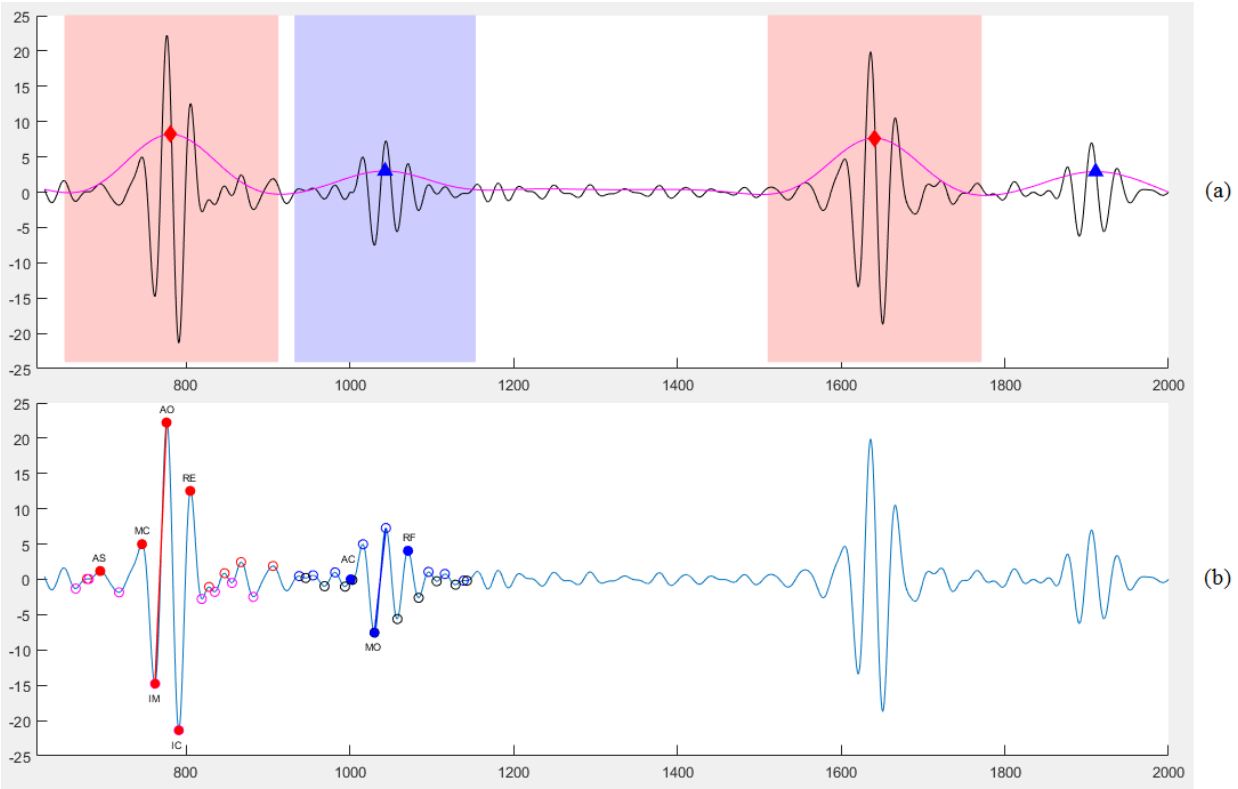

Figure 3.26 An example of event detection. (a) Detected systolic (red diamond) and diastolic (blue triangle) phases with searching intervals (red and blue rectangles) (b) Detected cardiac events with largest systolic slope (red line) and diastolic slope (blue line).

3.7 Real-time Mode of Cardiac Events Detection

In the Matlab framework, after splitting channel data form the received packages, each channel processing stream is fed continuously 1000 samples at a time. A buffer is used to store

new feeding data for phase and event detections. Figure 3.27 shows the overview of the technique to detect cardiac events in real-time.

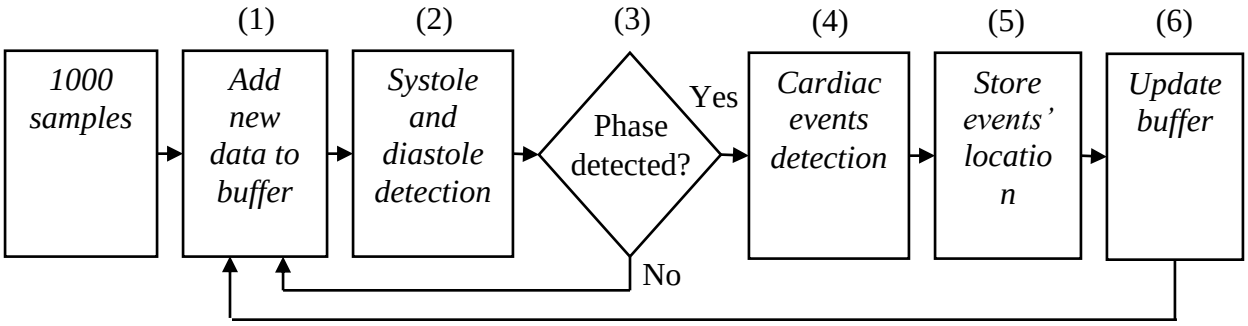

Figure 3.27 Block diagram of the real-time event detection.

There are total 6 steps in the block diagram. In the 1st step, 1000 data samples are added to the processing buffer. The two algorithms to detect the systolic and diastolic phases are applied in the 2nd step. After that, if no systolic and diastolic phases are found due to the lack of data, the processing buffer will be added another 1000 data samples. Once systolic and diastolic phases are identified, event detection will be applied to locate and save cardiac points in the 4th and 5th steps. In the last step, depending on the phase detection method used; there are two different ways to remove the processed data off the processing buffer before adding new data.

For the phase detection algorithm using *moving average threshold*, the last detected systolic phase is always kept back in processing buffer for the next detection. The data from the beginning of the processing buffer to the point which is 50 ms ahead of the maximum right before the last detected systolic are deleted. The reason of doing that is to ensure having enough maxima of the SCG energy signal in the processing buffer to calculate the average thresholds. Figure 3.28(a) and (b) illustrate *X* signs (on a red circle) in sub-graphs (iv) as the points to be removed for updating processing buffer.

For phase detection algorithm using *interpolation*, the last detected systolic phase is also kept back in the processing buffer. However, the data are deleted from the beginning of the processing buffer to the point which is 50 ms ahead of the last detected systole. The reason for doing that is to ensure the interpolation signal having at least two minima in the processing buffer for phase detection. Figure 3.28(a) and (b) illustrate *X* signs (on a red diamond) in sub-

graphs (iv) as the points to be cut up to for updating processing buffer and star signs as minima of interpolation signal.

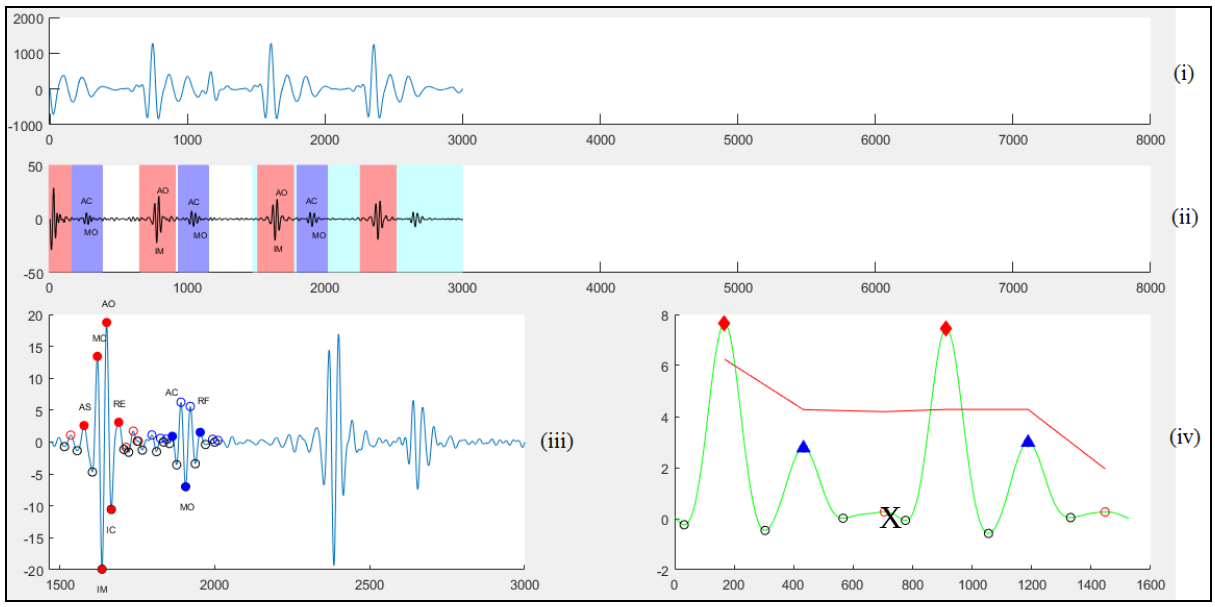

(a)

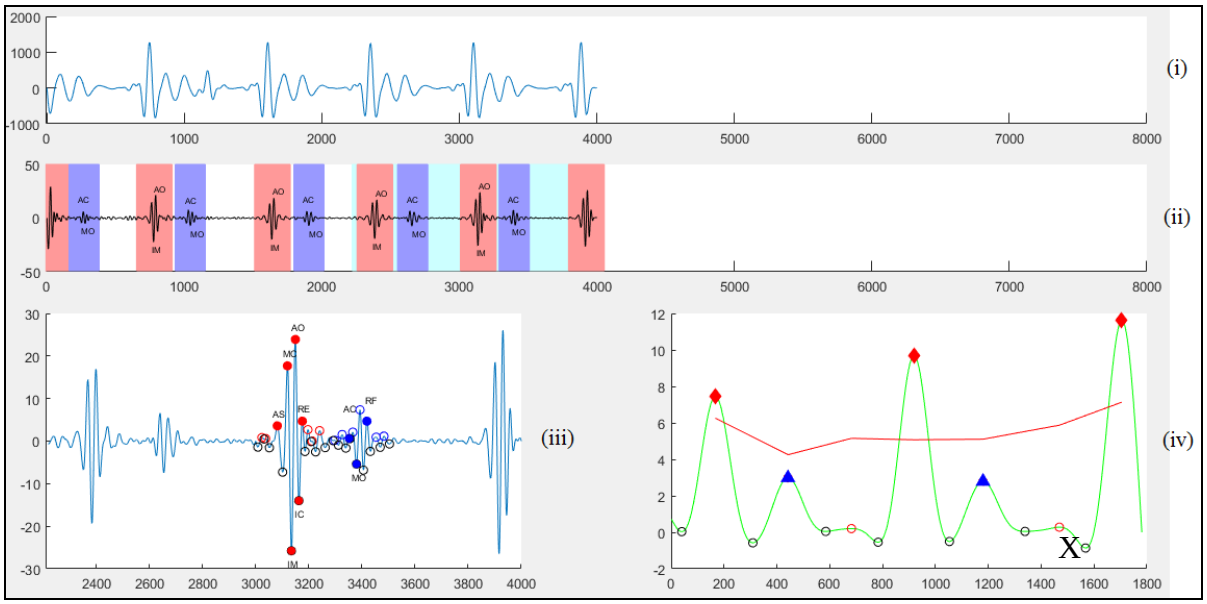

(b)

Figure 3.28 Real-time detection using moving average threshold. (a) Detection at the 3rd second. (b) Detection at the 4th second. (i) ECG signal. (ii) Searching intervals (systoles are red rectangles, and diastoles are blue rectangles), detected events and processing buffer (cyan rectangle) in 8-second window view. (iii) Detected events in processing buffer. (iv) Red line is moving average threshold. Red diamonds are systolic phases. Blue triangles are diastolic phases. Green line is SCG energy signal. Red and black circles are maxima and minima of SCG energy signal.

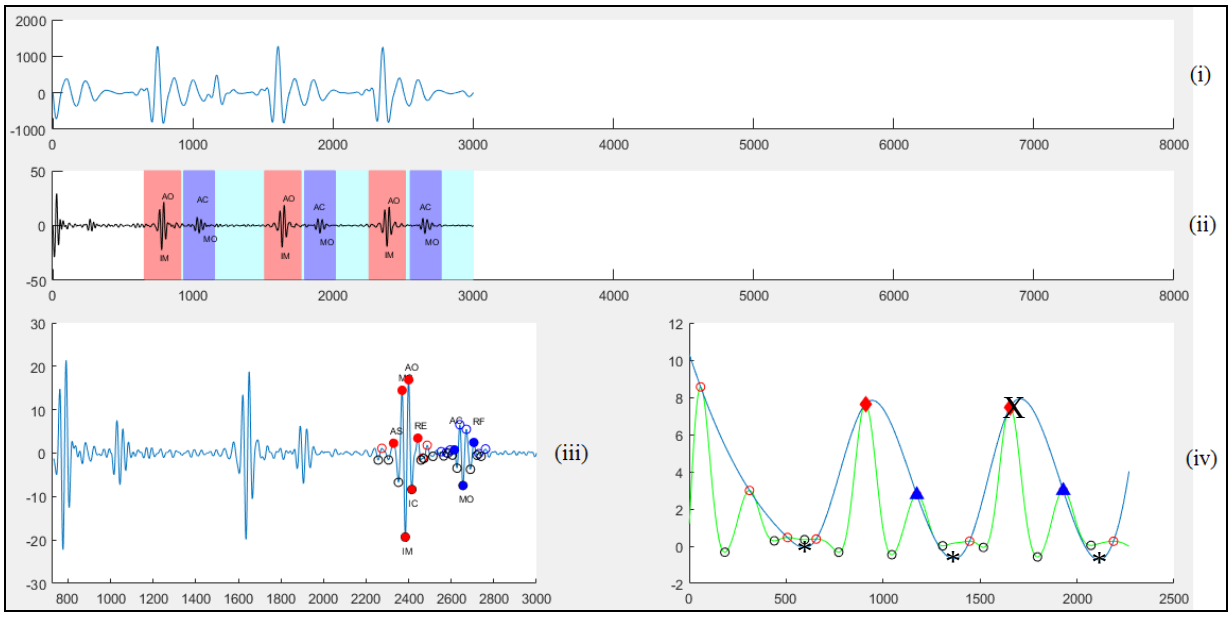

(a)

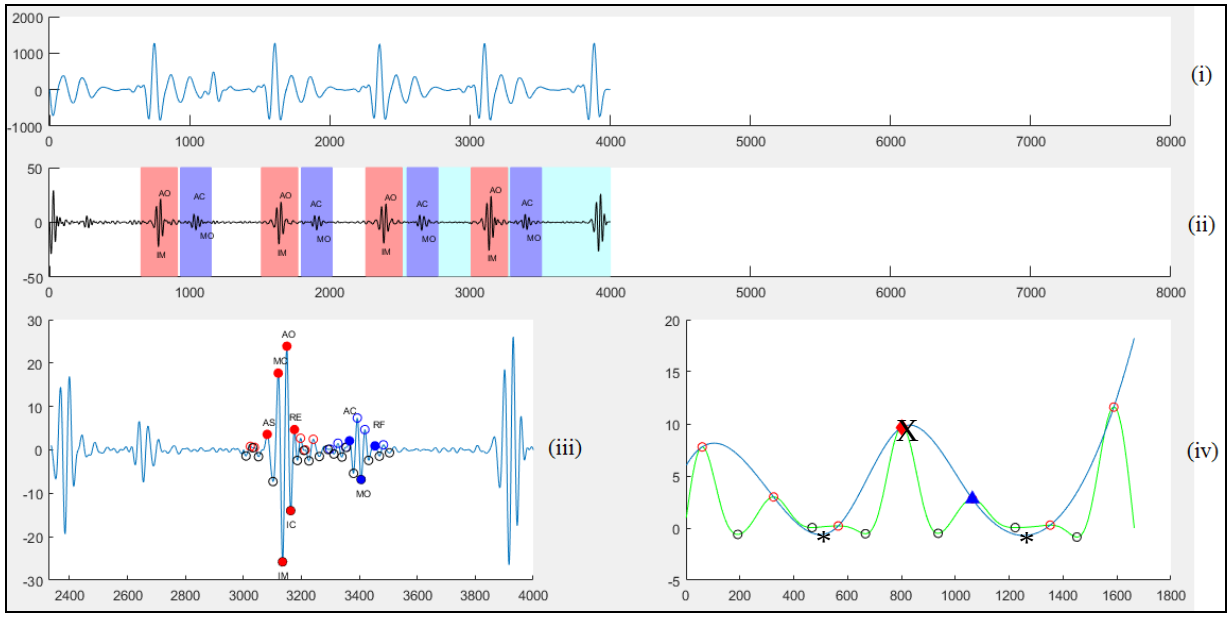

(b)

Figure 3.29 Real-time detection using interpolation. (a) Detection at the 3rd second. (b) Detection at the 4th second. (i) ECG signal. (ii) Searching intervals (systoles are red rectangles, and diastoles are blue rectangles), detected events and processing buffer (cyan rectangle) in 8-second window view. (iii) Detected events in processing buffer. (iv) Detected phases using interpolation. Red diamonds are systolic phases. Blue triangles are diastolic phases. Green line is SCG energy signal. Red and black circles are maxima and minima of SCG energy signal. Stars are minima of interpolation.

CHAPTER 4
RESULTS AND DISCUSSION

All results and discussion related to four sections in the method chapter will be reported in this chapter. First section describes the trials to evaluate the wireless DAQ system. In the next section, the advantages and disadvantages of various placements of the pair accelerometers will be compared. Data will be shown in third section to illustrate the different performance among noise removal techniques. In the last section, the detection algorithms for systolic/diastolic phases and events will be explained; the procedures to evaluate the algorithms will also be detailed and shown in this section.

4.1 Wireless Data Acquisition System

This section contains all the tests including data reliability and power consumption to exam the wireless DAQ system performance which is described in Section 3.1 of Chapter 3. However, because this is not the main purpose of this study and only direct mode was used to collect data; the assessment just applies simple procedures to test the wireless DAQ on direct mode only.

4.1.1 Data reliability

There are two scenarios to test the reliability of the system. For both tests, the laptop was connected directly to the self-AP of the wireless DAQ, and Wi-Fi Analyzer app was used to measure the signal strength on laptop.

In the first scenario, the ping test will be performed in 1 minute on the laptop. The command used is ping *–l 1460 192.168.1.2 –t* with –l is number of bytes want to send, -t means sending package continuously until get stop command. The number of byte is 1460 because it is the longest package that TCP protocol can carry without fragment. The distance between the laptop and the DAQ increases from 9m to the distance appearing loss or out of range of the Wi-Fi signal. Distance, latency, and length of data are tabulated in the table below to evaluate the connection.

Table 4.1 Ping results.

#	Distance (m)	Signal strength (dBm)	Number of bytes	Average latency (ms)	Loss percent (%)	Number of sent package	Notes
1	9	-71	1460	<1ms	0	60	light of sight
2	9	-79	1460	<1ms	0	59	through one wooden door
3	9	-85	1460	<1ms	0	62	through two wooden doors
4	13	-83	1460	<1ms	0	56	light of sight
5	13	-92	1460	<1ms	0	62	through one wooden door
6	13	out of range	NA	NA	NA	NA	through two wooden doors

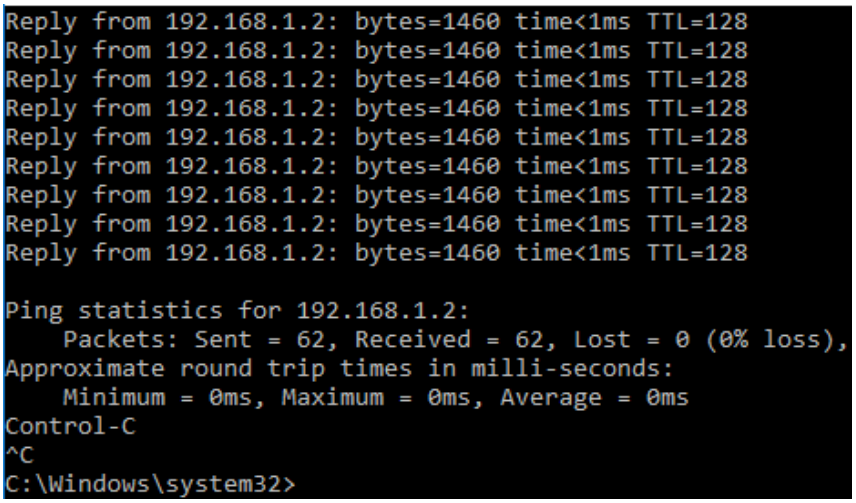

Figure 4.1 An example of ping test.

In the second test, all ADC inputs of the DAQ are connected directly to a defined signal source (2 V peak-to-peak, 1.2 V offset, 2 Hz) and start the acquisition on the laptop as usual in one minute. Then, compare the acquired data in the saved text file to the defined signal sources on the amplitude and frequency using LabChart software. LabChart can import the data in text file with tab delimiter and calculate the frequency and peak-to-peak voltage. The distance between the laptop and the DAQ is around 9m. With the good signal, LabChart calculated the frequency is 1.9980 Hz and the peak-to-peak voltage is 2032 mV which are very close to the defined signal sources.

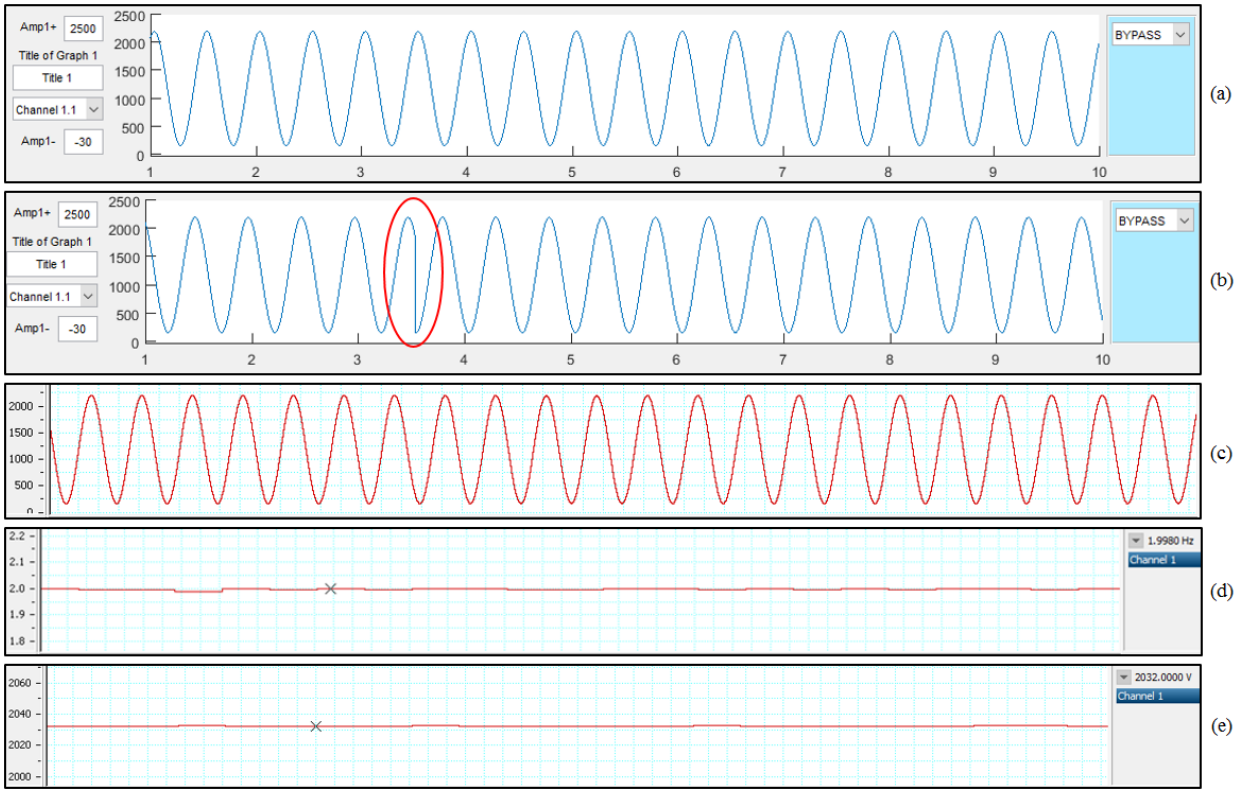

Figure 4.2 (a) Received data without dropped packages on Matlab framework. (b) Received data with one package dropped (red oval) on Matlab framework. (c) Good saved data in text file on LabChart. (d) Frequency of saved data calculated by LabChart. (e) Peak-to-peak voltage of saved data calculated by LabChart.

For the normal setting of the system, the DAQ transmits data using its own antenna to the receiving unit. The range is around 13 m in a home or office setting (non-line of sight) and can be greater than 20 m in outdoor (light of sight). The system is very reliable if the signal strength is above -93 dBm. If the signal strength is lower than -93 dBm, dropped packages will occur and it will cause the corrupted signal in the saved data. The unit also has the capacity of connecting to the existing Wi-Fi system of a home or an office. In this scenario, the transmitting range of the DAQ to the receiving unit is extended depending on the location between the two with respect to the central Wi-Fi.

4.1.2 Power consumption

The DAQ consumes 135 mA off the +3.3 V DC power supply while transmitting the data. A slightly lower power usage when it receives data (125 mA) from a computer. A low standby power of 70 μA was observed while the DAQ is in the standby mode. For a full-charged 3.7V, 800 mAh rechargeable LiPo battery, the unit can continuously operate for over 5 hours.

4.2 Motion Noise Removal Techniques with Different Placements of the Two Sensors

The results shown here are related to Section 3.3 and 3.4 in Chapter 3. With the simulation, the results of noise removal on both SUBTRACTOR and ADDER are ideal because the noise on both input signals are the same. However, in the real world, both accelerometers do not respond in the same way, so the perfect results of noise removal will not be as expected.

The outcomes of motion noise removal methods are divided into four sub-sections. The first one studies the technique using only one accelerometer with an analog band-pass filter. The second part consists the results of using two accelerometers with analog ADDER/ SUBTRACTOR and the analog band-pass filter. In the third part, all accelerometer signals will be fed directly into the DAQ and be processed in the Matlab framework, and the results of this configuration will be discussed. The last part examines the outcomes of using two accelerometers with AGC. All techniques are applied on two types of motion noise including gentle movement and walking with three ways of sensor placement comprising *horizontal, vertical* and *diagonal*. Because only digital processing technique uses all three-axis data, all remaining techniques will be shown only z-axis waveform. All the following figures and signal measurements are acquired from LabChart Reader software on data sets of one subject. The length of the signals in the figures is five seconds. The signal measurements include peak-to-peak voltage (Vpp), frequency and signal-to-noise ratio (SNR) of systolic and diastolic phases are calculated by the variance of systolic and diastolic phases over the variance of noise in quiescence period between a diastole and the following systole.

4.2.1 Motion noise removal using one accelerometer

In subpart 4.2.1.1, the performance of one accelerometer with the band-pass filter handling gentle movement with three ways of sensors placement is discussed. In the subpart 4.2.1.2, the same procedure is analyzed but coping with walking motion.

4.2.1.1 Coping with gentle motion

With one accelerometer placed on the sternum and an analog second-order band-pass filter, the gentle motion can be removed satisfactorily. All systolic and diastolic phases can be observed clearly with or without referring to ECG signal as seen in Figure 4.3(a). Without the ECG reference, the highest-energy portions of the output signal should be systoles, and lower-energy portions of output signal should be diastoles. With the ECG reference, the high-energy portions of the output signal locating near to the QRS complex indicated as red rounded rectangle in Figure 4.3(a) can be considered as systolic phases, and the lower-energy portions of output signal positioning close to the T wave shown as blue rounded rectangle in Figure 4.3(a) can be accepted as diastolic phase.

Figure 4.3(b) illustrates the red oval as systolic phase and the blue oval as diastolic phase. There is very small SCG signal residing in the gentle-motion z-axis signal which is pointed as the red circle in Figure 4.3(c). Table 4.2 shows the average measurements on all identified systoles and diastoles of output signal in Figure 4.2(b). With high total gain of amplifier and filter, which is approximately 480, the average swing of all recognized systoles and diastoles are high and approximately half of maximum wing 2.5 V. The average Vpp of the gentle movement in Figure 4.3(c) is around 325 mV, and its frequency is only around 1 Hz. Therefore, the gentle motion should be eliminated of the SCG signal by the band-pass filter.

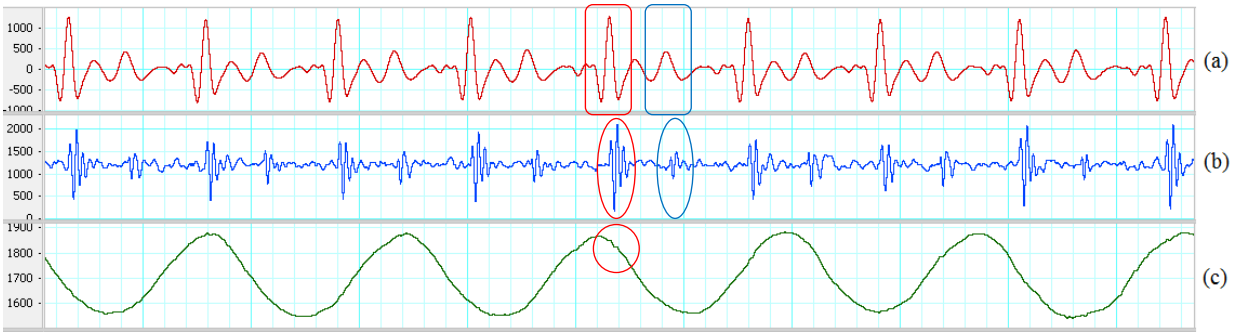

Figure 4.3 One sensor with filter on gentle movement. (a) Filtered ECG (5-20 Hz). Red rounded rectangle indicates a QRS complex. Blue rounded rectangle shows a T wave. (b) Filtered SCG. Red oval indicates a systole. Blue oval indicates a diastole. (c) Z-axis. Red circle illustrates a small residing SCG signal.

Table 4.2 Signal measurements of using one accelerometer on gentle motion.

Average Systolic Vpp (mV)	Average Diastolic Vpp (mV)	Average Systolic SNR	Average Diastolic SNR
1481.5	659.3	30.1	5.6

4.2.1.2 Coping with walking motion

The same set-up as in section 4.2.1.1 does not deal effectively with walking noise. The walking causes high rate of change in acceleration when the subject is stepping on the ground because the acceleration suddenly changes from a certain value to zero in a very short period. The Vpp of the walking z-axis is just about 260 mV which is smaller than the gentle movement, and the measured frequency in walking period is around 2 Hz which is expected to be removed successfully by the band-pass filter. However, the frequency of walking portions indicated by the brown oval in Figure 4.4(c) is still in the range of band-pass filter (20-50 Hz), so the high acceleration combining with high total gain of the amplifier and filter dominate many portions of the SCG signal and causes saturation on those segments. The information in saturation segment cannot be recovered accurately in the detection step.

Table 4.3 shows the average measurements on all identified systoles and diastoles of the output signal in Figure 4.4(b). Only one systole and one diastole in total eight phases can only be identified with ECG reference which are illustrated in order as red and blue ovals in Figure 4.4(b). All remaining phases are distorted by walking illustrated by orange oval. There still has small residing SCG signal on the portions of walking z-axis signal which has low rate of change and their outputs can be recognized when referring to ECG signal. The red circle depicts a small residing SCG signal on z-axis signal in Figure 4.4(c).

Table 4.3 Signal measurements of using one accelerometer on walking motion

Total systole	Detected systole	Total diastole	Detected diastole	Average detected systolic Vpp (mV)	Average detected diastolic Vpp (mV)	Average distorted Vpp (mV)	Average detected systolic SNR	Average detected diastolic SNR
9	1	8	1	1227	513	2500	1	0.1

Although one systolic and diastolic phase can be determined, they have very small amplitude comparing with the amplitude of walking distortion that will lead to false results in phase detection. The noise amplitude in quiescence period is very large comparing to the amplitude of identified systole and diastole, so their SNRs will be lower than one. In addition, the speed of walking or how fast the subject stepping on the ground also affects the output signal. If the high acceleration does not overlay on top of the systolic or diastolic phases, those phases can be identified with ECG reference.

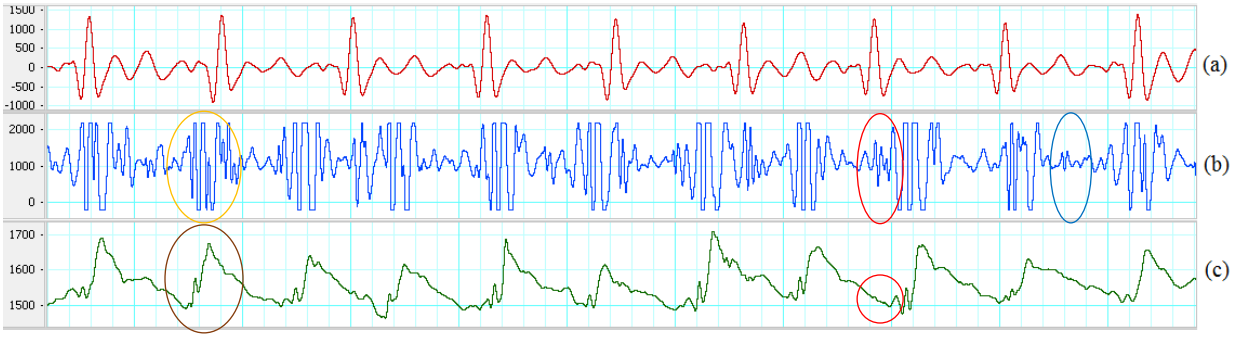

Figure 4.4 One sensor with filter on walking noise. (a) Filtered ECG (5-20 Hz). (b) Filtered SCG (20-50 Hz). Orange oval illustrates a distortion. Red oval indicates a recognized systole. Blue oval indicates a recognized diastole. (c) Z-axis with walking noise. Red circle illustrates a residing SCG signal. Brown oval indicates a high-energy walking portion.

4.2.2 Analog processing on two accelerometers

This sub-section consists of the results of using SUBTRACTOR and ADDER to scope with gentle and walking motion in different positions of two sensors including *horizontal, vertical* and *diagonal*.

4.2.2.1 Using SUBTRACTOR

In subpart 4.2.2.1.1, the performance of SUBTRACTOR coping mild movement with three ways of sensor placement is discussed. In the subpart 4.2.2.1.2, coping with walking motion is studied on the same procedure.

4.2.2.1.1 Coping with gentle motion

The two accelerometers placed *horizontal*, *vertical* and *diagonal* on the chest with SUBTRACTOR and the analog band-pass filter can eliminate the gentle motion effectively. All systolic and diastolic phases can be determined with or without the need of ECG signal. Table 4.4 shows the average measurements on all recognized systoles and diastoles of the output signals on three types of sensor placement with SUBTRACTOR and gentle movement. The systolic Vpp of the output signals in Figure 4.5(b), 4.6(b) and 4.7(b) are about three times lower than using one accelerometer, and the diastolic Vpp of the output signals are about two times smaller than using one accelerometer. The SNRs of *horizontal* and *vertical* placement alternate. The *vertical* sensors cope well with the noise on systolic portions, so the average systolic SNR of *vertical* placement is bigger than *horizontal* placement. On the other hand, the *horizontal* sensors cope better with the noise on diastolic portions, so the average diastolic SNR of *horizontal* placement is bigger than *vertical* placement. The *diagonal* placement handles the noise best on both systolic and diastolic portions that leads to high SNRs of both systoles and diastoles. The measured frequency of the gentle movement is around 0.9 Hz for all three sensor positions, so the analog band-pass can deal with it without any difficulty.

Table 4.4 Signal measurements of using two sensors with SUBTRACTOR on gentle motion

Sensor placements	Average Systolic Vpp (mV)	Average Diastolic Vpp (mV)	Average Systolic SNR	Average Diastolic SNR
Two *horizontal* sensors	414.7	294.1	34.4	14.3
Two *vertical* sensors	418.2	162.8	49.5	8
Two *diagonal* sensors	539	281	48	14.9

The red and blue ovals show determinable systole and diastole in Figure 4.5(b), 4.6(b) and 4.7(b). There are also small SCG signals on z-axis of the sensor placed close to the heart which is indicated as red circles in Figure 4.5(c), 4.6(c) and 4.7(c).

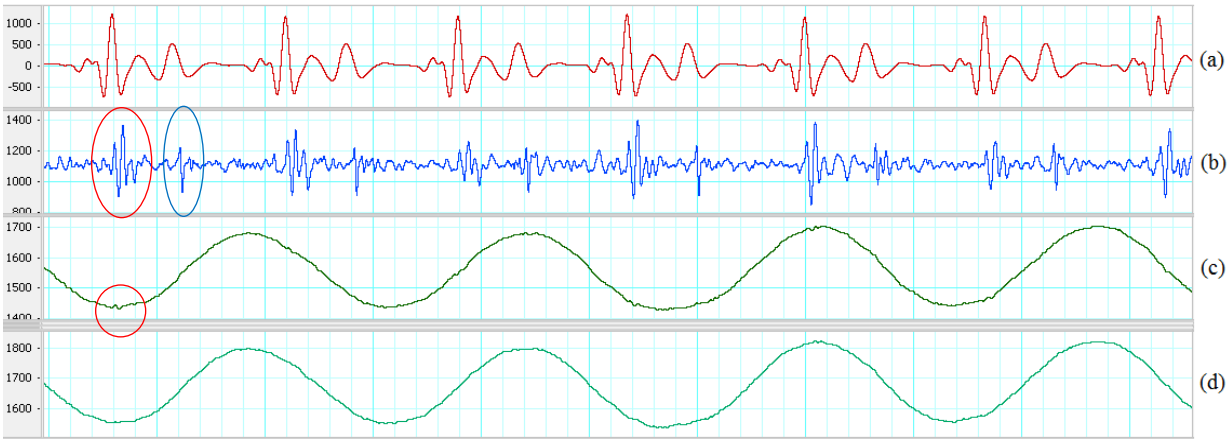

Figure 4.5 Two *horizontal* sensors with SUBTRACTOR on gentle movement. (a) Filtered ECG (5-20 Hz). (b) Filtered SCG (20-50 Hz). Red oval indicates an identified systolic. Blue oval indicates a recognized diastolic. (c) First sensor z-axis. Red circle indicates a small SCG signal. (d) Second sensor z-axis.

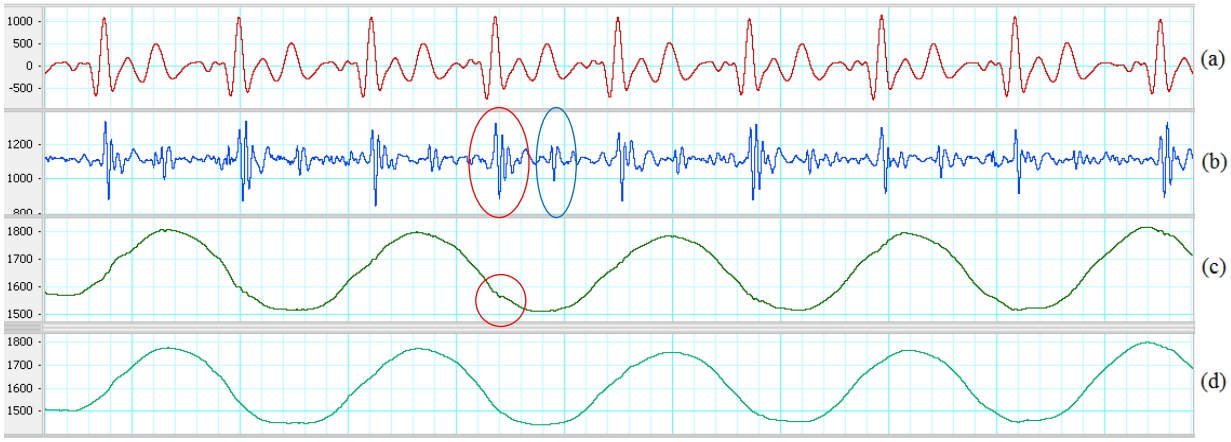

Figure 4.6 Two *vertical* sensors with SUBTRACTOR on gentle movement. (a) Filtered ECG (5-20 Hz). (b) Filtered SCG (20-50 Hz). Red oval indicates an identified systolic. Blue oval indicates a recognized diastolic. (c) First sensor z-axis. Red circle indicates a small SCG signal. (d) Second sensor z-axis.

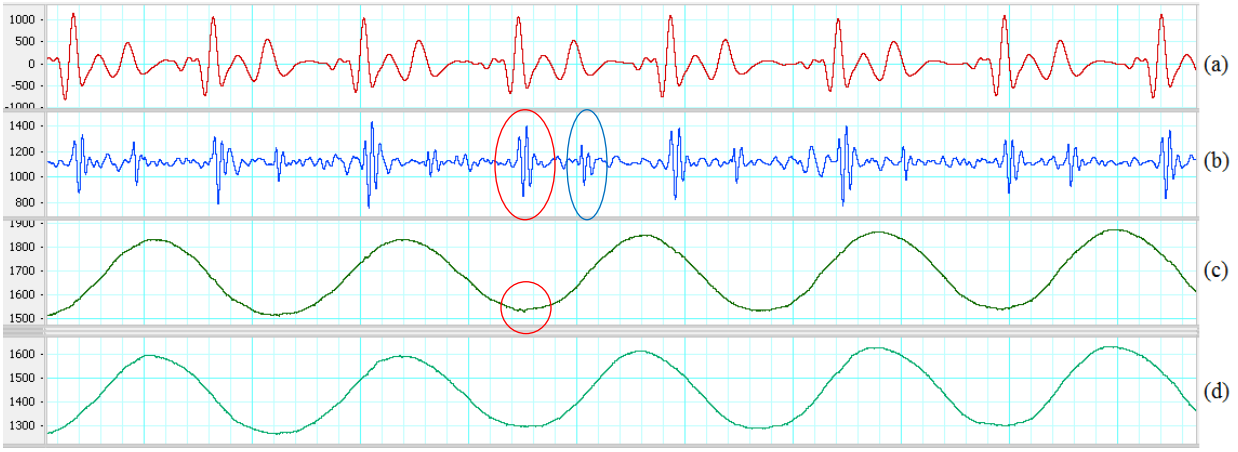

Figure 4.7 Two *diagonal* sensors with SUBTRACTOR on gentle movement. (a) Filtered ECG (5-20 Hz). (b) Filtered SCG (20-50 Hz). Red oval indicates an identified systolic. Blue oval indicates a recognized diastolic. (c) First sensor z-axis. Red circle indicates a small SCG signal. (d) Second sensor z-axis.

4.2.2.1.2 Coping with walking motion

The two accelerometers placed *horizontal*, *vertical* and *diagonal* on the chest with SUBTRACTOR and the analog band-pass filter can deal with walking noise better than using only one accelerometer. At least, no saturation is caused by walking motion even with the same high total gain when using one accelerometer. Although the SUBTRACTOR used high-performance common-mode rejection to suppress the walking noise and keep the output signal in range with the DAQ inputs, two sensors do not react in the same way with walking motion which are shown by brown ovals in Figure 4.8(c)(d), 4.9(c)(d) and 4.10(c)(d). The results of different reaction are some distortion signals indicated by the orange ovals in Figure 4.8(b), 4.9(b) and 4.10(b).

The different reaction of the two accelerometers may be due to the sensor error or sensor placement where both sensor axes are not laid on the same planes. The unaligned sensor placement can be observed by the dissimilar baseline values of two z-axis signals in Figure 4.8(c)(d), 4.9(c)(d) and 4.10(c)(d). Another reason of different reaction can be each sensor placed on the half side of the chest creating different force-propagation path from each foot to each sensor when walking.

Table 4.5 shows the average measurements on all recognized systoles and diastoles of output signals on three ways of sensor placement with SUBTRACTOR and walking motion. The SNR results may change due to how synchronized between high-energy portions of walking and systoles/diastoles. If they are in sync either with systoles or diastoles, those portions will be distorted and unidentified. If high-energy portions of walking stay in quiescence period of output signals, both systoles and diastoles can be recognized with ECG reference. The average Vpp of distortion of *horizontal* placement is smallest comparing two other ones. It means that the *horizontal* placement should handle the noise well which can increase the chance to determine cardiac phases. Two *diagonal* sensors do not remove the noise effectively because the average Vpp of distortion is quite high.

Table 4.5 Signal measurements of using two sensors with SUBTRACTOR on walking motion

Sensor placements	Total systole	Detected systole	Total diastole	Detected diastole	Average detected systolic Vpp (mV)	Average detected diastolic Vpp (mV)	Average distorted Vpp (mV)	Average detected systolic SNR	Average detected diastolic SNR
Two *horizontal* sensors	7	5	7	7	524.4	272.8	427.2	4.8	0.7
Two *vertical* sensors	9	9	8	0	368.6	N/A	699.3	4.2	N/A
Two *diagonal* sensors	9	9	9	4	613.4	338	1478.7	0.2	0.07

The z-axis of both sensors placed *vertical* on the chest in Figure 4.9(c) and 4.9(d) look quite similar comparing to the *horizontal* placement. Besides the sensor error and sensor placement, two accelerometers placing on the same *vertical* line on the center of the chest may create almost identical force-propagation path from each foot to each sensor which results in similar response of both sensors. However, there still has different response from both *vertical* accelerometers which is depicted by the orange and brown ovals in Figure 4.9(b), 4.9(c) and 4.9(d).

The z-axis of both sensors placed *diagonal* on the chest in Figure 4.10(c) and 4.10(d) look much different comparing to the *horizontal* placement. The causes should be the same with the *horizontal* and *vertical* placement which are the sensor error and sensor placement. Another reason can be the force-propagation paths are different on both vertical and horizontal directions comparing to only *horizontal* or *vertical* placement. One example of different response from both *diagonal* accelerometers which is illustrated by the orange and brown ovals in Figure 4.10(b), 4.10(c) and 4.10(d). The red blue ovals show the determinable systoles and diastoles in Figure 4.8(b), 4.9(b) and 4.10(b). There are also small SCG signals on z-axis of the sensor placed close to the heart which are indicated in red circles in Figure 4.8(c), 4.9(c) and 4.10(c).

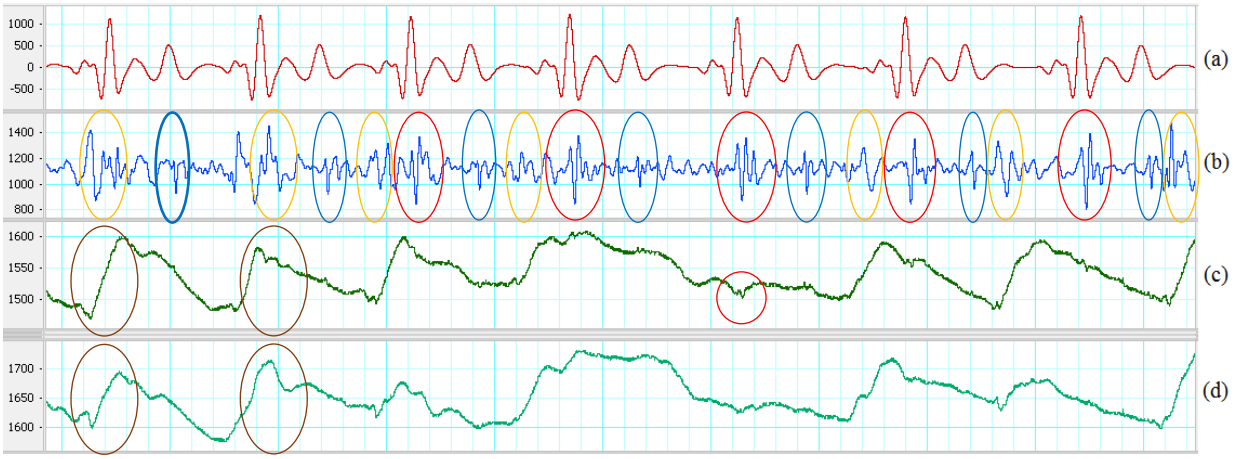

Figure 4.8 Two *horizontal* sensors with SUBTRACTOR on walking motion. (a) Filtered ECG (5-20 Hz). (b) Filtered SCG (20-50 Hz). Red ovals illustrate recognized systoles. Blue ovals indicate detected diastoles. Orange ovals show results of different reaction. (c) First sensor z-axis. Red circle indicates a small SCG signal. Brown ovals show high-energy portion of walking (d) Second sensor z-axis. Brown ovals indicate high-energy portion of walking.

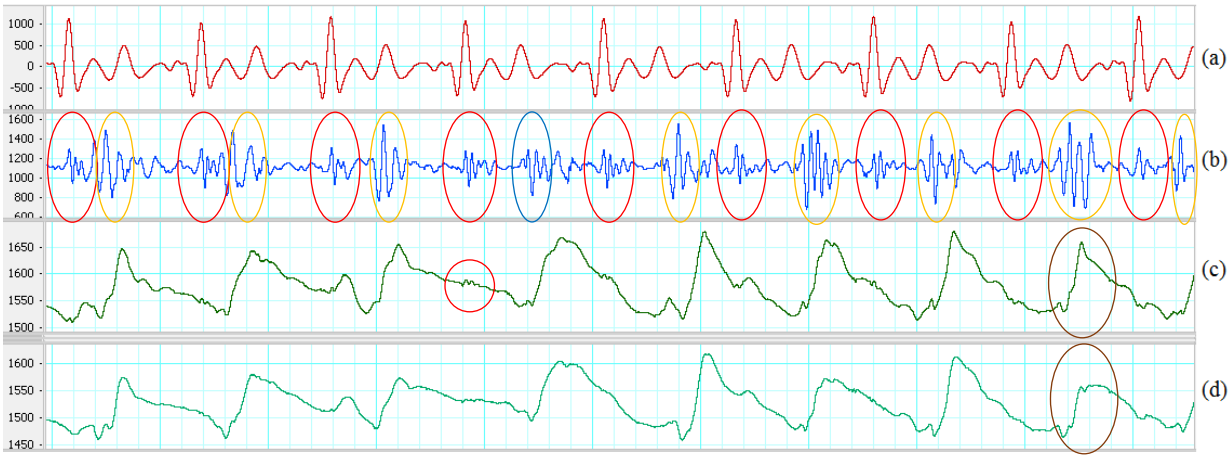

Figure 4.9 Two *vertical* sensors with SUBTRACTOR on walking motion. (a) Filtered ECG (5-20 Hz). (b) Filtered SCG (20-50 Hz). Red ovals illustrate recognized systoles. Blue ovals indicate detected diastoles. Orange ovals show results of different reaction. (c) First sensor z-axis. Red circle indicates a small SCG signal. Brown oval shows a high-energy portion of walking (d) Second sensor z-axis. Brown oval indicates a high-energy portion of walking.

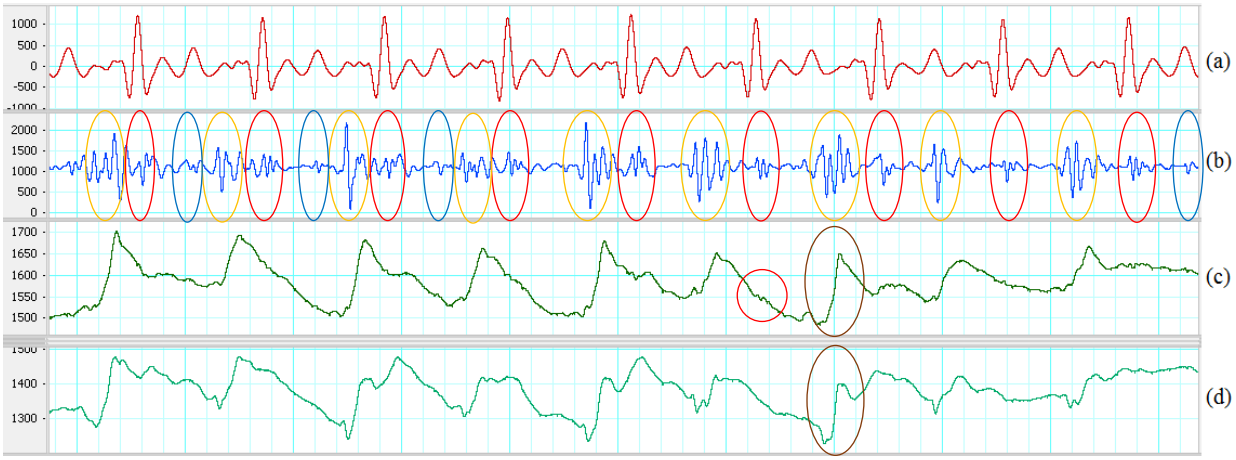

Figure 4.10 Two *diagonal* sensors with SUBTRACTOR on walking motion. (a) Filtered ECG (5-20 Hz). (b) Filtered SCG (20-50 Hz). Red ovals illustrate recognized systoles. Blue ovals indicate detected diastoles. Orange ovals show results of different reaction. (c) First sensor z-axis. Red circle indicates a small SCG signal. Brown oval shows a high-energy portion of walking (d) Second sensor z-axis. Brown oval indicates a high-energy portion of walking.

4.2.2.2 Using ADDER

In subpart 4.2.2.2.1, the performance of the ADDER coping mild movement with three ways of sensors placement is discussed. In the subpart 4.2.2.2.2, the same procedure is studied but coping with walking motion.

4.2.2.2.1 Coping with gentle motion

The two accelerometers placed *horizontal*, *vertical* and *diagonal* on the chest with ADDER and the analog band-pass filter can remove most of the gentle motions. With or without the need of ECG, all cardiac phases can be identified. The average measurements on all recognized systoles and diastoles of output signals on three types of sensor placement with ADDER and gentle movement are displayed in Table 4.6. The systolic Vpp of the output signals in Figure 4.11(b), 4.12(b) and 4.13(b) are around two times higher than using SUBTRACTOR and close to 1.9 V of the method using one accelerometer. Although the ADDER has high average Vpp on the output signals, their systolic and diastolic SNRs are not higher than the SUBTRACTOR for all three positions of the sensors. It means that the ADDER does not work well on motion noise comparing to the SUBTRACTOR. It enlarges not only the systolic and diastolic portions significantly but also the noise level at the output. The *vertical* sensors have the worst performance in the three positions. Besides, because of the sensor error, placing two accelerometers in the opposite directions for the ADDER can also make more difference in the response of the two accelerometers. Another reason of different reaction may be due to the dissimilar force-propagation path corresponding to sensor positions which is discussed in section 4.2.2.1.

Table 4.6 Signal measurements of using two sensors with ADDER on gentle motion.

Sensor placements	Average Systolic Vpp (mV)	Average Diastolic Vpp (mV)	Average Systolic SNR	Average Diastolic SNR
Two *horizontal* sensors	1390.3	799.2	31.8	13.9
Two *vertical* sensors	1081.3	490.2	16.9	3.1
Two *diagonal* sensors	1600.9	850.1	32.2	8.6

The red and blue ovals show examples of determinable systole and diastole in Figure 4.11(b), 4.12(b) and 4.13(b). There are also small SCG signals on the z-axis which are indicated as the red circles in Figure 4.11(c), 4.12(c) and 4.13(c).

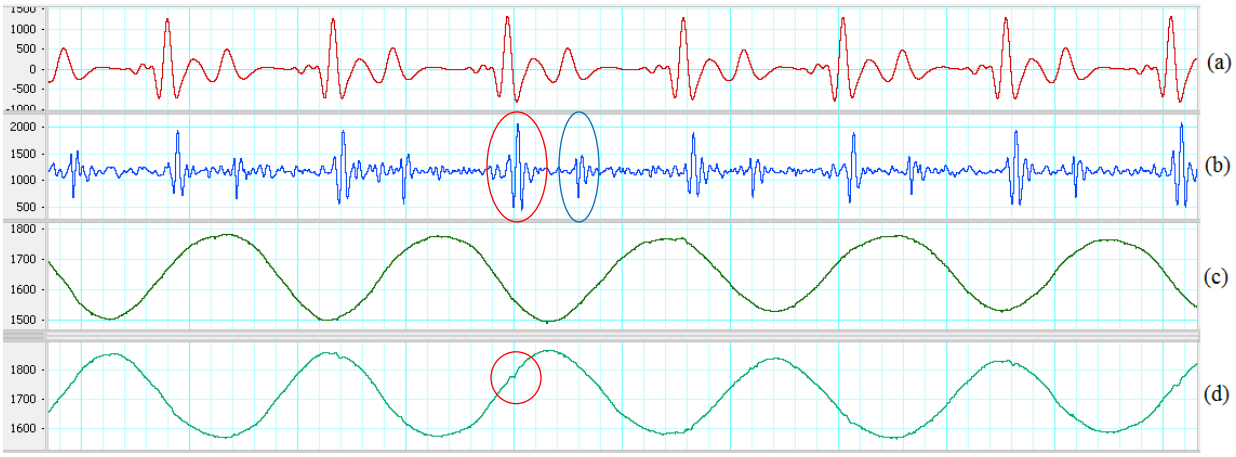

Figure 4.11 Two *horizontal* sensors with ADDER on gentle movement. (a) Filtered ECG (5-20 Hz). (b) Inverted and filtered SCG (20-50 Hz). Red oval indicates a recognized systole. Blue oval indicates an identified diastole. (c) First sensor z-axis. (d) Second sensor z-axis. Red circle indicates a small SCG signal.

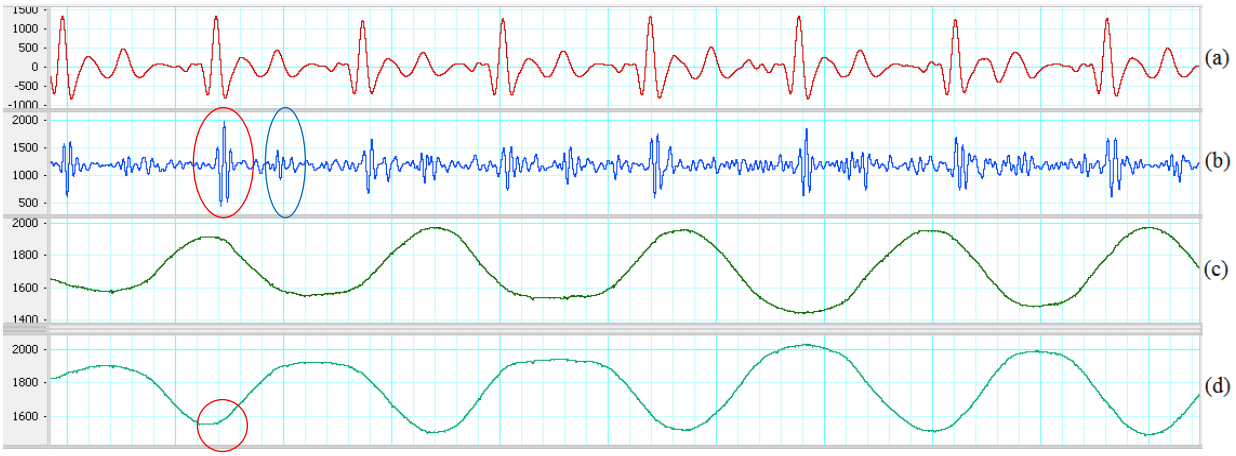

Figure 4.12 Two *vertical* sensors with ADDER on gentle movement. (a) Filtered ECG (5-20 Hz). (b) Inverted and filtered SCG (20-50 Hz). Red oval indicates a recognized systole. Blue oval indicates an identified diastole. (c) First sensor z-axis. (d) Second sensor z-axis. Red circle indicates a small SCG signal.

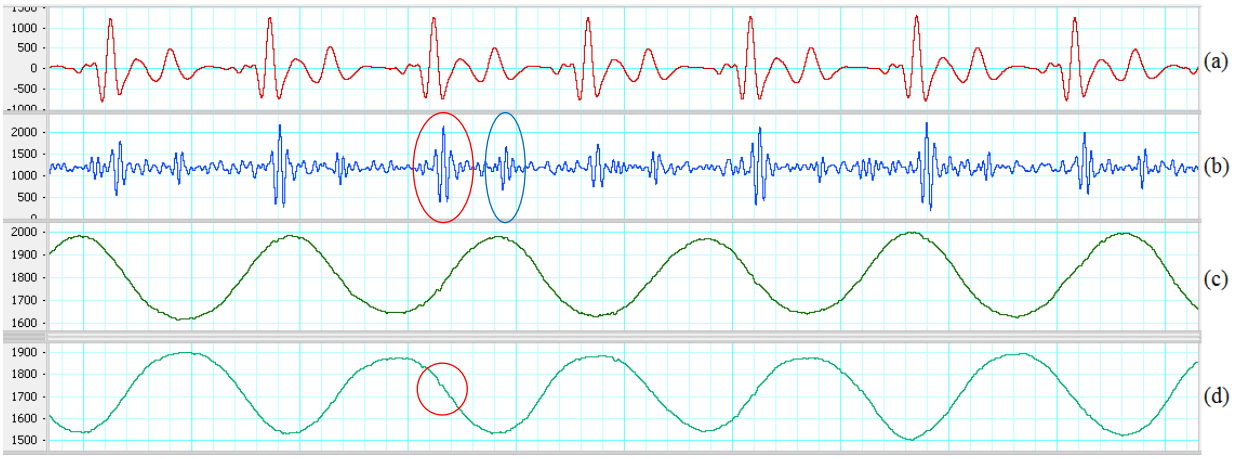

Figure 4.13 Two *diagonal* sensors with ADDER on gentle movement. (a) Filtered ECG (5-20 Hz). (b) Inverted and filtered SCG (20-50 Hz). Red oval indicates a recognized systole. Blue oval indicates an identified diastole. (c) First sensor z-axis. (d) Second sensor z-axis. Red circle indicates a small SCG signal.

4.2.2.2.2 Coping with walking motion

The two accelerometers placed *horizontal*, *vertical* and *diagonal* on the chest with ADDER and the analog band-pass filter cannot tackle walking motion efficaciously. Some saturation caused by walking motion appears on many portions of the output signals. Saturation also results in the loss of information and false solutions in the detection step. The possible cause is that the ADDER cannot eliminate totally the walking noise with high-frequency portions, so the difference of the two z-axis signals is significant. The high inequality combining with high amplification gain leads to saturation on the output signal. In addition, sensor error and the opposite direction of placement, the dis-similar force-propagation path corresponding to sensor positions which discussed in section 4.2.2.1 can be another reason of different response.

Table 4.7 displays the performance of using two accelerometers with ADDER on walking motion. The output of both sensors placed *horizontal* in Figure 4.14(b) has least saturation portions comparing to the *vertical* and *diagonal* placements. Fortunately, the distorted portions of the *horizontal* placement do not exist all the time in the quiescence period, so its systolic and diastolic SNRs has higher values than two others. However, the saturation dominates many systoles and diastoles, so only few of the phases are detected. The distorted portions of the *vertical* and *diagonal* placements unfortunately lay mainly in the quiescence period. Therefore,

their SNRs are smaller than one even though almost systoles and diastoles are determined with ECG reference.

Table 4.7 Signal measurements of using two sensors with ADDER on walking motion.

Sensor placements	Total systole	Detected systole	Total diastole	Detected diastole	Average detected systolic Vpp (mV)	Average detected diastolic Vpp (mV)	Average distorted Vpp (mV)	Average detected systolic SNR	Average detected diastolic SNR
Two *horizontal* sensors	9	6	8	3	2324.8	1244.3	2176.4	21.1	3
Two *vertical* sensors	7	5	7	5	1018.6	564.4	2366.6	1.3	0.3
Two *diagonal* sensors	9	9	8	7	1836.1	1012.1	2385.3	0.4	0.1

The red and blue ovals illustrate examples of determinable systole and diastole in Figure 4.14(b), 4.15(b) and 4.16(b). There are also small SCG signals on z-axis of the second sensor, and they are indicated as the red circles in Figure 4.14(c), 4.15(c) and 4.16(c). The different responses on all *horizontal*, *vertical* and *diagonal* placements are depicted by the orange and brown ovals in Figure 4.14(b)(c)(d), 4.15(b)(c)(d) and 4.16(b)(c)(d).

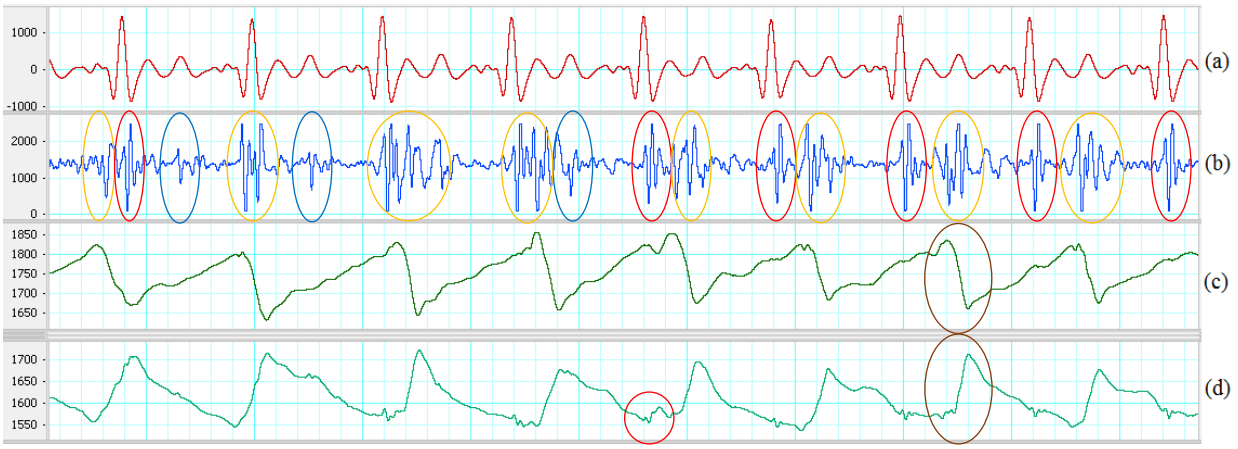

Figure 4.14 Two *horizontal* sensors with ADDER on walking motion. (a) Filtered ECG (5-20 Hz). (b) Inverted and filtered SCG (20-50 Hz). Red ovals illustrate recognized systoles. Blue ovals indicate detected diastoles. Orange ovals show results of different reaction. (c) First sensor z-axis. Brown oval shows a high-energy portion of walking (d) Second sensor z-axis. Brown oval indicates a high-energy portion of walking. Red circle indicates a small SCG signal.

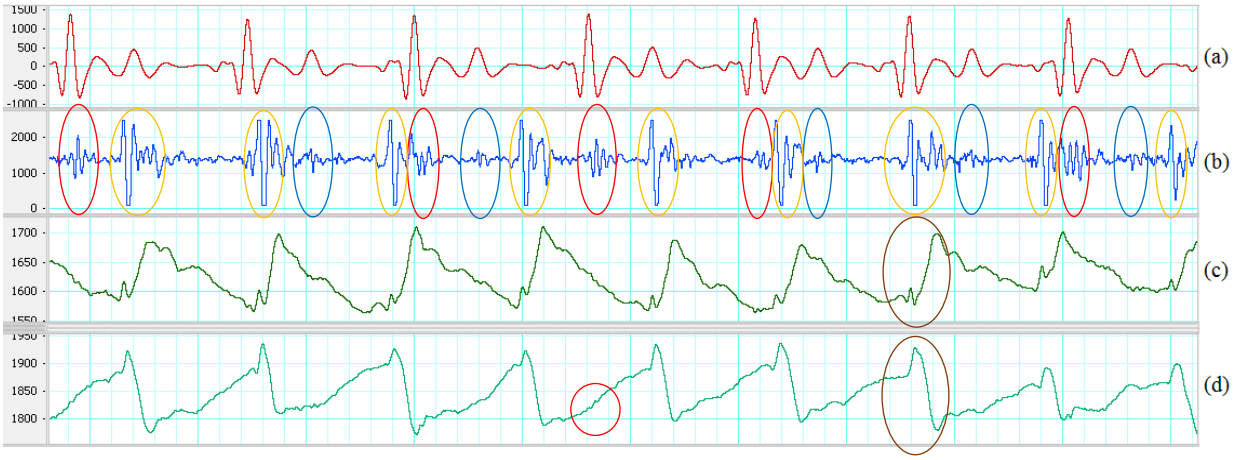

Figure 4.15 Two *vertical* sensors with ADDER on walking motion. (a) Filtered ECG (5-20 Hz). (b) Inverted and filtered SCG (20-50 Hz). Red ovals illustrate recognized systoles. Blue ovals indicate detected diastoles. Orange ovals show results of different reaction. (c) First sensor z-axis. Brown oval shows a high-energy portion of walking (d) Second sensor z-axis. Brown oval indicates a high-energy portion of walking. Red circle indicates a small SCG signal.

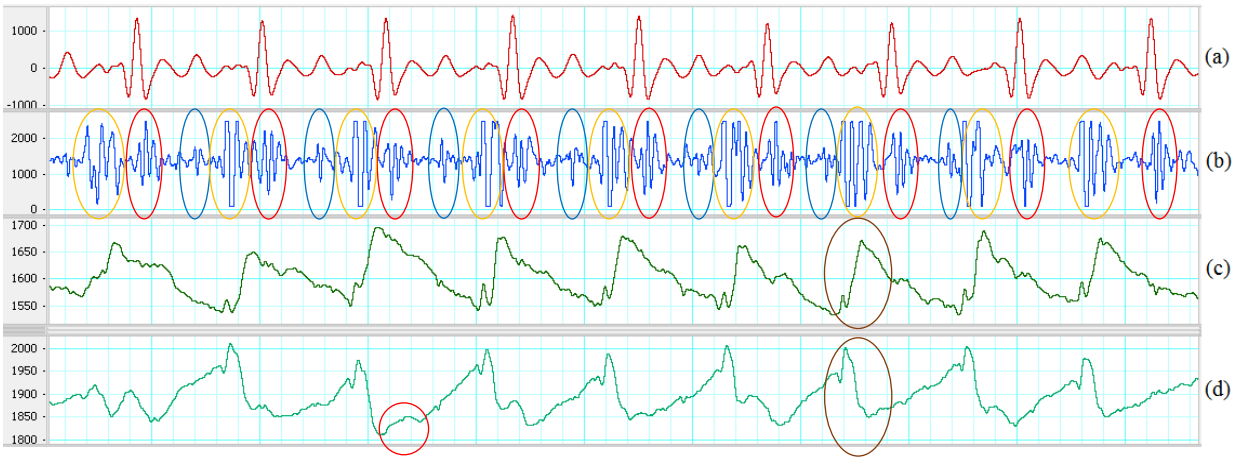

Figure 4.16 Two *diagonal* sensors with ADDER on walking motion. (a) Filtered ECG (5-20 Hz). (b) Inverted and filtered SCG (20-50 Hz). Red ovals illustrate recognized systoles. Blue ovals indicate detected diastoles. Orange ovals show results of different reaction. (c) First sensor z-axis. Brown oval shows a high-energy portion of walking (d) Second sensor z-axis. Brown oval indicates a high-energy portion of walking. Red circle indicates a small SCG signal.

4.2.3 Digital processing of two accelerometers

For easy to follow, two equations to combine data from two accelerometers in section 3.4.4 are rewritten.

$$\text{TOTAL\_ACC} = \sqrt{(x_1 - x_2)^2 + (y_1 - y_2)^2 + (z_1 - z_2)^2} \tag{3.1}$$

where x_1, y_1, z_1 are the data of three-axis of the first accelerometer and x_2, y_2, z_2 are the data of three-axis of the second accelerometer.

$$\text{Z\_ACC} = \text{abs}\,(z_1 - z_2) \tag{3.2}$$

where abs is the absolute function and z_1, z_2 are the z-axis data of two accelerometers.

The following sub-sections comprises the results of using Equation (3.1) - *total acceleration* and Equation (3.2) - *z-axis acceleration* to cope with gentle and walking motion in three places of the two sensors including *horizontal*, *vertical* and *diagonal*. The gentle and walking data sets applied the above equations belong to analog processing with SUBTRACTOR because both sensors placing on the same directions for all axes have a better similarity on the reaction than placing on opposite directions when using ADDER. Hence, the results of both equations will also be compared to the results of analog processing with SUBTRACTOR.

4.2.3.1 Coping with gentle motion

Both equations can eliminate the gentle motion successfully. All systolic and diastolic phases are identifiable referring to ECG signal, but the output signal of the SUBTRACTOR in Figure 4.17(b) is lagged 15 ms compared to the outputs of *total acceleration* in Figure 4.17(c) and *z-axis acceleration* in Figure 4.17(d). The reason is the delay of the instrumentation amplifier and the band-pass filter in analog processing method.

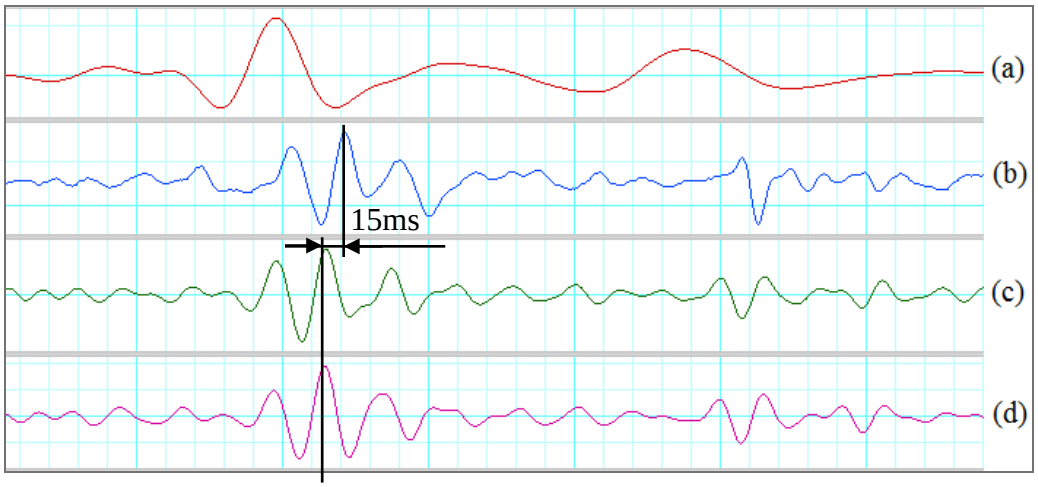

Figure 4.17 A delay between digital processing and analog processing. (a) Filtered ECG. (b) Filtered SCG with SUBTRACTOR (*subtraction*). (c) Filtered *total acceleration*. (d) Filtered *z-axis acceleration*.

Table 4.8 shows the average measurements on all identified systoles and diastoles of the output signals including *subtraction*, *total acceleration* and *z-axis acceleration* on three types of sensor placement. The average Vpp of systoles and diastoles of the *subtraction* is always greater than the *total acceleration* and *z-axis acceleration*, but its SNRs are always smaller than the *total acceleration* and *z-axis acceleration*. It means that the analog processing may also increase the output noise level through the process while digital processing suppresses the noise better at the output.

Between *total acceleration* and *z-axis acceleration*, the average Vpp of systoles and diastoles are quite close to each other when placing the two sensors on *horizontal* and *diagonal*, but the SNRs of *total acceleration* are smaller than *z-axis acceleration* for *horizontal* placement while its SNRs are larger than *z-axis acceleration* for *diagonal* placement. The reasons for these

are that the *z-axis acceleration* deal better with noise than *total acceleration* for *horizontal* placement and vice versa for *diagonal* placement.

For *vertical* placement, the average Vpp of systoles and diastoles of *total acceleration* are greater than *z-axis acceleration*, but the SNRs of both *total acceleration* and *z-axis acceleration* are not much different. It means that although *total acceleration* may gather information of all three axes to achieve better Vpp, it can also accumulate the noise at output from all three axes rather than the noise only on one axis as *z-axis acceleration*.

Table 4.8 Signal measurements of two sensors with digital processing on gentle motion

Sensor placements and methods		Average Systolic Vpp (mV)	Average Diastolic Vpp (mV)	Average Systolic SNR	Average Diastolic SNR
Two *horizontal* sensors	Subtraction	414.7	294.1	34.4	14.3
	Total acceleration	6.3	3.7	67.5	21.7
	Z-axis acceleration	6.2	3.6	75.3	23
Two *vertical* sensors	Subtraction	418.2	162.8	49.5	8
	Total acceleration	13.3	5.5	69.9	11.3
	Z-axis acceleration	6.6	2.4	67.8	9.7
Two *diagonal* sensors	Subtraction	539	281	48	14.9
	Total acceleration	11.7	4.7	84.7	17.8
	Z-axis acceleration	9.4	4.1	78.1	20.4

The red and blue ovals show examples of determinable systole and diastole in Figure 4.18(b), 4.19(b) and 4.20(b). There are also small SCG signals on the z-axis of the first sensor indicated as red circles in Figure 4.18(c), 4.19(c) and 4.20(c).

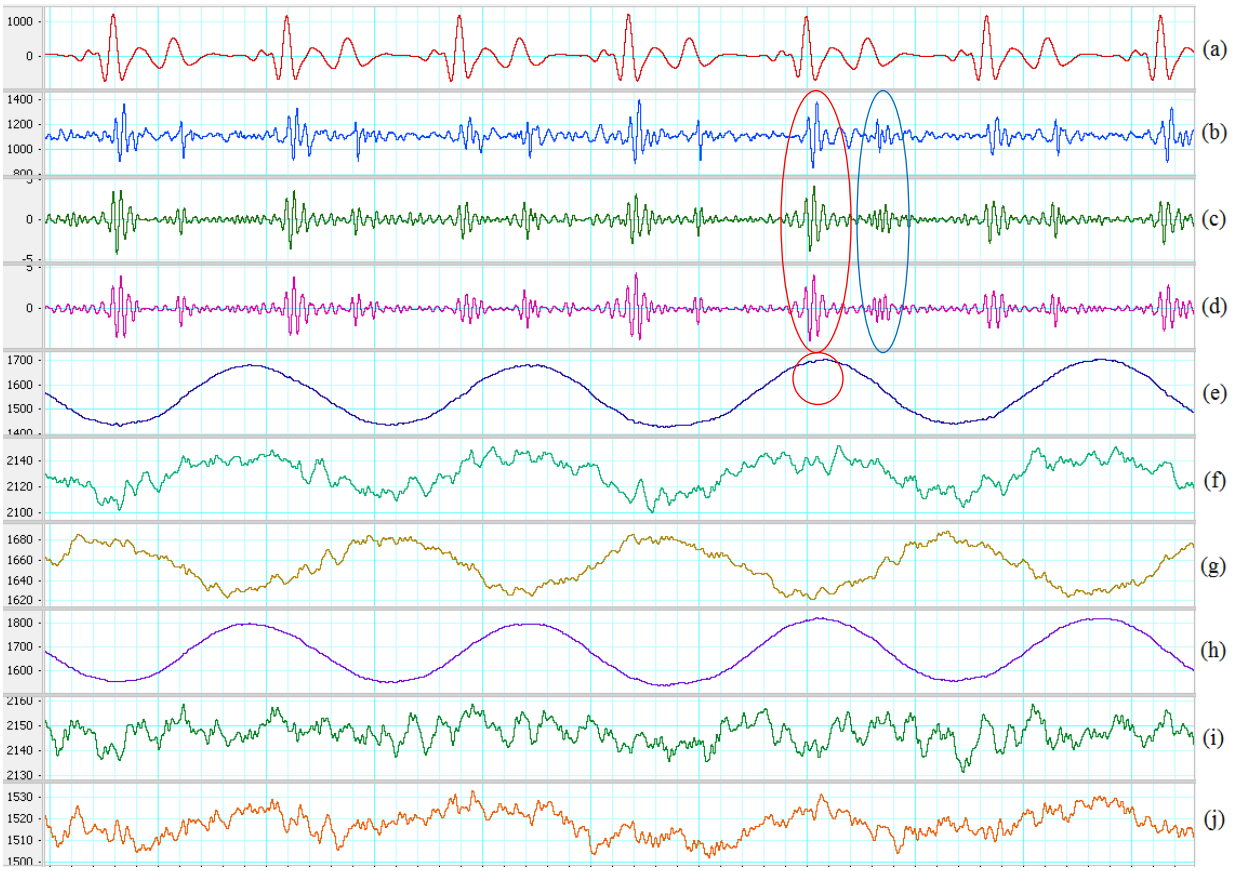

Figure 4.18 Two *horizontal* sensors with digital processing on gentle movement. (a) Filtered ECG (5-20 Hz). (b) Filtered SCG with SUBTRACTOR (*subtraction*). (c) Filtered *total acceleration*. (d) Filtered *z-axis acceleration*. Red oval indicates a recognized systole. Blue oval indicates a determined diastole. (e) First sensor z-axis. Red circle indicates a small SCG signal. (f) First sensor y-axis. (g) First sensor x-axis. (h) Second sensor z-axis. (i) Second sensor y-axis. (j) Second sensor x-axis.

Figure 4.19 Two *vertical* sensors with digital processing on gentle movement. (a) Filtered ECG (5-20 Hz). (b) Filtered SCG with SUBTRACTOR (*subtraction*). (c) Filtered *total acceleration*. (d) Filtered *z-axis acceleration*. Red oval indicates a recognized systole. Blue oval indicates a determined diastole. (e) First sensor z-axis. Red circle indicates a small SCG signal. (f) First sensor y-axis. (g) First sensor x-axis. (h) Second sensor z-axis. (i) Second sensor y-axis. (j) Second sensor x-axis.

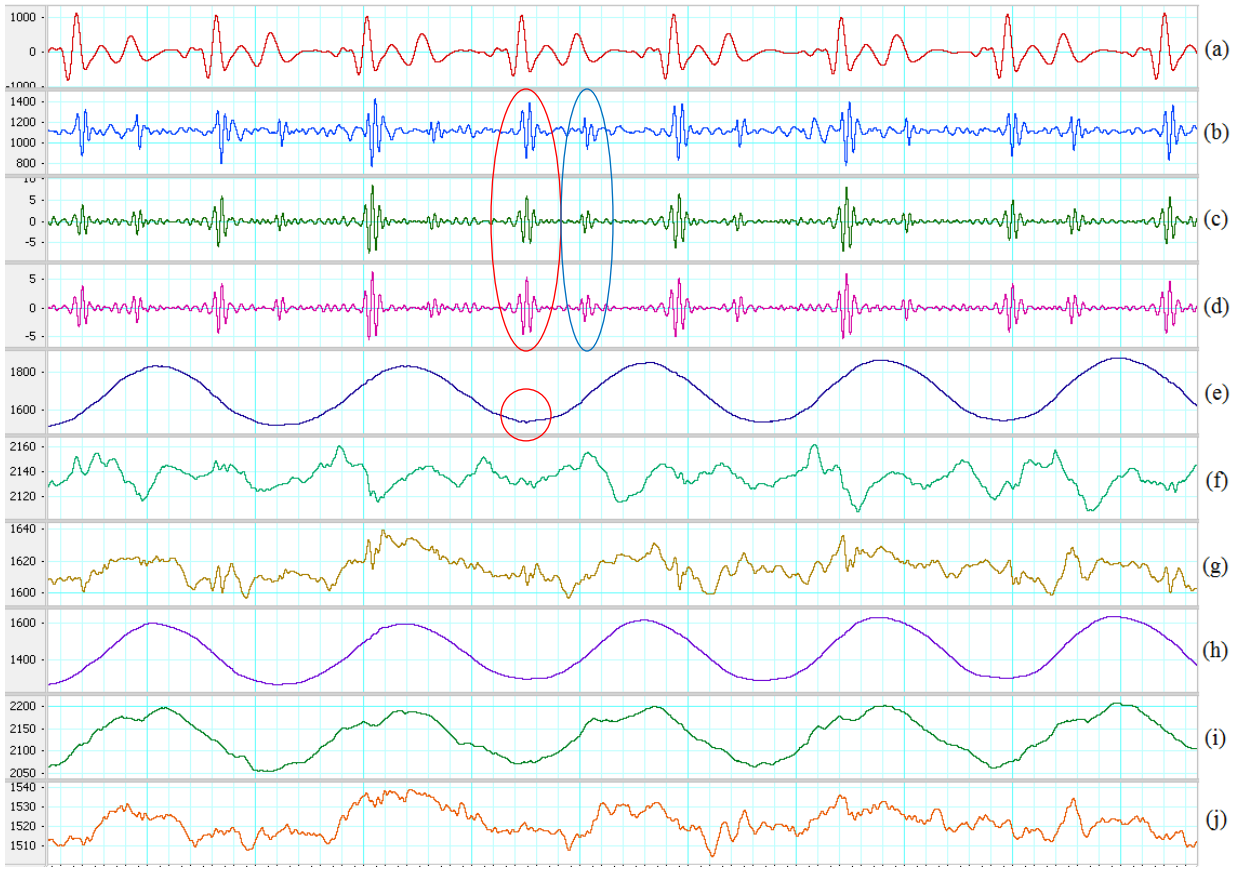

Figure 4.20 Two *diagonal* sensors with digital processing on gentle movement. (a) Filtered ECG (5-20 Hz). (b) Filtered SCG with SUBTRACTOR (*subtraction*). (c) Filtered *total acceleration*. (d) Filtered *z-axis acceleration*. Red oval indicates a recognized systole. Blue oval indicates a determined diastole. (e) First sensor z-axis. Red circle indicates a small SCG signal. (f) First sensor y-axis. (g) First sensor x-axis. (h) Second sensor z-axis. (i) Second sensor y-axis. (j) Second sensor x-axis.

4.2.3.2 Coping with walking motion

Both equations cannot totally get rid of walking motion on the data sets, but they suppress the noise better on some portions comparing to the SUBTRACTOR. Examples can be seen in the fifth cardiac period which are indicated by the green ovals in Figure 4.21(b)(c)(d) and 4.22(b)(c)(d).

For the *diagonal* placement, outputs of the SUBTRACTOR and two equations are quite the same. It means that the two equations do not reduce much noise than the SUBTRACTOR in this position. Table 4.9 shows the average measurements on all recognized systoles and diastoles of

the output signals using two equations of digital processing on walking data. Although the number of detected systoles and diastoles are mostly the same, the SNRs of both *total acceleration* and *z-axis acceleration* are virtually better than using the SUBTRACTOR only. The best results of SNRs belongs to *z-axis acceleration* on *horizontal* and *vertical* placements and *total acceleration* on *diagonal* placement. However, the SNR values of *z-axis acceleration* on *horizontal* and *vertical* placement are much greater than the *total acceleration* on *diagonal* placement. Hence, *z-axis acceleration* still has the best performance overall.

Table 4.9 Signal measurements of two sensors with digital processing on walking motion

Sensor placements and methods		Total systole	Detected systole	Total diastole	Detected diastole	Average detected systolic Vpp (mV)	Average detected diastolic Vpp (mV)	Average distorted Vpp (mV)	Average detected systolic SNR	Average detected diastolic SNR
Two *horizontal* sensors	Subtraction	**7**	5	**7**	7	524.4	272.8	427.2	4.8	0.7
	Total acceleration		5		7	6.4	3.2	10.66	6	0.8
	Z-axis acceleration		7		7	6.9	3.5	4.1	9.3	2.2
Two *vertical* sensors	Subtraction	**9**	9	**8**	0	368.6	N/A	699.3	4.2	N/A
	Total acceleration		9		1	10.3	5.09	12.4	3.9	0.8
	Z-axis acceleration		9		0	5.8	N/A	8.9	11.5	N/A
Two *diagonal* sensors	Subtraction	**9**	9	**9**	4	613.4	338	1478.7	0.2	0.07
	Total acceleration		9		3	13.7	4.9	15.9	3.9	0.09
	Z-axis acceleration		9		3	10.1	4.4	20.7	1.1	0.04

The red and blue ovals show determinable systoles and diastoles in Figure 4.21(b)(c)(d), 4.22(b)(c)(d) and 4.23(b)(c)(d). There are small SCG signals on the z-axis signal which are indicated as red circles in Figure 4.21(e), 4.22(e) and 4.23(e).

Figure 4.21 Two *horizontal* sensors with digital processing on walking motion. (a) Filtered ECG (5-20 Hz). (b) Filtered SCG with SUBTRACTOR (*subtraction*). (c) Filtered *total acceleration*. (d) Filtered *z-axis acceleration*. Red ovals indicate recognized systoles. Blue ovals indicate determined diastoles. Orange ovals show results of different response. Green ovals illustrate better noise suppression. (e) First sensor z-axis. Red circle indicates a small SCG signal. (f) First sensor y-axis. (g) First sensor x-axis. Brown oval indicates high-energy portion of walking. (h) Second sensor z-axis. (i) Second sensor y-axis. (j) Second sensor x-axis. Brown oval indicates high-energy portion of walking.

Figure 4.22 Two *vertical* sensors with digital processing on walking motion. (a) Filtered ECG (5-20 Hz). (b) Filtered SCG with SUBTRACTOR (*subtraction*). (c) Filtered *total acceleration*. (d) Filtered *z-axis acceleration*. Red ovals indicate recognized systoles. Blue ovals indicate determined diastoles. Orange ovals show results of different response. Green ovals illustrate better noise suppression. (e) First sensor z-axis. Red circle indicates a small SCG signal. (f) First sensor y-axis. (g) First sensor x-axis. Brown oval indicates high-energy portion of walking. (h) Second sensor z-axis. (i) Second sensor y-axis. (j) Second sensor x-axis. Brown oval indicates high-energy portion of walking.

Figure 4.23 Two *diagonal* sensors with digital processing on walking motion. (a) Filtered ECG (5-20 Hz). (b) Filtered SCG with SUBTRACTOR (*subtraction*). (c) Filtered *total acceleration*. (d) Filtered *z-axis acceleration*. Red ovals indicate recognized systoles. Blue ovals indicate determined diastoles. Orange ovals show results of different response. (e) First sensor z-axis. Red circle indicates a small SCG signal. (f) First sensor y-axis. (g) First sensor x-axis. Brown oval indicates high-energy portion of walking. (h) Second sensor z-axis. (i) Second sensor y-axis. (j) Second sensor x-axis. Brown oval indicates high-energy portion of walking.

4.2.4 Fusion processing of two accelerometers

In subpart 4.2.4.1, the performance of fusion processing scoping mild movement with three ways of sensor placement is discussed. In the subpart 4.2.4.2, the same procedure is studied but coping with walking motion.

4.2.4.1 Coping with gentle motion

Although the idea of changing gain is to avoid the saturation with maximum output swing, the noise is added more in some portions which reduces several detected systoles and diastoles even with gentle motion. The transparent green rectangles in Figure 4.24(b), Figure 4.25(b) and

Figure 4.26(b) illustrate the periods which are reduced gain after a detection of saturation. In those regions, the diastoles are detectable and the noise level is lower than other regions. The gain then increases slowly which may introduce high-level noises which are indicated by green ovals in Figure 4.24(b), Figure 4.25(b) and Figure 4.26(b). The average Vpp of detected systoles and diastoles in Table 4.10 are quite similar and close to 1.9 V of the method using one accelerometer. The average SNRs of identified systoles may be generally a bit higher than using fixed-gain SUBTRACTOR, but the average SNRs of diastoles are much lower compared to the fixed-gain SUBTRACTOR. The introduced noise in some portions when changing the gain can be the reason. The average noise still has high amplitude which would lead to false results in detection.

Table 4.10 Signal measurements of using two sensors with AGC on gentle motion

Sensor placements	Total systole	Detected systole	Total diastole	Detected diastole	Average detected systolic Vpp (mV)	Average detected diastolic Vpp (mV)	Average distorted Vpp (mV)	Average detected systolic SNR	Average detected diastolic SNR
Two *horizontal* sensors	9	9	9	5	2017.3	573	1078	52.6	2.8
Two *vertical* sensors	8	8	8	8	2234.6	569	592.7	36	1.6
Two *diagonal* sensors	9	9	8	8	1949.3	557.6	629	43.7	2.3

The red and blue ovals depict determined systoles and diastoles in Figure 4.24(b), 4.25(b) and 4.26(b). There are also small SCG signals on z-axis signal which are indicated as red circles in Figure 4.24(c), 4.25(c) and 4.26(c).

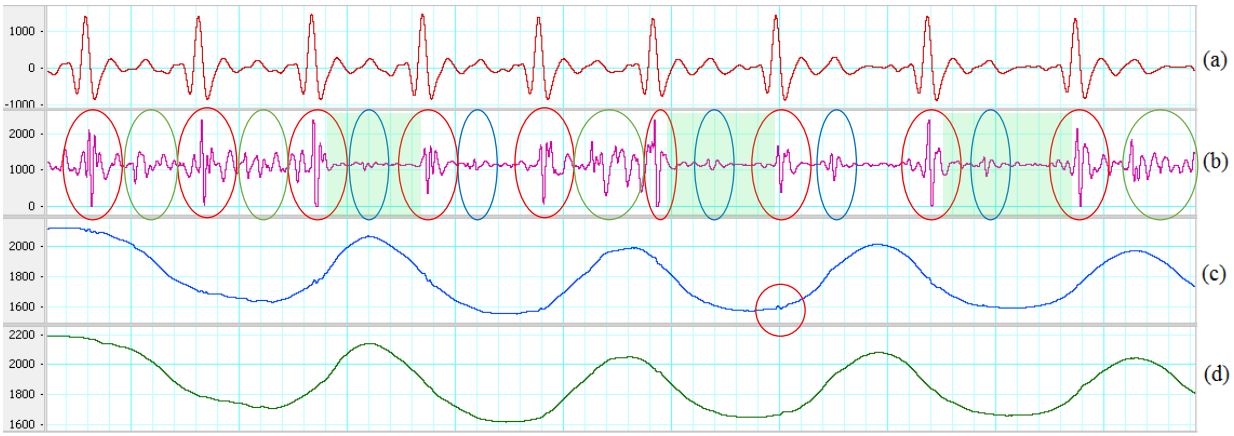

Figure 4.24 Two *horizontal* sensors with AGC on gentle motion. (a) Filtered ECG (5-20 Hz). (b) Filtered SCG (20-50 Hz). Green ovals show the introduced noise. Red ovals indicate recognized systoles. Blue ovals indicate determined diastoles. Transparent green rectangles are periods with reduced gain after a detected saturation. (c) First sensor z-axis. Red circle indicates a small SCG signal. (d) Second sensor z-axis.

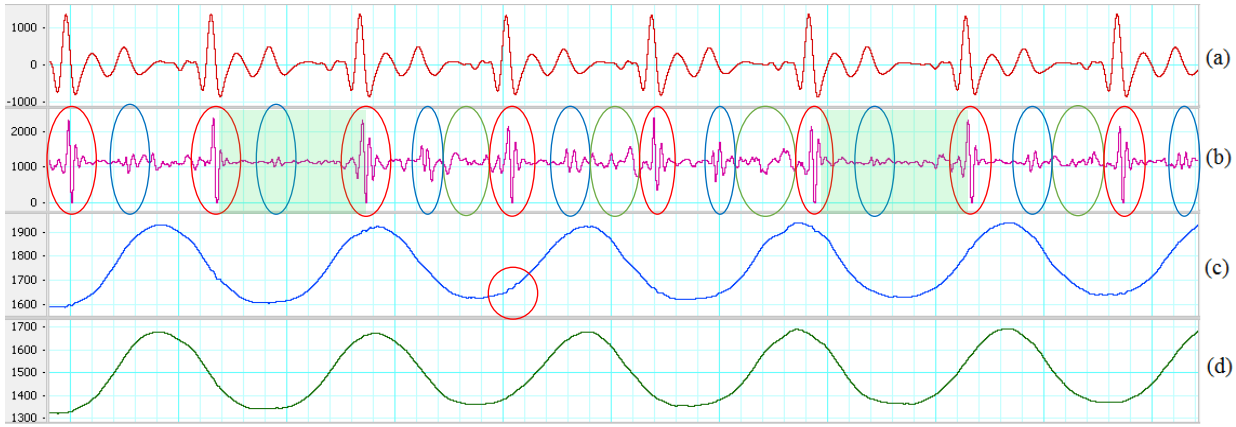

Figure 4.25 Two *vertical* sensors with AGC on gentle motion. (a) Filtered ECG (5-20 Hz). (b) Filtered SCG (20-50 Hz). Green ovals show the introduced noise. Red ovals indicate recognized systoles. Blue ovals indicate determined diastoles. Transparent green rectangles are periods with reduced gain after a detected saturation. (c) First sensor z-axis. Red circle indicates a small SCG signal. (d) Second sensor z-axis.

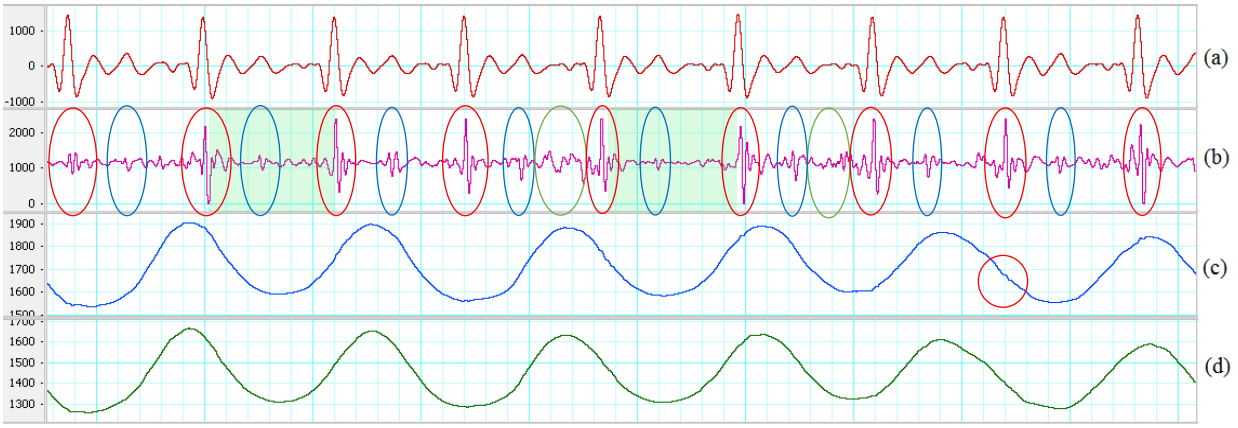

Figure 4.26 Two *diagonal* sensors with AGC on gentle motion. (a) Filtered ECG (5-20 Hz). (b) Filtered SCG (20-50 Hz). Green ovals show the introduced noise. Red ovals indicate recognized systoles. Blue ovals indicate determined diastoles. Transparent green rectangles are periods with reduced gain after a detected saturation. (c) First sensor z-axis. Red circle indicates a small SCG signal. (d) Second sensor z-axis.

4.2.4.2 Coping with walking motion

The same configuration of AGC on the SUBTRACTOR decreases even more number of detected systoles and diastoles on walking motion. The introduced noise of the AGC method combining with walking motion increase significant noise level at the output. The transparent green rectangles in Figure 4.27(b), Figure 4.28(b) and Figure 4.29(b) indicate the reduced-gain periods. In those regions, the noise level is much lower than the other regions.

According to Table 4.11, the average Vpp of all detected systoles and diastoles do not improve considerably compared to the fixed-gain SUBTRACTOR, and the mean of their SNRs are greatly smaller than the fixed-gain SUBTRACTOR in overall. The average noise levels are also much higher than fixed-gain SUBTRACTOR on walking motion.

The red and blue ovals illustrate the recognized systoles and diastoles in Figure 4.27(b), 4.28(b) and 4.29(b). There are also small SCG signals on z-axis signals which are indicated as red circles in Figure 4.27(c), 4.28(c) and 4.29(c).

Table 4.11 Signal measurements of using two sensors with AGC on walking motion

Sensor placements	Total systole	Detected systole	Total diastole	Detected diastole	Average detected systolic Vpp (mV)	Average detected diastolic Vpp (mV)	Average distorted Vpp (mV)	Average detected systolic SNR	Average detected diastolic SNR
Two *horizontal* sensors	8	6	8	6	1355.5	469.6	1918.4	24.5	0.8
Two *vertical* sensors	8	2	7	7	804	368.4	1870.1	0.07	0.6
Two *diagonal* sensors	9	5	8	4	468	322	2083.2	0.8	0.3

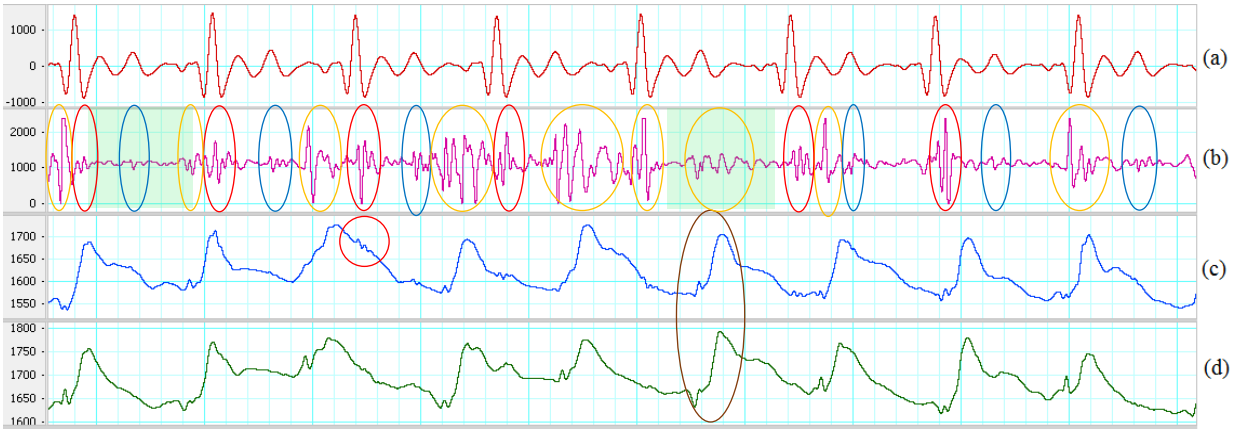

Figure 4.27 Two *horizontal* sensors with AGC on walking motion. (a) Filtered ECG (5-20 Hz). (b) Filtered SCG (20-50 Hz). Orange ovals show results of different response and introduced noise. Red ovals indicate recognized systoles. Blue ovals indicate detected diastoles. Transparent green rectangles are periods with reduced gain after a detected saturation. (c) First sensor z-axis. Red circle indicates a small SCG signal. (d) Second sensor z-axis.

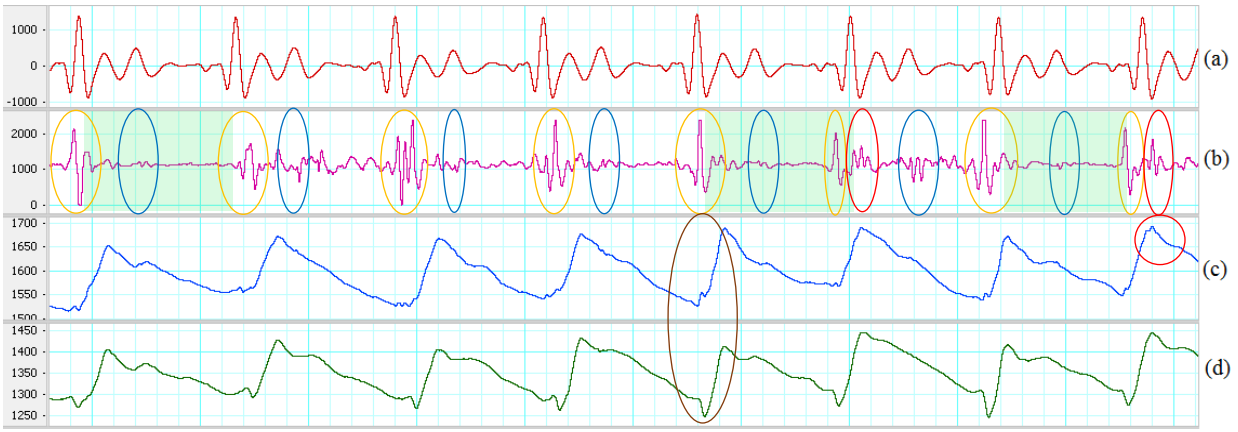

Figure 4.28 Two *vertical* sensors with AGC on walking motion. (a) Filtered ECG (5-20 Hz). (b) Filtered SCG (20-50 Hz). Orange ovals show results of different response and introduced noise. Red ovals indicate recognized systoles. Blue ovals indicate detected diastoles. Transparent green rectangles are periods with reduced gain after a detected saturation. (c) First sensor z-axis. Red circle indicates a small SCG signal. (d) Second sensor z-axis.

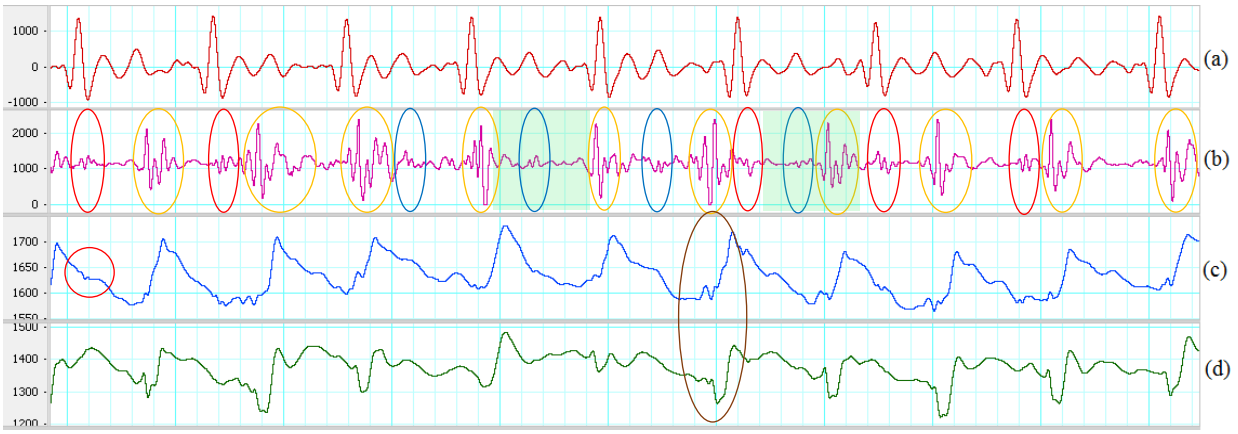

Figure 4.29 Two *diagonal* sensors with AGC on walking motion. (a) Filtered ECG (5-20 Hz). (b) Filtered SCG (20-50 Hz). Orange ovals show results of different response and introduced noise. Red ovals indicate recognized systoles. Blue ovals indicate detected diastoles. Transparent green rectangles are periods with reduced gain after a detected saturation. (c) First sensor z-axis. Red circle indicates a small SCG signal. (d) Second sensor z-axis.

4.3 Systolic and Diastolic Phase Detection

The digital processing is much simpler in configuration than analog and fusion processing and the performance is also better. In addition, the results of three placements of sensors are not significantly different while the *horizontal* placement using only one flexible band to keep all sensors on the chest which is easy way to set up on the subjects. Therefore, the detection part applies only on stationary data sets using two *horizontal* accelerometers and digital processing. Three equations were used in the digital processing again are re-written for easier to follow:

$$\text{TOTAL\_ACC} = \sqrt{(x_1 - 1650)^2 + (y_1 - 1650)^2 + (z_1 - 1650)^2} \quad (4.1)$$

where x_1, y_1, z_1 are the data of three-axis of one accelerometer which was placed close to the heart and had strong SCG signal with motion. Because the accelerometers are powered at 3.3V, the zero-acceleration point is at the center which is 1.65V for an equivalent of 1650 in ADC data.

$$\text{TOTAL\_ACC} = \sqrt{(x_1 - x_2)^2 + (y_1 - y_2)^2 + (z_1 - z_2)^2} \quad (4.2)$$

where x_1, y_1, z_1 are the data of three-axis of the first accelerometer, and x_2, y_2, z_2 are the data of three-axis of the second accelerometer.

$$\text{Z\_ACC} = \text{abs}\,(z_1 - z_2) \quad (4.3)$$

where abs is the absolute function, and z_1, z_2 are the z-axis data of two accelerometers.

The ECG is used as standard timing marker to locate and evaluate the output signal after removing motion noise. The ECG is applied a zero-phase filtering in range 5-15 Hz to retain the QRS complex and timing for comparison. However, the data of accelerometer has no delay due to signals are fed directly into the DAQ while ECG has a small delay of 58 ms because of the analog amplification and filtration. Hence, all ECG data are shifted ahead 58 samples to compensate for the delay.

The SCG filtered with bandpass (20-50 Hz) is manually annotated the position of systolic phases by locating the AO peaks and diastolic phases by the MO peaks. The manual annotation is also referenced to the ECG timing to maximize the accuracy [56]. The AO point is the peak of the upward slope starting by the IM point which is the nadir of the downward slope following by

the QRS complex. The MO point is the second nadir of the downward slope following the AC point which is a sharp down steepness near the end of the T wave of ECG.

The error rate and the missing rate between the results processed by the algorithms and by the manual annotation are recorded and compared. The error rate is calculated based on the location of each systole or diastole of automatic detection methods and searches backward and forward within an interval of 70 ms called tolerance. If there is one manual annotated systole or diastole inside that range, that detected systole or diastole will be marked as correct. If not, it will be marked as fault; and an error counter will increase one unit. Then, the total of error count was compared with the total manual annotated systoles or diastoles to obtain the error rate. The missing rate is calculated based on the location of each systole or diastole of manual annotation and look backward and forward within the same tolerant interval. If there is one automatic detected systole or diastole, that manual annotated systole or diastole will be marked as detected one. If not, it will be marked as missing; and a missing counter will increase one. After that, the total of missing count is compared with the total manual annotated systoles or diastoles to obtain the missing rate. The calculation times are also measured to estimate the performance of the two algorithms.

Table 4.12 shows the results of eight subjects including the error rate and the missing rate of both methods using Equation (3.3) which is total acceleration of only one sensor. Based on the average of eight subjects, the mean error and missing rates is under 4 % for systolic detection and 9 % for diastolic detection. The errors and missing rate of detection of the moving average method is a bit better than interpolation method. However, both methods have higher error and missing rate of diastolic detection than systolic detection. The moving average has an excellent result on subject 1. Subject 8 is a special case who has very weak diastolic signal on one accelerometer, so it causes the high error and missing rate of diastolic detection of both algorithms.

When applying Equation (3.1) which is *total acceleration* of two sensors in moving average threshold and interpolation methods, the results are virtually much better than only one accelerometer except for the special case – subject 8. Table 4.13 indicates the missing rates of systoles of moving average threshold and interpolation method including subject 8 are as twice as higher than one accelerometer in Table 4.12. The reason is when combining all data of two

sensors of subject 8, the energy levels of diastoles are sometimes higher than systoles which make moving average threshold method cannot work well. However, the error rates of diastoles of moving average threshold and interpolation methods including subject 8 decrease around twice.

When applying Equation (3.2) which is *z-axis acceleration* of two sensors in moving average threshold and interpolation methods, the results are quite similar with *total acceleration* and better than only one accelerometer also except the special case – subject 8. Table 4.14 illustrates the missing rates of systoles of moving average threshold and interpolation methods with subject 8 increase while the error rates of diastoles of both methods including subject 8 decrease comparing to one accelerometer in Table 4.12.

The average calculation time of the moving average algorithm is 0.0752 second while the interpolation algorithm spends the average time of 0.0835 second on the same one-minute length of data. The reason is the interpolation technique required more calculation to interpolate all query points from the peaks, so it causes a bit longer time to run comparing with moving average method.

Table 4.12 The error and missing rates of moving average threshold and interpolation algorithms with Equation (3.3) on eight subjects.

Sub-jects	Manual				Moving average				Interpolation			
	Heart rate	S:D ratio	Total Sys.	Total Dias.	Systole (%)		Diastole (%)		Systole (%)		Diastole (%)	
					Error	Miss	Error	Miss	Error	Miss	Error	Miss
1	78.7±2.7	0.50±0.06	84	84	0	0	0	0	0	1.2	0	1.2
2	88.7±3.8	0.55±0.09	90	90	0	4.4	4.4	8.8	1.1	3.3	4.4	6.6
3	75.2±2.9	0.57±0.09	76	77	1.3	0	1.3	1.3	0	1.3	0	2.6
4	98.9±4.3	0.65±0.10	100	100	0	0	8	8	0	1	5	6
5	76.4±4.3	0.55±0.04	80	79	5	1.2	5	1.2	5	7.5	5	6.3
6	79.7±2.3	0.67±0.10	84	84	2.3	14.2	5.9	17.8	4.7	7.1	7.1	9.5
7	70.6±4.5	0.53±0.12	72	73	4.1	0	5.4	2.7	5.5	0	6.8	2.7
8	102.0±3.2	0.72±0.11	105	106	0	3.8	20.7	26.4	1.9	4.7	30.1	33.9
avg	83.77	0.59	76.8	77.0	1.59	2.95	6.34	8.28	2.3	3.26	7.3	8.6
σ	11.52	0.07	11.4	11.4	2	4.8	6.3	9.3	2.4	2.8	9.6	10.5
average without subject 8					1.8	2.8	4.3	5.7	2.3	3.1	4.0	5.0
σ without subject 8					2.1	5.3	2.8	6.4	2.6	3.1	2.9	2.9

Table 4.13 The error and missing rates of moving average threshold and interpolation algorithms with equation (3.1) on eight subjects.

Sub-jects	Manual				Moving average				Interpolation			
	Heart rate	S:D ratio	Total Sys.	Total Dias.	Systole (%)		Diastole (%)		Systole (%)		Diastole (%)	
					Error	Miss	Error	Miss	Error	Miss	Error	Miss
1	78.7±2.7	0.50±0.06	84	84	0	0	1.1	1.1	1.1	1.1	2.3	2.3
2	88.7±3.8	0.55±0.09	90	90	2.2	3.3	2.2	3.3	1.1	3.3	1.1	3.3
3	75.2±2.9	0.57±0.09	76	77	1.3	0	1.3	1.3	2.6	1.3	2.6	2.6
4	98.9±4.3	0.65±0.10	100	100	0	0	5	5	0	1	1	2
5	76.4±4.3	0.55±0.04	80	79	0	0	0	0	1.2	2.5	1.2	1.2
6	79.7±2.3	0.67±0.10	84	84	0	0	1.1	1.1	0	2.3	1.2	3.5
7	70.6±4.5	0.53±0.12	72	73	6.9	4.1	9.5	8.2	5.5	4.1	8.2	8.2
8	102.0±3.2	0.72±0.11	105	106	3.8	58	3.7	58.4	13.3	25.7	13.2	26.4
avg	83.77	0.59	76.8	77.0	1.78	8.18	2.99	9.8	3.1	5.16	3.85	6.19
σ	11.52	0.07	11.4	11.4	2.5	20.2	3.1	19.8	4.5	8.4	4.5	8.4
Average without subject 8					1.2	1.1	2.4	2.7	1.2	2.3	2.2	3.5
σ without subject 8					2.6	2.1	3.6	3.4	3.1	1.5	4.0	2.9

Table 4.14 The error and missing rates of moving average threshold and interpolation algorithms with equation (3.2) on eight subjects.

Sub-jects	Manual				Moving average				Interpolation			
	Heart rate	S:D ratio	Total Sys.	Total Dias.	Systole (%)		Diastole (%)		Systole (%)		Diastole (%)	
					Error	Miss	Error	Miss	Error	Miss	Error	Miss
1	78.7±2.7	0.50±0.06	84	84	0	0	0	0	0	1.2	0	1.2
2	88.7±3.8	0.55±0.09	90	90	0	2.2	0	2.2	0	2.2	0	2.2
3	75.2±2.9	0.57±0.09	76	77	1.3	0	1.3	1.3	0	1.3	0	2.6
4	98.9±4.3	0.65±0.10	100	100	0	0	5	5	0	1	3	4
5	76.4±4.3	0.55±0.04	80	79	0	0	0	0	0	2.5	0	1.2
6	79.7±2.3	0.67±0.10	84	84	0	0	1.1	1.1	0	2.3	1.2	3.5
7	70.6±4.5	0.53±0.12	72	73	6.9	5.5	9.5	9.5	8.3	5.5	10.9	9.5
8	102.0±3.2	0.72±0.11	105	106	5.7	58	5.6	58.4	16.1	29.5	16	30.1
avg	83.77	0.59	76.8	77.0	1.74	8.21	2.81	9.69	3.1	5.69	3.89	6.79
σ	11.52	0.07	11.4	11.4	2.9	20.2	3.5	19.9	6.0	9.7	6.1	9.8
average without subject 8					1.5	1.1	2.9	2.9	1.6	2.2	2.5	3.3
σ without subject 8					2.5	1.8	3.3	2.9	1.9	1.2	2.6	2.3

Figure 4.30 and Figure 4.31 depict how the length of average windows and scaler value are chosen based on the lowest average error and missing rates. The average rates were calculated on error and missing rates of eight subjects by varying the average windows size from 3 to 48 samples and the scaler value is from 1 to 1.4. The best window size is 3 samples, and the best scaler value is 1.1.

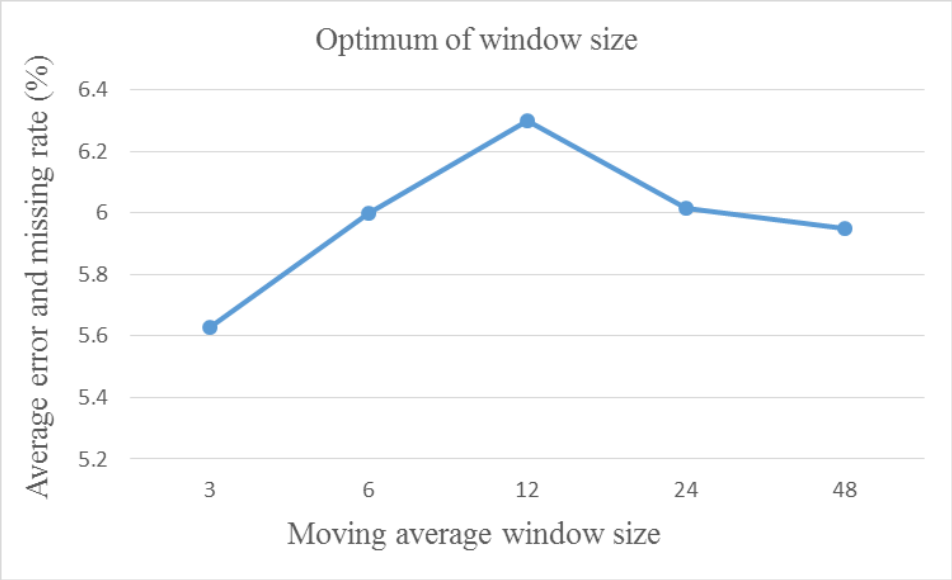

Figure 4.30 The optimum of window size for moving average threshold on eight subjects.

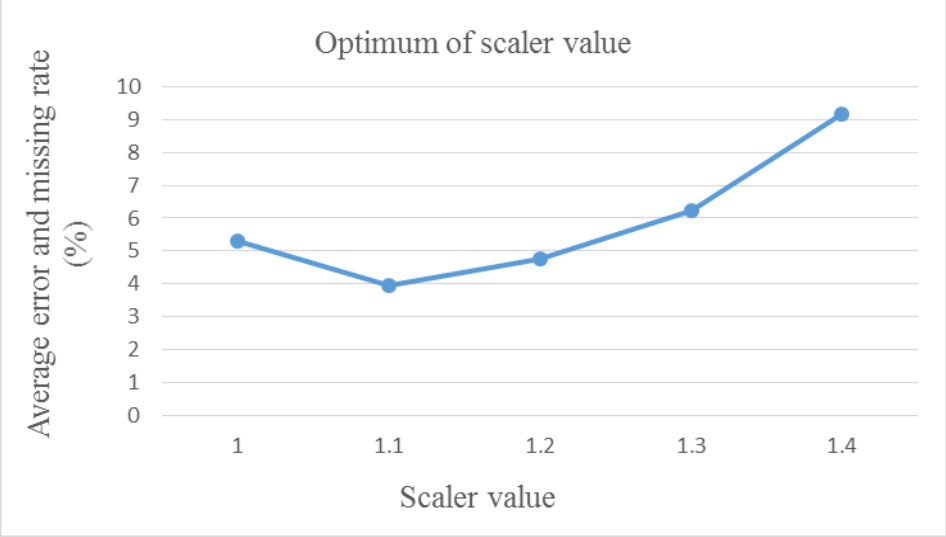

Figure 4.31 The optimum of scaler value for moving average threshold on eight subjects.

4.4 Summary of Results

With gentle motion, almost all noise removal techniques can recover most systolic and diastolic portions of the SCG signal. Although the techniques of using ADDER and using AGC have high Vpps on all three placements, in general, the SNRs of *total acceleration* and *z-axis acceleration* are much better than the others on all placements. The *total acceleration* and *z-axis acceleration* improve average systolic SNR around 2.4 times and average diastolic SNR around 3 times comparing to using only one accelerometer. Figure 4.32 illustrates the comparison of Vpps and SNRs of all sensor placements on gentle motion. Figure 4.34(a) shows the enhancements of the techniques using 2 sensors with gentle motion. Because the performance is not significant different among sensor placements when coping with type of motion, *horizontal* is selected as good position due to its ease of setting-up. The difference among sensor placements with gentle motion is illustrated in Figure 4.35.

With walking motion, all techniques cannot totally remove walking noise. The methods of using ADDER and using AGC have good Vpps on all three placements and highest systolic SNRs on *horizontal* position. The SNRs of *ADDER* and *z-axis acceleration* are mostly better than the others in all sensor positions; they enhance about 7.4 times of average systolic SNR and about 11.2 times of average diastolic SNR comparing to using one accelerometer. Figure 4.33 shows the comparison of Vpps and SNRs of all sensor placements on walking motion. Figure 4.34(b) shows the enhancements of the techniques using 2 sensors with walking motion. The performance of the horizontal placement is outstanding comparing with other positions when coping with walking motion. The difference among sensor placements with walking motion is shown in Figure 4.36. Moreover, using 2 accelerometers can increase the average number of recognizable systole and diastole on walking SCG signal to 71.3 % and 43.8 % respectively comparing to only one sensor which are 11 % and 12 %. Figure 4.37 illustrates the percentage of identified systole and diastole on walking motion.

About phase detection, Figure 4.38 shows the comparison of performance of two algorithms without the special case – subject 8. Both moving average threshold and interpolation algorithms have lower error and missing rate when applying on two sensors with *total acceleration* and *z-axis acceleration* than only one sensor. The average error and missing rate of using one sensor is 3.65 %. The average error and missing rates of *total acceleration* and *z-axis*

acceleration with moving average threshold are 1.85 % and 2.1 % respectively. The average error and missing rates of *total acceleration* and *z-axis acceleration* with interpolation are in order of 2.3 % and 2.4 %.

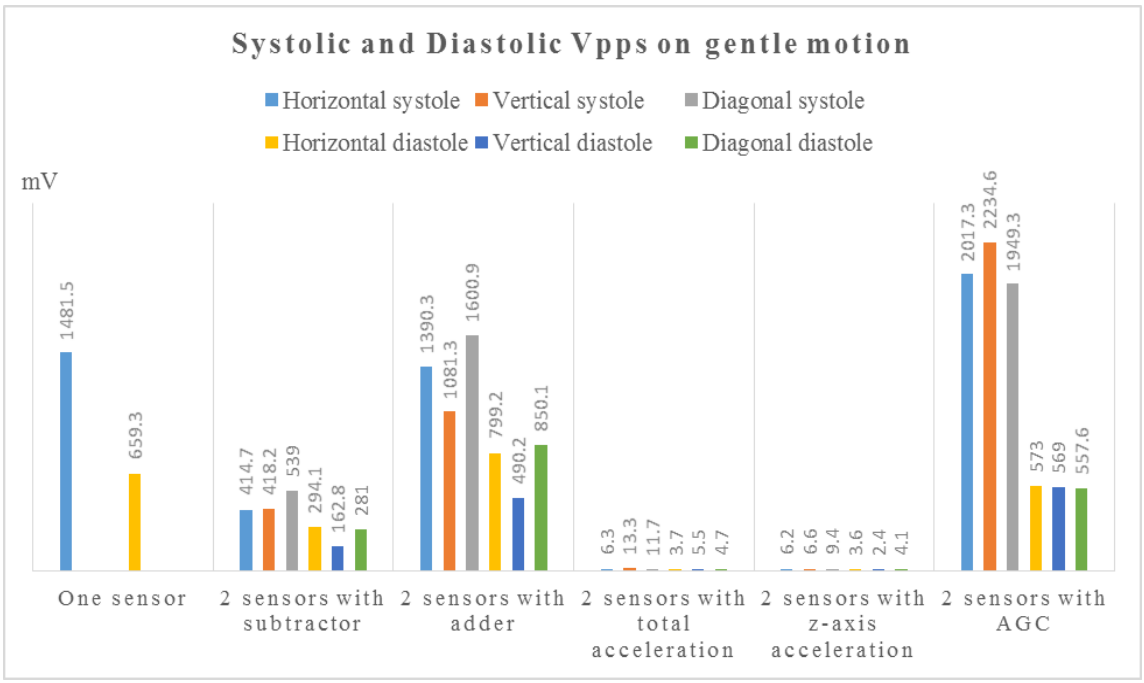

(a)

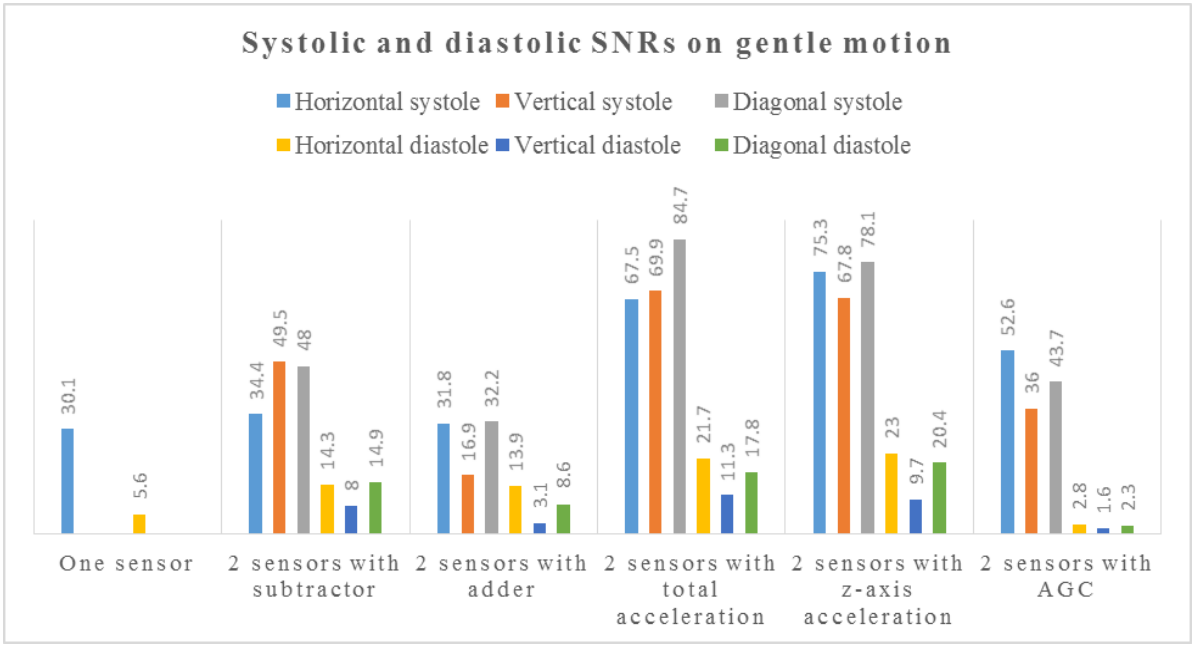

(b)

Figure 4.32 Comparison of Vpps and SNRs on gentle motion. (a) Vpps. (b) SNRs.

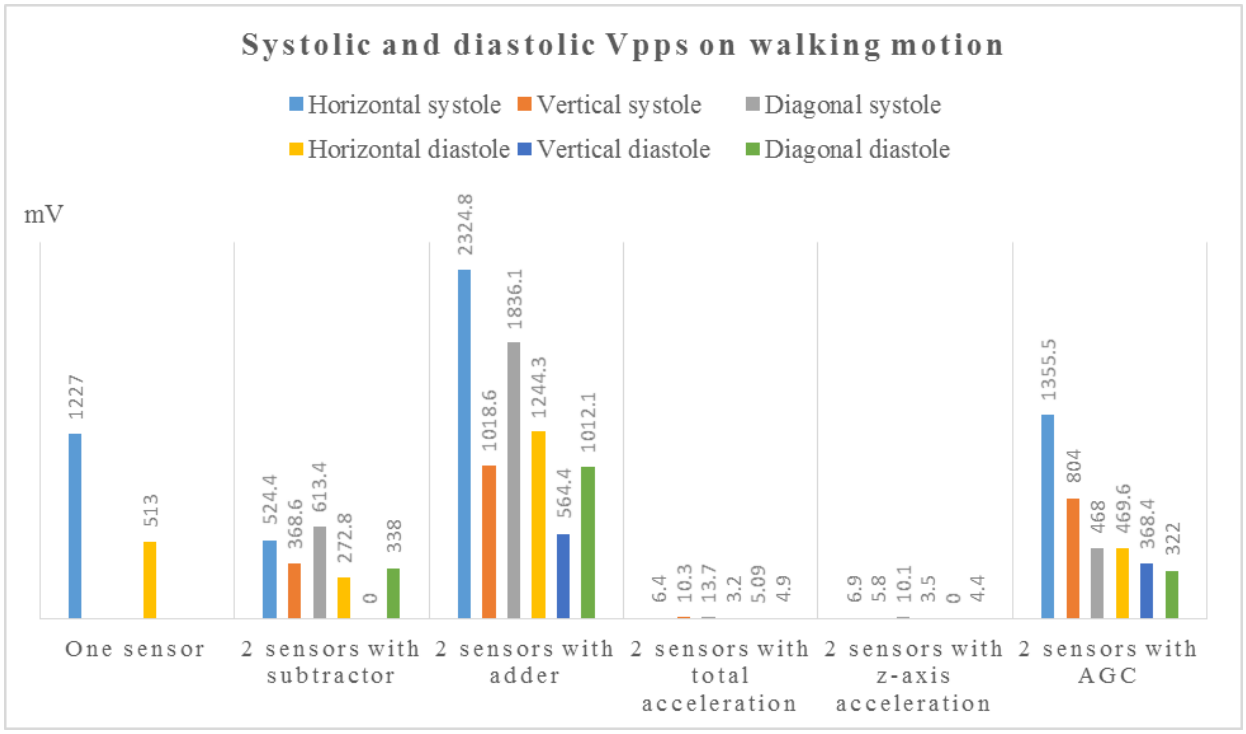

(a)

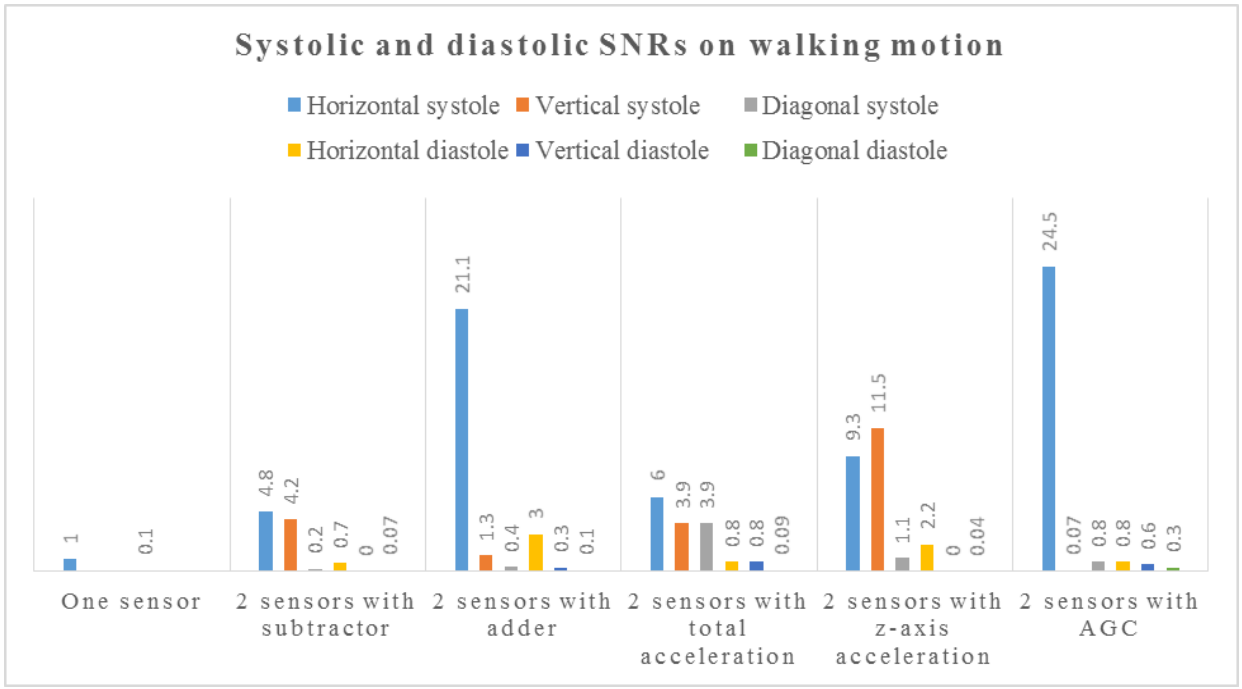

(b)

Figure 4.33 Comparison of Vpps and SNRs on walking motion. (a) Vpps. (b) SNRs.

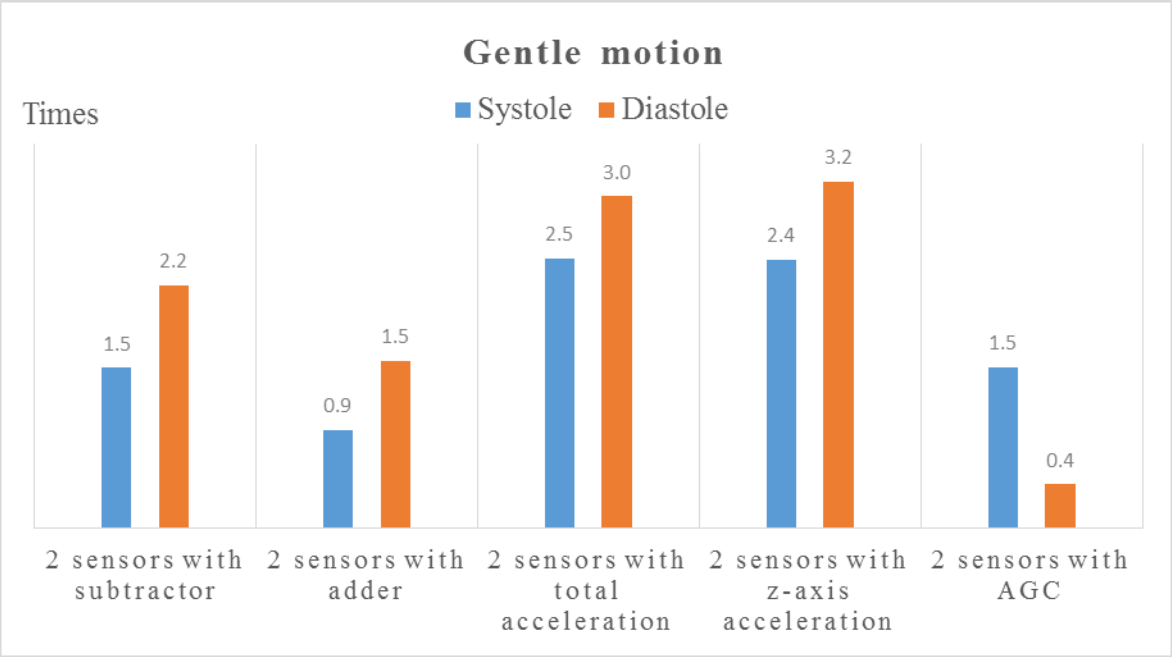

(a)

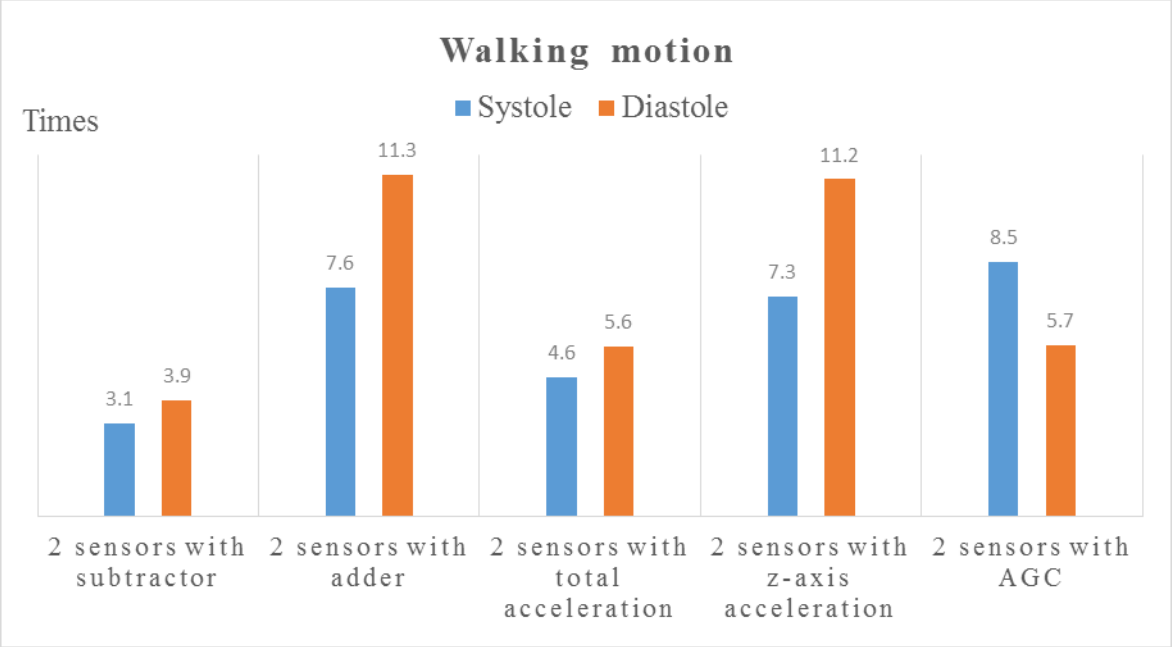

(b)

Figure 4.34 The comparison of ratios between average SNRs of one accelerometer and two accelerometers

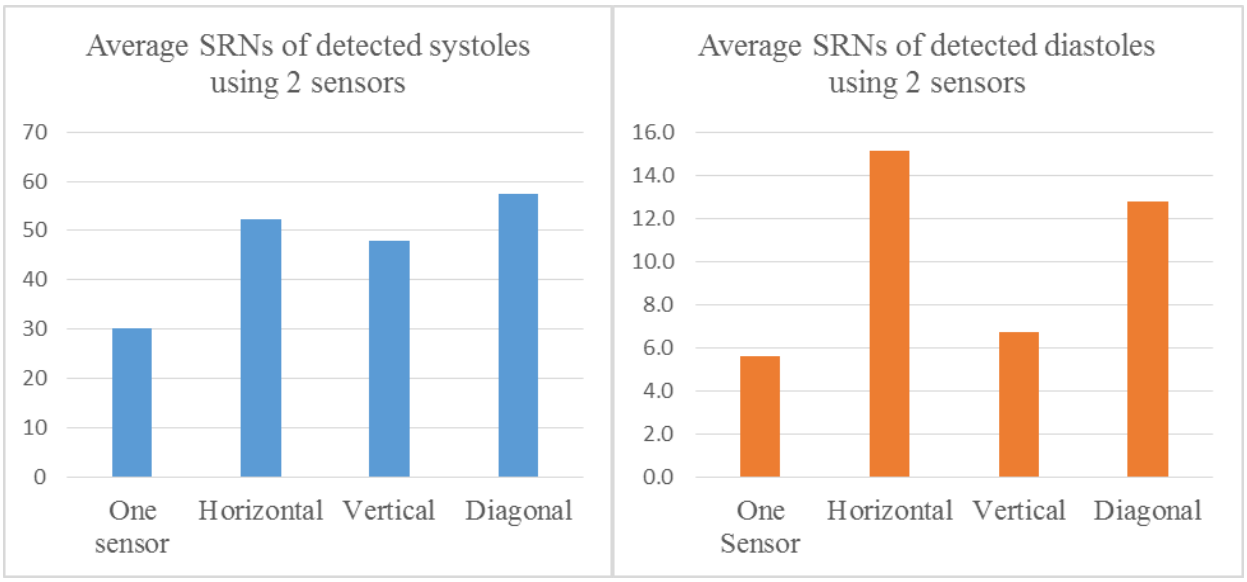

Figure 4.35 Average SRNs of detected systoles and diastoles of all techniques with gentle motion on three placements of two sensors.

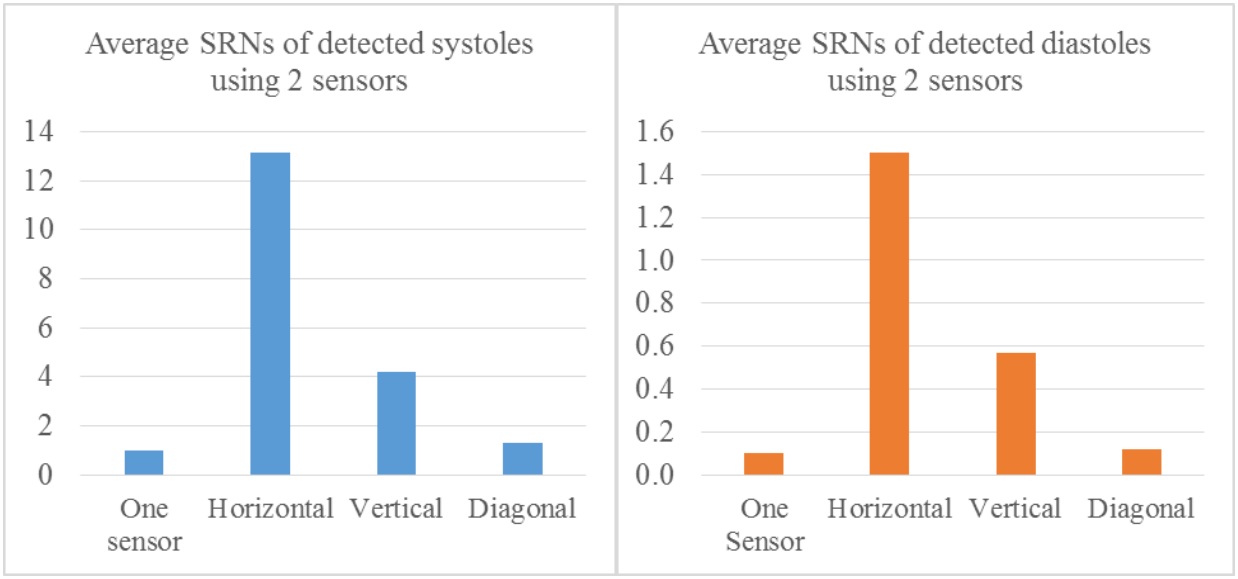

Figure 4.36 Average SRNs of detected systoles and diastoles of all techniques with walking motion on three placements of two sensors.

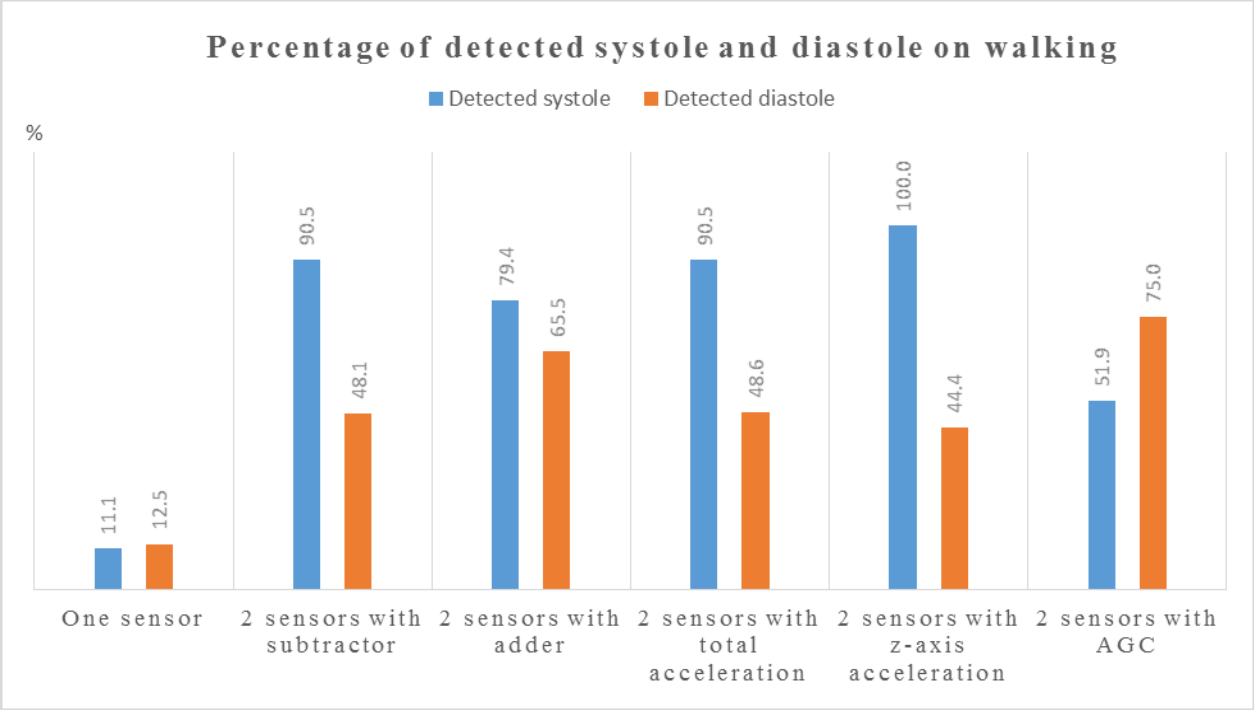

Figure 4.37 Percentage of identified systole and diastole on walking

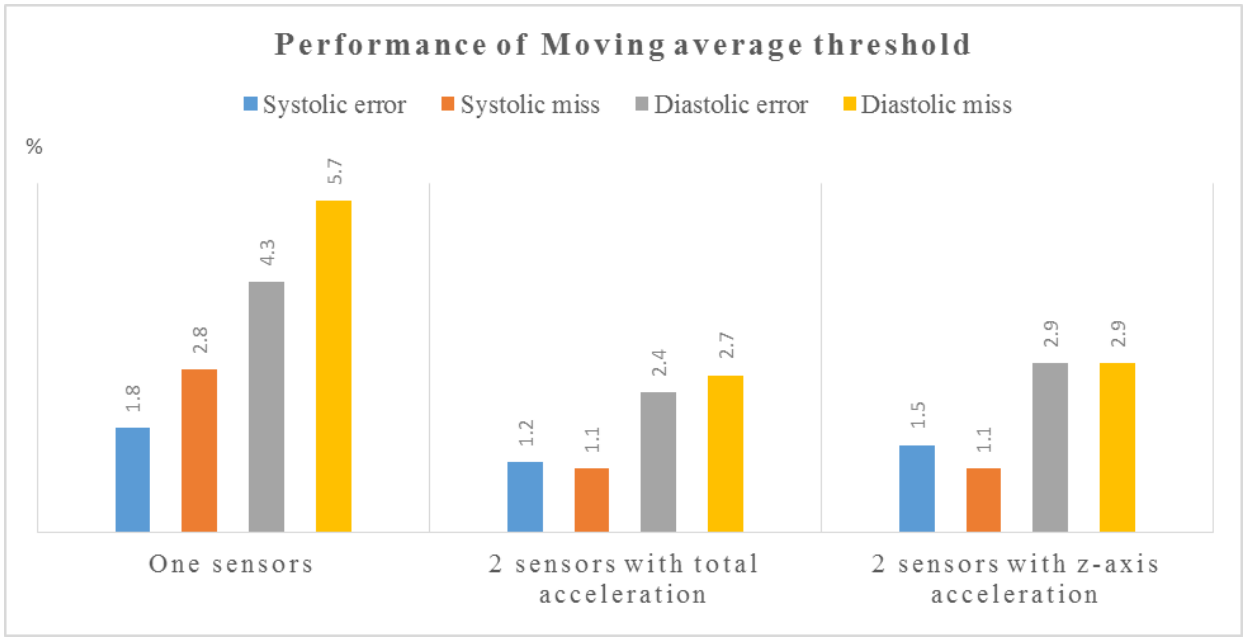

(a)

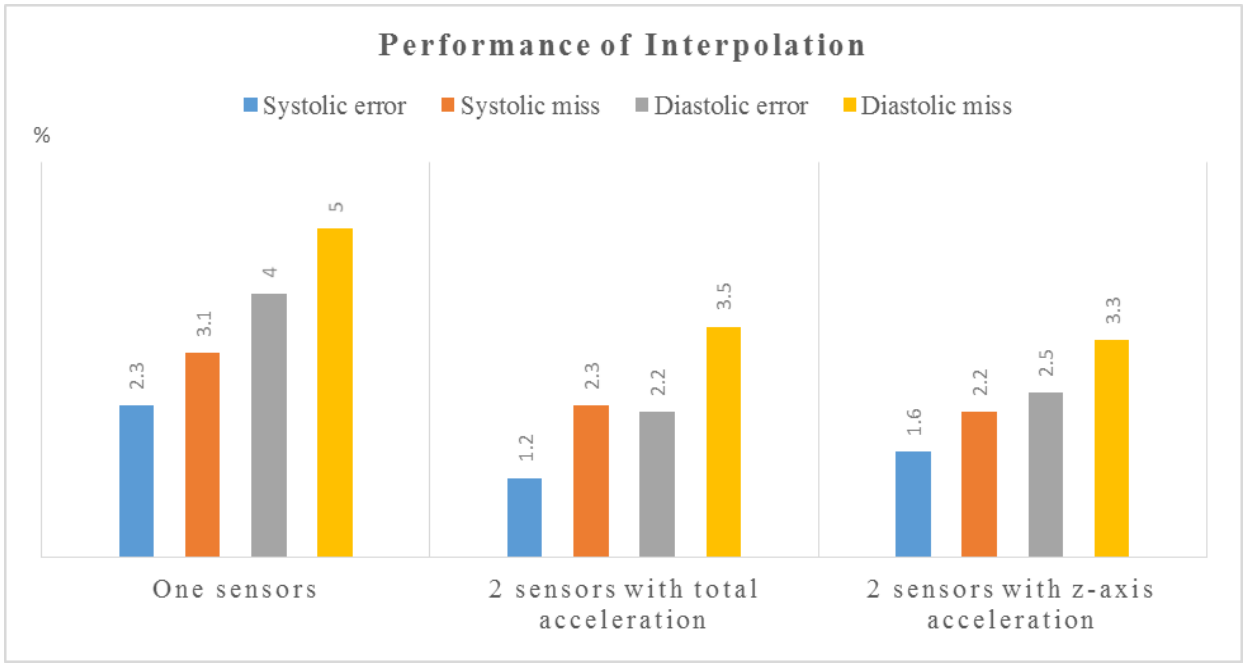

(b)

Figure 4.38 Comparison of performance of two algorithms without subject 8. (a) Moving average threshold. (b) Interpolation.

CHAPTER 5
CONCLUSION AND FUTURE WORK

In this chapter, all procedures conducting the research are summarized by a short discussion of each step. Then, possible future contributions of this work will be listed.

5.1 Summary

Heart disease is one of the most death causes in the world. To address this concern, many studies were developed to monitor and evaluate the heart performance. The main purpose of this study is also to observe the heart activities in long-term to reduce the risk of heart disease. Specifically, it studies the motion noise removal techniques using two accelerometers system on active people and detects the cardiac phases and events on SCG signal.

To achieve that, a wireless DAQ and a framework on Matlab were firstly developed to collect and analyze data with motion on eight voluntary subjects without any record of heart disease. The wireless DAQ provides good and reliable data with high resolution 16-bit and high sampling rate 1k sample-per-second in a range around 13 m indoor and more than 20 m outdoor. However, the data will be corrupted when the SNR of Wi-Fi signal drops under -93 dBm which causes packages loss. Flexibility of the Matlab framework allows the users to implement and test the algorithms in processing streams in real-time fashion. With low power consumption, the unit can continuously operate for over 5 hours with a full-charged 800 mAh rechargeable battery.

Secondly, the wireless DAQ combining with analog front-ends and algorithms on the Matlab framework were also used to examine the motion removal techniques on the subjects while they were making soft movement or walking. There are three main procedures to remove the motion noise including *analog processing*, *digital processing* and *fusion processing*. They were tested on three placements of sensors including *horizontal*, *vertical* and *diagonal* with two kinds of motion noise comprising gentle movement and walking. The less-noise bandwidth of SCG signal was also analyzed on walking and running data of five subjects which is from 20 to 50 Hz.

With gentle motion, almost all noise removal techniques can recover most systolic and diastolic portions of the SCG signal. The frequency of gentle motion is out of range of band-pass filter, so it can be removed completely. Although the techniques of using ADDER and using AGC have good Vpps on all three placements, the SNRs of *total acceleration* and *z-axis acceleration* are much better than the others on all placements. The *total acceleration* and *z-axis acceleration* improve average systolic SNR around 2 times and average diastolic SNR around 3 times comparing to using only one accelerometer. Because the performance is not significant different among sensor placements when coping with gentle motion, placing the sensor horizontally is the best as the sensor setup is very simple.

With walking motion, all techniques cannot totally remove walking noise. Although the Vpp of walking motion is smaller than the Vpp of gentle motion, the frequency of some walking portions still in the range of bandpass filter, so they are amplified and overlap some parts of the SCG signal. Again, the methods of using ADDER and using AGC have good Vpps on all three placements and highest systolic SNRs on *horizontal* position. The SNRs of ADDER and *z-axis acceleration* are still mostly better than the others in all sensor positions. The SNRs of *ADDER* and *z-axis acceleration* are generally better than the others in all sensor positions; they enhance about 7 times of average systolic SNR and about 11 times of average diastolic SNR comparing to using one accelerometer. The performance of horizontal placement is outstanding comparing with other positions when coping with walking motion.

The *total acceleration* can enhance the SNRs with gentle motion by gather all information from three axes, but with walking motion, the *total acceleration* may accumulate the noise from three axes which causes lower SNRs comparing with ADDER and *z-axis acceleration.* The SNR results with walking motion may vary due to how synchronization between high-energy portions of walking motion with systoles/diastoles. If they are in-sync either with systoles or diastoles, those portions will be distorted and unidentified. If high-energy portions of walking stay in quiescence period of output signals, both systoles and diastoles can be recognized with ECG reference.

The reasons of less effectiveness of walking motion removal might be due to different reaction of two sensors to the motion. It can be caused by the manufactured error of sensors or unaligned placement of the two sensors. The sensor reacts more similar with low-frequency

noise such as kind movement than high-frequency noise like walking, and the more the two sensors responses are different, the more the distortion appears on output signal.

Thirdly, two phase-detection algorithms were applied on stationary data sets of digital processing and *horizontal* placement of eight subjects to locate the systoles and diastoles. The total acceleration of only one sensor was also calculated for comparison purpose. Both algorithms have lower error and missing rate when applying on two sensors with *total acceleration* and *z-axis acceleration* than only one sensor. The interpolation technique required much calculation to interpolate all query points from the peaks, so it causes a bit longer time to run comparing with moving average method. The algorithms are good with less-noise signal such as gentle movement, but not with noisy signal such as walking. It should still need the ECG as timing reference for improving accuracy of phase detection with walking motion.

Finally, rely on detected systolic and diastolic phases, the event-detection algorithm searches inside intervals to locate cardiac events using two outstanding characteristics of the SCG signal. Because both methods are not too complex due to the techniques and the processing time, they can absolutely be employed in real-time applications. To employ on microcontroller, the moving average method is recommended because the interpolation function is quite complicated to be implemented in a microcontroller.

5.2 Contributions

The first contribution of this thesis is the design and construction of a low-cost and opened-structure wireless DAQ. All settings including protocol, embedded firmware and digital interfaces are controlled by user comparing to the other closed-design commercial DAQs. Commercially available DAQs are very expensive with wireless connection and do not support the modification of the core firmware for other purpose such as the AGC technique using in this thesis work (the adaptation of external amplification gain based on input saturation). The self-developed wireless DAQ has also potential to connect digital-interface sensors which cannot be achieved by a normal commercial DAQ. Another intention of the wireless DAQ is embedding all detection algorithms into the microcontroller to save power for raw data transmission and to test the wearable capability for outdoor activities.

The second contribution is the novelty of noise removal techniques using two accelerometers instead of only one as previous studies. To the best knowledge of the author, these noise removal methods using two sensors have not been yet examined. Although there are few studies worked on the data of three axes of accelerometer, they used only one accelerometer and focused on 3-D space. In this study, the combination of three axes of the two accelerometers using total acceleration was investigated and showed the enhancement in the results. In addition, the three positions of two sensors were tested to confirm which one can achieve the best quality SCG which has also not been conducted by any previous research.

The last contributions of this study are two algorithms to locate the systolic and diastolic phases on the filtered SCG using two sensors. These two algorithms differ from other algorithms in other research which requires the ECG as timing reference or uses complex techniques such as EMD or wavelet transform. EMD and wavelet transform require high computation time and cannot run in real-time mode. The proposed algorithms in this thesis are less complex and applicable to real-time application with lower error and missing rate comparing to one accelerometer method. The cardiac events detection algorithm based on the maximum slope between maxima and minima of the filtered SCG using two sensors is also first proposed.

5.3 Future work

The heart is believed to push the chest not only on the direction but also on the rotation, so to improve the performance of noise removal, the sensor fusion which combines the accelerometers and gyroscopes in only one sensor called inertial measurement unit (IMU) can be used instead of only accelerometers.

In this study, the dissimilar response from two sensors could be caused by unaligned placement which means both sensors are not placed on the same plane. To overcome this situation, a calibration procedure should be developed to compensate the different reaction of the two sensors. The fixed systolic interval in moving average threshold algorithm is working well on people have normal heartrate ranging from 80 to 90 bpm. However, there will be a problem when the heart rate goes lower or higher than that range because the systolic interval varies when the heart rate changes. To improve the overall performance, an adaptive systolic interval should be used instead of the fixed one. To do that, a regression line between the heart rate and the systolic interval should be calculated. For step 5 in the phase detection, low-pass filtering, the

cut-off frequency should also be adaptive to the heart rate to maximize accuracy. From the above regression line, the heart rate can also be divided into small ranges, then each range has a different cut-off frequency. Based on the continuous updating average heartbeat, one can apply appropriated systolic interval and low-pass cut-off frequency to increase the accuracy.

With walking motion, to improve the accuracy of phase detection, portions of walking motion with high rate of change should be tracked. When they are greater than a value which can be optimized by practice, the phase detection should avoid that segment which may be distorted by walking motion. On the other hand, the ECG components can be used as a reference to avoid noisy segments in detection step.

In the event detection, the searching intervals for cardiac events is fixed to 260 ms for systolic points and 220 ms for diastolic points which are good for people with normal heart rate ranging from 80 to 90 bpm. When the heart rate changes, the searching intervals will vary longer or shorter. Therefore, adaptive searching intervals should be designed to improve the accuracy of event detection and the performance of the algorithm.

REFERENCES

[1] World Health Organization. (2017). The top 10 causes of death. Retrieved from http://www.who.int/mediacentre/factsheets/fs310/en/

[2] Public Health Agency of Canada. (2017). Heart Disease in Canada. Retrieved from https://www.canada.ca/en/public-health/services/publications/diseases-conditions/heart-disease-canada.html

[3] Khan, M. I. G. (2005). *Heart disease diagnosis and therapy : a practical approach* (2nd ed.). Totowa, N.J.: Humana Press.

[4] Jain, P. K., & Tiwari, A. K. (2014). Heart monitoring systems—A review. *Computers in Biology and Medicine, 54*, 1-13. doi:http://dx.doi.org/10.1016/j.compbiomed.2014.08.014

[5] Wcislik, M., Pozoga, M., & Smerdzynski, P. (2015). Wireless Health Monitoring System. *IFAC-PapersOnLine, 48*(4), 312-317. doi:http://dx.doi.org/10.1016/j.ifacol.2015.07.053

[6] Augustyniak, P. (2011). Wearable wireless heart rate monitor for continuous long-term variability studies. *Journal of Electrocardiology, 44*(2), 195-200. doi:http://dx.doi.org/10.1016/j.jelectrocard.2010.11.014

[7] Di Rienzo, M., Meriggi, P., Rizzo, F., Vaini, E., Faini, A., Merati, G., . . . Castiglioni, P. (2011). A wearable system for the seismocardiogram assessment in daily life conditions. *Conf Proc IEEE Eng Med Biol Soc, 2011*, 4263-4266. doi:10.1109/IEMBS.2011.6091058

[8] Fezari, M., Rasras, R., & Emary, I. M. M. E. (2015). Ambulatory Health Monitoring System Using Wireless Sensors Node. *Procedia Computer Science, 65*, 86-94. doi:http://dx.doi.org/10.1016/j.procs.2015.09.082

[9] Sardini, E., & Serpelloni, M. (2010). Instrumented wearable belt for wireless health monitoring. *Procedia Engineering, 5*, 580-583. doi:http://dx.doi.org/10.1016/j.proeng.2010.09.176

[10] Pandian, P. S., Mohanavelu, K., Safeer, K. P., Kotresh, T. M., Shakunthala, D. T., Gopal, P., & Padaki, V. C. (2008). Smart Vest: Wearable multi-parameter remote physiological monitoring system. *Medical Engineering & Physics, 30*(4), 466-477. doi:http://dx.doi.org/10.1016/j.medengphy.2007.05.014

[11] Lee, Y.-D., & Chung, W.-Y. (2009). Wireless sensor network based wearable smart shirt for ubiquitous health and activity monitoring. *Sensors and Actuators B: Chemical, 140*(2), 390-395. doi:http://dx.doi.org/10.1016/j.snb.2009.04.040

[12] Cannon, C. P., & Khan, M. G. (2008). *Rapid ECG Interpretation*: Humana Press.

[13] Auer, R., Bauer, D. C., Marques-Vidal, P., Butler, J., Min, L. J., Cornuz, J., . . . Health, A. B. C. S. (2012). Association of major and minor ECG abnormalities with coronary heart disease events. *JAMA, 307*(14), 1497-1505. doi:10.1001/jama.2012.434

[14] Stern, S., Tzivoni, D., & Stern, Z. (1975). Diagnostic accuracy of ambulatory ECG monitoring in ischemic heart disease. *Circulation, 52*(6), 1045-1049.

[15] Zanetti, J. M., Poliac, M. O., & Crow, R. S. (1991, 23-26 Sep 1991). *Seismocardiography: waveform identification and noise analysis.* Paper presented at the [1991] Proceedings Computers in Cardiology.

[16] Wilson, R. A., Bamrah, V. S., Lindsay, J., Schwaiger, M., & Morganroth, J. (1993). Diagnostic accuracy of seismocardiography compared with electrocardiography for the anatomic and physiologic diagnosis of coronary artery disease during exercise testing. *The American Journal of Cardiology, 71*(7), 536-545. doi:http://dx.doi.org/10.1016/0002-9149(93)90508-A

[17] Salerno, D. M., & Zanetti, J. (1991). Seismocardiography for monitoring changes in left ventricular function during ischemia. *Chest, 100*(4), 991-993.

[18] Salerno, D. M., Zanetti, J. M., Green, L. A., Mooney, M. R., Madison, J. D., & Van Tassel, R. A. (1991). Seismocardiographic changes associated with obstruction of coronary blood flow during balloon angioplasty. *The American Journal of Cardiology, 68*(2), 201-207. doi:http://dx.doi.org/10.1016/0002-9149(91)90744-6

[19] Crow, R., Salerno, D. M., Hunnan, P., & Zanetti, J. M. (1991). Seismocardiography for measurement of left ventricular performance at rest and immediately post exercise. *Journal of the American College of Cardiology, 17*(2), A352. doi:http://dx.doi.org/10.1016/0735-1097(91)92374-U

[20] Libonati, J. R., Colby, A. M., Caldwell, T. M., Kasparian, R., & Glassberg, H. L. (1999). Systolic and diastolic cardiac function time intervals and exercise capacity in women. *Med Sci Sports Exerc, 31*(2), 258-263.

[21] Ovadia, M., Gear, K., Thoele, D., & Marcus, F. I. (1995). Accelerometer Systolic-Time Intervals as Fast-Response Sensors of Upright Posture in the Young. *Circulation, 92*(7), 1849-1859.

[22] Jerosch-Herold, M., Zanetti, J., Merkle, H., Poliac, L., Huang, H., Mansoor, A., . . . Wilke, N. (1999). The seismocardiogram as magnetic-field-compatible alternative to the electrocardiogram for cardiac stress monitoring. *International Journal of Cardiac Imaging, 15*(6), 523-531. doi:Doi 10.1023/A:1006364518204

[23] Korzeniowska-Kubacka, I., & Piotrowicz, R. (2002). Seismocardiography - a noninvasive technique for estimating left ventricular function. Preliminary results. *Przegl Lek, 59*(9), 774-776.

[24] Korzeniowska-Kubacka, I., Bilinska, M., & Piotrowicz, R. (2005). Usefulness of seismocardiography for the diagnosis of ischemia in patients with coronary artery disease. *Ann Noninvasive Electrocardiol, 10*(3), 281-287. doi:10.1111/j.1542-474X.2005.00547.x

[25] Iwona Korzeniowska-Kubacka, Beata Kuśmierczyk-Droszcz, Maria Bilińska, Barbara Dobraszkiewicz-Wasilewska, Krzysztof Mazurek, & Ryszard Piotrowicz. (2006). Seismocardiography - a non-invasive method of assessing systolic and diastolic left ventricular function in ischaemic heart disease. *Cardiology Journal, 13*(4), 319-324.

[26] Tavakolian, K., Khosrow-Khavar, F., Kajbafzadeh, B., Marzencki, M., Rohani, S., Kaminska, B., & Menon, C. (2012). Seismocardiographic adjustment of diastolic timed vibrations. *Conf Proc IEEE Eng Med Biol Soc, 2012*, 3797-3800. doi:10.1109/EMBC.2012.6346794

[27] Khosrow-khavar, F., Tavakolian, K., Soleimani-Nouri, M., Kaminska, B., & Menon, C. (2013). A new seismocardiography segmentation algorithm for diastolic timed vibrations. *Conf Proc IEEE Eng Med Biol Soc, 2013*, 7278-7281. doi:10.1109/EMBC.2013.6611238

[28] Tavakolian, K., Khosrow-Khavar, F., Kajbafzadeh, B., Marzencki, M., Blaber, A. P., Kaminska, B., & Menon, C. (2013). Precordial acceleration signals improve the performance of diastolic timed vibrations. *Medical Engineering & Physics, 35*(8), 1133-1140. doi:http://dx.doi.org/10.1016/j.medengphy.2012.12.001

[29] Di Rienzo, M., Vaini, E., Castiglioni, P., Merati, G., Meriggi, P., Parati, G., . . . Rizzo, F. (2013). Wearable seismocardiography: Towards a beat-by-beat assessment of cardiac mechanics in ambulant subjects. *Autonomic Neuroscience, 178*(1–2), 50-59. doi:https://doi.org/10.1016/j.autneu.2013.04.005

[30] Becker, M., Roehl, A. B., Siekmann, U., Koch, A., de la Fuente, M., Roissant, R., . . . Hein, M. (2014). Simplified detection of myocardial ischemia by seismocardiography. Differentiation between causes of altered myocardial function. *Herz, 39*(5), 586-592. doi:10.1007/s00059-013-3851-x

[31] Shafiq, G., Tatinati, S., & Veluvolu, K. C. (2016, 16-20 Aug. 2016). *Automatic annotation of peaks in seismocardiogram for systolic time intervals.* Paper presented at the 2016 38th

Annual International Conference of the IEEE Engineering in Medicine and Biology Society (EMBC).

[32] Shafiq, G., Tatinati, S., Ang, W. T., & Veluvolu, K. C. (2016). Automatic Identification of Systolic Time Intervals in Seismocardiogram. *6*, 37524. doi:10.1038/srep37524

http://dharmasastra.live.cf.private.springer.com/articles/srep37524#supplementary-information

[33] Khosrow-khavar, F., Tavakolian, K., Blaber, A. P., Zanetti, J. M., Fazel-Rezai, R., & Menon, C. (2015). Automatic Annotation of Seismocardiogram With High-Frequency Precordial Accelerations. *IEEE Journal of Biomedical and Health Informatics, 19*(4), 1428-1434. doi:10.1109/JBHI.2014.2360156

[34] Khosrow-Khavar, F., Tavakolian, K., & Menon, C. (2015). Moving toward automatic and standalone delineation of seismocardiogram signal. *Conf Proc IEEE Eng Med Biol Soc, 2015*, 7163-7166. doi:10.1109/EMBC.2015.7320044

[35] Laurin, A., Khosrow-Khavar, F., Blaber, A. P., & Kouhyar, T. (2016). Accurate and consistent automatic seismocardiogram annotation without concurrent ECG. *Physiological Measurement, 37*(9), 1588.

[36] Rivero, I., Valdes, E., & Valdes, F. E. (2016). Robust Detection of AO and IM Points in the Seismocardiogram Using CWT. *Ieee Latin America Transactions, 14*(11), 4468-4473. doi:10.1109/Tla.2016.7795816

[37] Jain, P. K., Tiwari, A. K., & Chourasia, V. S. (2016). Performance analysis of seismocardiography for heart sound signal recording in noisy scenarios. *J Med Eng Technol, 40*(3), 106-118. doi:10.3109/03091902.2016.1139203

[38] Yang, C. X., & Tavassolian, N. (2016). Motion Artifact Cancellation of Seismocardiographic Recording From Moving Subjects. *Ieee Sensors Journal, 16*(14), 5702-5708. doi:10.1109/Jsen.2016.2573269

[39] Javaid, A. Q., Ashouri, H., Dorier, A., Etemadi, M., Heller, J. A., Roy, S., & Inan, O. T. (2017). Quantifying and Reducing Motion Artifacts in Wearable Seismocardiogram Measurements During Walking to Assess Left Ventricular Health. *IEEE Trans Biomed Eng*, *64*(6), 1277-1286. doi:10.1109/TBME.2016.2600945

[40] Gordon, J. W. (1877). Certain Molar Movements of the Human Body produced by the Circulation of the Blood. *J Anat Physiol*, *11*(Pt 3), 533-536.

[41] Henderson, Y. (1905). The mass-movements of the circulation as shown by a recoil curve. *American Journal of Physiology*, *14*(3), 287-298.

[42] Starr, I., & Noordergraaf, A. (1967). *Ballistocardiography in cardiovascular research*. Philadelphia and Montreal: Lippincott.

[43] Starr, I., Rawson, A. J., Schroeder, H. A., & Joseph, N. R. (1939). Studies on the estimation of cardiac output in man, and of abnormalities in cardiac function, from the heart's recoil and the blood's impacts; the ballistocardiogram. *American Heart Journal*, *18*(4), 506. doi:http://dx.doi.org/10.1016/S0002-8703(39)90682-4

[44] Dock, W., Mandelbaum, H., & Mandelbaum, R. (1953). *Ballistocardiography, the Application of the Direct Ballistocardiograph to Clinical Medicine*. USA: C.V. Mosby publishing company.

[45] Elliott, R. V., Packard, R. G., & Kyrazis, D. T. (1954). Acceleration ballistocardiography; design, construction, and application of a new instrument. *Circulation*, *9*(2), 281-291.

[46] Mounsey, P. (1957). Praecordial ballistocardiography. *Br Heart J*, *19*(2), 259-271.

[47] Scarborough, W. R., Talbot, S. A., Braunstein, J. R., Rappaport, M. B., Dock, W., Scarborough, W. R., . . . Starr, I. (1956). Proposals for Ballistocardiographic Nomenclature and Conventions: Revised and Extended. *Report of Committee on Ballistocardiographic Terminology*, *14*(3), 435-450. doi:10.1161/01.cir.14.3.435

[48] Junnila, S., Akhbardeh, A., Barna, L. C., Defee, I., & Varri, A. (2006). A wireless ballistocardiographic chair. *Conf Proc IEEE Eng Med Biol Soc, 1*, 5932-5935. doi:10.1109/IEMBS.2006.259814

[49] Junnila, S., Akhbardeh, A., Varri, A., & Koivistoinen, T. (2005, 2-4 Nov. 2005). *An EMFi-film sensor based ballistocardiographic chair: performance and cycle extraction method.* Paper presented at the IEEE Workshop on Signal Processing Systems Design and Implementation, 2005.

[50] Lindqvist, A., Pihlajamaki, K., Jalonen, J., Laaksonen, V., & Alihanka, J. (1996). Static-charge-sensitive bed ballistocardiography in cardiovascular monitoring. *Clin Physiol, 16*(1), 23-30.

[51] Vehkaoja, A., Rajala, S., Kumpulainen, P., & Lekkala, J. (2013). Correlation approach for the detection of the heartbeat intervals using force sensors placed under the bed posts. *Journal of Medical Engineering & Technology, 37*(5), 327-333. doi:10.3109/03091902.2013.807523

[52] Inan, O. T., Etemadi, M., Wiard, R. M., Giovangrandi, L., & Kovacs, G. T. (2009). Robust ballistocardiogram acquisition for home monitoring. *Physiol Meas, 30*(2), 169-185. doi:10.1088/0967-3334/30/2/005

[53] Bozhenko, B. S. (1961). Seismocardiography - a new method in the study of functional conditions of the heart. *Ter Arkh, 33*, 55-64.

[54] Baevskii, R. M., Egorov, A. D., & Kazarian, L. A. (1964). The Method of Seismocardiography. *Kardiologiia, 18*, 87-89.

[55] Salerno, D., & Zanetti, J. (1990). Seismocardiography: A new technique for recording cardiac vibrations. concept, method, and initial observations. *Journal of cardiovascular technology, 9*(2), 111-118.

[56] Crow, R. S., Hannan, P., Jacobs, D., Hedquist, L., & Salerno, D. M. (1994). Relationship between Seismocardiogram and Echocardiogram for Events in the Cardiac Cycle. *American Journal of Noninvasive Cardiology*, *8*(1), 39-46.

[57] Pandia, K., Inan, O. T., Kovacs, G. T. A., & Giovangrandi, L. (2012). Extracting respiratory information from seismocardiogram signals acquired on the chest using a miniature accelerometer. *Physiological Measurement*, *33*(10), 1643-1660. doi:10.1088/0967-3334/33/10/1643

[58] Dinh, A. (2011). Design of a Seismocardiography Using Tri-Axial Accelerometer Embedded with Electrocardiogram. *World Congress on Engineering and Computer Science, II*, 782-785.

[59] Inan, O. T., Migeotte, P. F., Park, K. S., Etemadi, M., Tavakolian, K., Casanella, R., . . . Di Rienzo, M. (2015). Ballistocardiography and Seismocardiography: A Review of Recent Advances. *IEEE Journal of Biomedical and Health Informatics*, *19*(4), 1414-1427. doi:10.1109/Jbhi.2014.2361732

[60] Zanetti, J. M., & Tavakolian, K. (2013). Seismocardiography: past, present and future. *Conf Proc IEEE Eng Med Biol Soc, 2013*, 7004-7007. doi:10.1109/EMBC.2013.6611170

[61] Akhbardeh, A., Tavakolian, K., Gurev, V., Lee, T., New, W., Kaminska, B., & Trayanova, N. (2009). Comparative analysis of three different modalities for characterization of the seismocardiogram. *Conf Proc IEEE Eng Med Biol Soc*, *2009*, 2899-2903. doi:10.1109/IEMBS.2009.5334444

[62] Gurev, V., Tavakolian, K., Constantino, J., Kaminska, B., Blaber, A. P., & Trayanova, N. A. (2012). Mechanisms Underlying Isovolumic Contraction and Ejection Peaks in Seismocardiogram Morphology. *J Med Biol Eng*, *32*(2), 103-110.

[63] Lin, W. Y., Chou, W. C., Chang, P. C., Chou, C. C., Wen, M. S., Ho, M. Y., . . . Lee, M. Y. (2016). Identification of Location Specific Feature Points in a Cardiac Cycle Using a

Novel Seismocardiogram Spectrum System. *IEEE Journal of Biomedical and Health Informatics, PP*(99), 1-1. doi:10.1109/JBHI.2016.2620496

[64] LPC1768/66/65/64 - 32-bit ARM Cortex-M3 microcontroller Datasheet. (2009). (pp. 72): NXP Semiconductors. Retrieved from http://www.nxp.com/documents/data_sheet/LPC1768_66_65_64.pdf.

[65] ADS131E0x 4-, 6-, and 8-Channel, 24-Bit, Simultaneously-Sampling, Delta-Sigma ADC. (2017). (pp. 73): Texas Instruments Incorporated. Retrieved from http://www.ti.com/lit/ds/sbas561c/sbas561c.pdf.

[66] Young, S. S. (2001). *Computerized data acquisition and analysis for the life sciences: a hands-on guide*: Cambridge University Press.

[67] WizFi210 Datasheet. (2013). (pp. 26): WIZnet Co. Retrieved from http://www.wiznet.io/wp-content/uploads/wiznethome/WiFi%20Module/WizFi_210_220/Document/WizFi210_DS_V120E.pdf.

[68] ± 2g Tri-axis Accelerometer Specifications. (2014). (pp. 14): Kionix. Retrieved from http://www.mouser.com/ds/2/348/KXR94-2050%20Specifications%20Rev%203-844615.pdf.

[69] PS25255 EPIC QFN sensor, electrophysiology, low gain, low power Datasheet. (pp. 6): Plessey Semiconductors. Retrieved from http://www.plesseysemiconductors.com/wp-content/uploads/ps25255-epic-qfn-sensor-electrophysiology-low-gain-low-power-datasheet.pdf.

[70] AD623 - Single and Dual-Supply, Rail-to-Rail, Low Cost Instrumentation Amplifier. (2016). (pp. 26): Analog Devices, Inc. Retrieved from http://www.analog.com/media/en/technical-documentation/data-sheets/AD623.pdf.

[71] MCP6L01/1R/1U/2/4 - 1 MHz, 85 µA Op Amps. (2011). (pp. 38): Microchip Technology Inc. Retrieved from http://ww1.microchip.com/downloads/en/DeviceDoc/22140b.pdf.

[72] MCP433X/435X - 7/8-Bit Quad SPI Digital POT with Volatile Memory. (2010). (pp. 88): Microchip Technology Inc. Retrieved from http://ww1.microchip.com/downloads/en/DeviceDoc/22242A.pdf.

[73] Cooper, S., Cant, R., & Sparkes, L. (2014). Respiratory rate records: the repeated rate? *J Clin Nurs, 23*(9-10), 1236-1238. doi:10.1111/jocn.12234

[74] Vitikainen, A. M., Makela, E., Lioumis, P., Jousmaki, V., & Makela, J. P. (2015). Accelerometer-based automatic voice onset detection in speech mapping with navigated repetitive transcranial magnetic stimulation. *J Neurosci Methods, 253*, 70-77. doi:10.1016/j.jneumeth.2015.05.015

[75] Webster, J. G. (2009). *Medical Instrumentation Application and Design, 4th Edition*: Wiley Global Education.

[76] Mondal, T., Slorach, C., Manlhiot, C., Hui, W., Kantor, P. F., McCrindle, B. W., . . . Friedberg, M. K. (2014). Prognostic Implications of the Systolic to Diastolic Duration Ratio in Children With Idiopathic or Familial Dilated Cardiomyopathy. *Circulation-Cardiovascular Imaging, 7*(5), 773-780. doi:10.1161/Circimaging.114.002120

[77] Marcus, F., & He, D. (2006). Accelerometer-based method for cardiac function and therapy assessment: Google Patents. Retrieved from http://www.google.com/patents/US20060095085.